Reading the muddy compass

Relative paleointensities of the Earth's magnetic field derived from deep-sea sediments

Yvo S. Kok

Reading the muddy compass

Relative paleointensities
of the Earth's magnetic field
derived from deep-sea sediments

Reading the muddy compass

Relative paleointensities
of the Earth's magnetic field
derived from deep-sea sediments

Relatieve paleointensiteiten van het aardmagneetveld
afgeleid van diepzeesedimenten

(met een samenvatting in het Nederlands)

PROEFSCHRIFT

TER VERKRIJGING VAN DE GRAAD VAN DOCTOR AAN DE
UNIVERSITEIT UTRECHT, OP GEZAG VAN DE RECTOR MAGNIFICUS,
PROF. DR H.O. VOORMA, INGEVOLGE HET BESLUIT VAN HET
COLLEGE VOOR PROMOTIES IN HET OPENBAAR TE VERDEDIGEN
OP MAANDAG 23 NOVEMBER 1998 DES NAMIDDAGS TE 4.15 UUR

DOOR

Yvo Sander Kok

Geboren op 10 december 1970 te Den Burg

Promotoren: Prof. Dr L. Tauxe
               Scripps Institution of Oceanography
               University of California San Diego

               Prof. Dr J.D.A. Zijderveld
               Faculteit Aardwetenschappen
               Universiteit Utrecht

Co-promotor: Dr C.G. Langereis
               Faculteit Aardwetenschappen
               Universiteit Utrecht

*Déjà se pose devant nous cette trilogie inaccessible
à la pensée humaine, le Temps, la Vie et la Mort,
qui fait justement de la Géologie une science si mystérieuse
et si poignante, parce que c'est elle qui s'approche le plus
de ces inconnues, mais sans pouvoir les saisir.*

MAURICE LUGEON, 1913

Ter nagedachtenis aan mijn opa

Contents

Chapter 1

General introduction

One of the interesting features of our living planet is its small but noticeable magnetic field. Some kinds of bacteria and animals intuitively use the Earth's magnetic field to navigate, e.g. during their annual migrations. Mankind discovered the potential of the magnetic force through the use of compasses that point towards the magnetic North. However, the geomagnetic field directions are not stable and corrections for the difference between magnetic and geographic poles are crucial for positioning purposes. Historical registrations not only show variations in the direction of the magnetic field, but also the intensity of geomagnetic field varies with time. The knowledge of these time-dependent properties of the magnetic field results in a better understanding of the processes in the inner part of our planet that drive the 'geodynamo'. The nature and evolution of the geodynamo are some of the most intriguing and unknown features of Earth sciences.

The direct observations of the geomagnetic field only span a very small fraction of the geological history. Fortunately, rocks containing certain iron oxides and iron sulfides record information on the prevailing magnetic field during their formation. The magnetic signal in rocks is very weak, but modern equipment allows paleomagnetists to extract geomagnetic data as far back as the Archaean (2.5–4 billion years ago). Thanks to this phenomenon, we have discovered that the geomagnetic field has reversed its polarity very often during Earth's history. The last major geomagnetic reversal occurred approximately 780 thousand years ago.

Paleomagnetism has solved many geological questions; e.g. the magnetic directions registered in rocks allow to reconstruct the plate tectonic movements for the last hundreds of million years. Another example of paleomagnetism as a geological tool are studies that use the well-known sequence of the magnetic polarity intervals for dating purposes (magnetostratigraphy). Less straightforward than paleomagnetic direction determinations are the studies on the long-term behavior

1

of the *strength* of the magnetic field: paleointensity research. The intensity data constitute a fundamental aspect of the geomagnetic field.

For all paleomagnetic investigations it is crucial to isolate the primary magnetic component from the total natural remanent magnetization (NRM) vector, which should be analyzed in sufficient detail. Paleomagnetists use demagnetization techniques to discriminate the primary magnetization from secondary additions. In essence, two procedures are routinely used to progressively analyze the NRM of the rock and to isolate the primary component: in zero-magnetic field, samples are either exposed to elevated temperatures (thermal demagnetization), or to alternating fields (AF demagnetization).

Paleointensity determinations require laboratory experiments that mimic nature. Volcanics acquire their primary magnetization after cooling through the blocking temperatures of their magnetic minerals. Therefore, stepwise thermal demagnetization of NRM is compared with acquisition of artificial thermal remanence in a known laboratory field to unravel the strength of the paleofield that is recorded in the rock. In principle, this technique provides *absolute* paleointensities of the geomagnetic field. A practical drawback is that a continuous temporal record cannot be constructed because of the discontinuous extrusion of lavas, in contrast to sedimentary rocks. Sedimentary sequences have the advantage that they span long and continuous time intervals, and can both be sampled and correlated on a global basis. The major drawback in these studies is the lack of knowledge on the acquisition process of detrital remanent magnetization (DRM). It is assumed that magnetic particles have a small preference to align with the ambient magnetic field when settling at the ocean floor. Sedimentary NRM intensity is in first order proportional to the Earth's magnetic field during deposition, but also varying processes like sedimentary input, bioturbation, consolidation, and compaction affect the NRM. Analogous to the thermal experiments for volcanic rocks, the deposition at the ocean floor can be imitated by redeposition experiments. However, the redeposition conditions in the laboratory will never approach the continuum of physical processes at the ocean floor. Thus, the bottle-neck in sedimentary paleointensity studies is the largely unknown sedimentary NRM acquisition process, but despite this flaw, sediments can provide valuable information.

Since not only the paleointensity, but also grain size, concentration, type and amount of magnetic minerals influence the NRM intensity, it is crucial for sedimentary paleointensity studies that NRM is properly corrected. Approximations for the 'magnetizability' of NRM are magnetic susceptibility χ or laboratory induced remanences which are used to normalize NRM. The paleointensities of the ancient field obtained in this way are relative estimates, which are obtained in a much simpler and faster manner than from the better-understood volcanic rocks.

A problem encountered in all rocks is that parts of the measured remanences are not primary magnetizations but contaminations (secondary magnetizations).

Water content, pressure, temperature, and many other physical parameters can vary considerably after formation of the rock, also when it is taken from its 'habitat', either by human or tectonic forces. This causes secondary magnetizations that can often be recognized during the demagnetization procedure. They can subsequently be eliminated, especially when the later, secondary magnetizations are acquired in an ambient magnetic field that is different from the direction of the primary magnetic component.

Secondary magnetization connected to viscous relaxation can be hard to detect when acquired in the same field as the primary remanence. The process of acquisition of viscous remanent magnetization (VRM) will effect all grain-size populations to some extent, even if all physical parameters remain constant, as long as it is exposed to an external field for a sufficiently long period. Sedimentary magnetization acquisition is a rather inefficient process. Therefore, the maximum or equilibrium magnetization is mostly much larger than the DRM vector. Relaxation towards the equilibrium magnetization can have relatively large consequences for the total NRM. Volcanics that carry thermo-remanent magnetizations (TRM), have primary magnetizations much closer to the equilibrium magnetization. The time constant controlling the rate of VRM acquisition for a given grain size, temperature and mineral type is the relaxation time τ that spans from milliseconds to astronomical durations. Magnetic components with short relaxation times (up to years) are often easily removed, whereas long-τ VRM (with τ up to circa two orders of magnitude longer than the age of the rocks) is more persistent against demagnetization. If in a particular sediment core the distributions of relaxation times were similar, the VRM contribution to the NRM of the young rocks can be drastically different from the those of the older. The effects of age dependence on the VRM contribution become more radical when the paleomagnetic field has changed its polarity in the meantime. Reversed magnetizations have recorded a magnetic component opposite to the present-day VRM, which always grows along the prevailing Earth's magnetic field. Variable distributions of relaxation times throughout a sedimentary sequence, depending on for instance variable grain-size distributions, can cause an even more complex record of VRM added to DRM. In that case a 'blanket' demagnetization of NRM may not be appropriate and can lead to erroneous interpretations.

In short, the primary detrital remanent magnetization must be discriminated from the total natural remanent magnetization. Long-relaxation time VRM depends mainly on the grain-size distributions and age, and varies considerably throughout a sedimentary sequence. Once a pure DRM component is isolated, normalization with a magnetizability renders a relative paleointensity estimate, as long as the factor is an appropriate reflection of the DRM acquisition mechanism.

1.1 Outline and summary of the thesis

This thesis has been structured in three parts: Part I discusses three methodological studies, Part II addresses the saw-toothed pattern observed in some paleointensity records spanning the last 4 million years, and Part III examines geomagnetic paleointensity stacks.

Part I: Relative paleointensity in sediments: Methods

In **Chapter 2** a pseudo-Thellier paleointensity method for normalizing sedimentary records is presented. It is comparable to the Thellier-Thellier technique [*Thellier and Thellier*, 1959] which compares unblocking of NRM with blocking of partial thermo-remanent magnetization (p-TRM). Instead of the thermal experiments, we use alternating field demagnetization of NRM and compare it with acquisition of anhysteretic remanent magnetization (ARM) to derive a more robust paleointensity estimate. We suggest that it has the advantage of removing variable amounts of VRM included in NRM.

Chapter 3 discusses a statistical method for Thellier-Thellier or pseudo-Thellier experiments. Conventionally, paleointensities are determined by linear regression of the best-fit line through NRM and laboratory induced remanences. With a jackknife resampling method, we successively remove data pairs from the set to recalculate the slope with the least-squares fit. The number of additional paleointensity estimates is treated as an uncertainty measure in the original determination. Unlike the standard deviation of the original paleointensity, jackknife resampling often produces asymmetric uncertainty bounds.

Chapter 4 uses the pseudo-Thellier method (described in Chapter 2) to estimate VRM contributions to NRM. While the relationship of demagnetization of a laboratory acquired stirred remanence is linear with ARM acquisition, that of NRM demagnetization and ARM acquisition is typically non-linear. The concave parts of the relating curve are suggested to be caused by VRM components that are demagnetized earlier than DRM. Since the coercivities of VRM and DRM partially overlap, also a fraction of the DRM is removed. For paleointensity determinations, these non-linear parts are avoided, but here we focus on the implications as long-relaxation time VRM indicators. In Chapter 2, the long-τ VRM contribution is estimated by the difference of the conventional NRM/ARM and the best-fit slope. Here we suggest a different method which does not require determining either paleointensity value. Results of our long-τ VRM suggest correlations with paleoclimate curves, and age-dependent growth of VRM. In addition, a distinct change in grain size is detected, and it appears that the long-τ VRM acquired during the Pleistocene is associated with short-τ effects detected in the laboratory environment.

Part II: Saw-toothed pattern in paleointensity records

The observation of a so-called "saw-toothed" pattern [*Valet and Meynadier*, 1993] has stimulated much discussion and debate in the paleomagnetic community. These investigators noted a remarkable triangular pattern in their paleointensity determinations for the last 4 million year. Within a stable polarity interval, progressive decay of the dipole intensity seems to lead up to polarity reversals, to be followed by high intensities of the next stable polarity zone. A rather unexpected behavior of the geodynamo would be inferred from this paleointensity pattern. Since their publication, several other studies confirmed the saw-toothed pattern, while some found no evidence for such behavior. **Chapter 5** suggests that the saw-toothed phenomenon is caused by cumulative viscous remanence. In particular, it addresses viscous magnetizations acquired over millions of years. A cumulative viscous remanence model that incorporates distributions of long relaxation times τ, e.g. 50±25 Myr, changes an originally constant absolute paleointensity value to a saw-toothed pattern like the one that *Valet and Meynadier* [1993] observed.

Chapter 6 examines in more detail one of the reversals of the record of *Valet and Meynadier* [1993]. We use thermal demagnetization techniques on a resampled collection and note that the asymmetric pattern disappears. We conclude that the saw-toothed pattern is caused by an artificial component obscuring the primary magnetizations. Moreover, the Thellier-Thellier experiments allow us to constrain parameters for our model of Chapter 5. The model reproduces the original asymmetrical offset around the reversal very well, strongly suggesting that the contamination causing the saw-toothed pattern is of long-τ viscous origin.

Our French colleagues attempt to categorically refute alternative explanations of the saw-toothed pattern. Recently, *Meynadier et al.* [1998] published a test of our model. In **Chapter 7** we argue that their refutation is built on a misinterpretation of our work. *Meynadier et al.* [1998] wrested one example of a relaxation time distribution used in Chapter 5 from its context and tested it against thermal blocking of real sediments. Logically, the characteristics vary considerably, since our example spans merely a subset of the extremely wide range of relaxation times present in the rock. We draw attention to the fact that the specific example 50±25 Myr is able to generate a saw tooth, but the existence of much longer relaxation times (i.e., $\gg$ 100 Myr) in the sediments is explicitly mentioned in Chapters 5 and 6. When the tooth of time works for a few million years, the influence of astronomical τ's on the viscous remanence calculations is negligible.

Part III: Stacks

Chapter 8 argues that published paleointensity records spanning the last 200 kyr are also affected by non-geomagnetic features. Two recent independently derived stacks of paleointensity estimates show good correspondence. The first—Sint-200 [_Guyodo and Valet_, 1996]—consists of a compilation of NRM intensity records corrected by one of the obvious normalizers. The second 200-kyr stack uses several normalized ^{10}Be records as an indication of cosmogenic production rate, which is translated to relative geomagnetic field intensity variations [_Frank et al._, 1997]. The overall agreement of NRM and ^{10}Be derived paleointensity data is optimistically explained as a validation of the use of techniques and material to obtain paleointensity variations. Alternatively, it is suggested that both records are—to a certain degree—still biased by Pleistocene climate. In general, climatically induced variations are evident in sedimentary sequences, for instance, oxygen isotopes (δ^{18}O) data from sediments can represent the glacial–interglacial chronology; hence, δ^{18}O data are often used to date and synchronize sedimentary records. Both paleointensity stacks—but especially the ^{10}Be data—show coherent features with the δ^{18}O data, suggesting that they display both geomagnetic field behavior _and_ climate. To test this contention, spectral-analysis techniques are used on the 200-kyr paleointensity stacks and on an individual record included in Sint-200. The latter paleointensity record indicates that NRM, ARM, but also their ratio is coherent with δ^{18}O. This is explained as an inadequacy in the normalization technique. More recently developed paleointensity determinations appear to suppress this influence.

Chapter 9 presents a paleointensity stack for the Matuyama Chron. Sedimentary magnetizations from 4 ODP cores from the Ontong-Java Plateau (OJP) are analyzed with thermal techniques. Thellier-Thellier experiments [_Thellier and Thellier_, 1959] are used to determine magnetic properties and indicate that a thermal demagnetization to 250°C can be used for paleointensity estimates. The correlated records form a coherent OJP stack, which is dated at reversal boundaries. There is no evidence in the OJP stack for a saw-toothed pattern. A coherent feature with two other data sets spanning the Matuyama Chron, is the occurrence of a 150-kyr periodicity. However, the time control of the OJP stack is not accurate, except for the 10 tie points at the reversals. This could—at least in part—explain why the three Matuyama paleointensity records show no other coherent frequencies.

Part I

Relative paleointensity in sediments: Methods

Chapter 2

Pseudo-Thellier approach

Abstract We present a method for normalizing sedimentary records for estimating relative paleointensity of the geomagnetic field, similar to that successfully used to obtain absolute paleointensity from thermally blocked remanences. It has the advantages that it is more effective in removing unwanted viscous remanence, thereby improving agreement among various records and that it allows the estimation of the uncertainty in the relative paleointensity calculated.

2.1   Introduction

Extracting paleointensity information from sedimentary sequences has been a frequent goal since the earliest days of paleomagnetism (e.g. *Johnson et al.* [1948]; see recent review by *Tauxe* [1993]). Laboratory redeposition experiments suggest that when properly stirred, sediments can carry a remanent magnetization that is linearly related to the ambient magnetic field (e.g. *Kent* [1973]). In practice, sediments always display some changes in "magnetizability" within a given sequence as a result of changes in, for example, concentration, grain size, and mineralogy of the magnetic phase. In addition, the original remanence may have been modified by subsequent processes, for example, by viscous or chemical remagnetization. Whereas separation of chemical and depositional components may be quite difficult, separation of viscous and depositional components may be achievable.

No laboratory experiment can duplicate the natural process of sedimentation exactly and laboratory redeposition is not in routine use. Given the difficulty of redeposition, most studies have relied on the use of some bulk magnetic property related to the magnetizability for normalization such as magnetic suscep-

---

tibility (χ), anhysteretic remanence (ARM) or isothermal remanence (IRM) (see *Tauxe* [1993] for a thorough discussion). Estimates of relative intensity (B^*) therefore are derived by dividing the natural remanence (NRM) by the normalizer of choice (e.g. χ, ARM or IRM for B^*_χ, B^*_A or B^*_I respectively). Each of these choices for normalization suffers from drawbacks that make them less than ideal as summarized by *Levi and Banerjee* [1976], *King et al.* [1983], *Tauxe* [1993], Moreover, none of these "brute force" estimates of B^* take into account the possible contribution of viscous remanence (VRM) to the NRM. In sediments deposited during the last 780,000 years (the Brunhes Chron), a VRM is likely to be nearly parallel to the primary detrital remanence (DRM), (*sensu Tauxe* [1993]) making it quite difficult to detect. In order to minimize the VRM contribution, *Levi and Banerjee* [1976] proposed that both the NRM and ARM (or IRM) be demagnetized at progressive treatment steps $(B^*_{A(A.F.)}$ or $(B^*_{I(A.F.)})$, respectively). This procedure was intended to identify some coercivity window that was more or less stable. This method is far preferable to the "brute force" method of using NRM with no demagnetization, but still has the difficulty that the parameter usually changes substantially as a function of demagnetization step; moreover, it is difficult to judge whether and when the VRM has been successfully removed. *Jackson et al.* [1988] introduced the use of a partial ARM (pARM). PARMs can be tuned to a particular coercivity window and could be used for normalization of the NRM fraction in the same coercivity window, whereby the portion of the NRM vector falling between two A.F. demagnetization treatment steps (say 30 and 50 mT) is calculated by vector subtraction. This partial NRM (pNRM) could then be normalized by the pARM acquired between the same two A.F. steps (here designated as $B^*_A[^{min}_{max}]$). This "vector difference" method is superior to the brute force methods, but still suffers from the fact that it is difficult to choose objectively the particular treatment steps as bounds for the partial remanences.

Finally, assessing the reliability of the various normalized remanences remains problematical. At present, the preferred procedure is to compare estimates of B^* derived from various methods of normalization and hope for some agreement. Since all methods of normalization are flawed in different ways, agreement among several brute force estimates has been thought to be a fairly powerful test of the reliability of the data (see e.g. *Tric et al.* [1992]). It is frequently argued that agreement among different contemporaneous records argues in favor of successful normalization. In fact, contemporaneous records of relative paleointensity are disappointingly dissimilar (see e.g. *Tauxe* [1993]). Although the general character of the records on time scales of tens of thousands of years is replicated, the amplitudes often differ by factors of two or three or more, even for the records from the same region. It was the disappointing comparison of replicate records of relative paleointensity that led us to seek an improved method for normalization.

Furthermore, if the NRM is composed of viscous and depositional components, most normalization techniques will fail to separate the two and the amplitude of

the normalized remanence records will be systematically biased. Good agreement may be obtained for inaccurate data.

In this paper, we present a method of normalization that not only conveniently separates VRM from DRM, but offers a means of assessing the uncertainty of the relative paleointensity estimate. The method is equally applicable to thermal demagnetization as to alternating field demagnetization should circumstances require it. We test the method on sediments recovered from the Ontong-Java Plateau.

2.2   Sample location and instrumentation

All specimens used here were taken from core RNDB 74p (2.06°N, 159.5°E and 2547 m water depth), acquired from the Ontong-Java Plateau during the Roundabout expedition in 1988. The magnetic properties of this high carbonate (over 95%) core are identical to those studied previously by *Tauxe and Wu* [1990]. The magnetization is carried by fine grained magnetite whose concentration and grain size is fairly uniform in the cores selected for study. Isotopic studies on RNDB74p demonstrate that the specimens discussed in the following are from oxygen isotopic stage 9 (M. Yasuda, pers. comm.) at some 6 meters depth below core top.

Remanence measurements were made on the CTF cryogenic magnetometer housed in the magnetically shielded room of the Fort Hoofddijk Paleomagnetic Laboratory at the University of Utrecht. Alternating field demagnetization was performed using an Sapphire Instruments SI-4 single axis demagnetizer. ARMs and pARMs were acquired in the same coil using a D.C. field of 0.05 mT which could be switched on and off electronically at specified field steps. IRMs were produced by the same electronics using a companion coil, so cross field calibration is quite good.

2.3   The pseudo-Thellier method of normalization

Our method is inspired by paleointensity studies using thermally blocked remanences and draws heavily on the techniques developed by *Thellier and Thellier* [1959] as enhanced by *Coe et al.* [1978]). The essence of the method is to compare directly the NRM contained in a particular coercivity or blocking temperature fraction with that acquired by an ARM or thermal remanence (TRM) in the same coercivity or blocking temperature fraction.

First, we measure the NRM, then demagnetize it in step wise fashion using fairly closely spaced steps. We perform a so-called "double demagnetization" in which the specimen is demagnetized along three orthogonal axes (x, y, z), measured, then demagnetized along -x, -y, -z and remeasured (see Figure 2.1a). The vector mean of the two measurements is calculated (see Figure 2.1b). Double
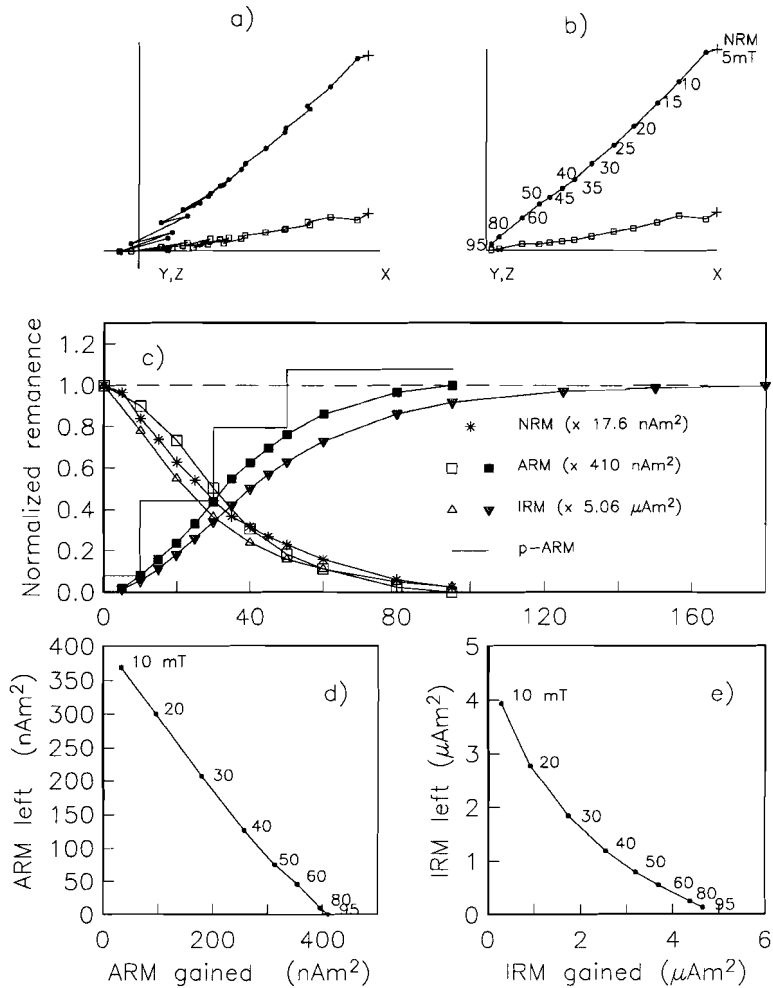
Figure 2.1: (a) Vector end-point diagram of step-wise A.F. demagnetization data. X and Y (solid symbols) are in the horizontal plane (unoriented with respect to North), and X and Z (open symbols) are in the vertical plane. Plusses mark the NRM data. Starting from the third demagnetization step, each demagnetization was carried out twice (see text); double demagnetization results in "zig-zagging". (b) Same as (a) but using vector average of double demagnetization steps. (c) Remanence normalized by specified values for each remanence type versus applied field (see text). (d) ARM left after demagnetization to a given peak field plotted on ARM gained at the same peak field value (squares in (c)). (e) Same as (d) but for IRM left on IRM gained (triangles in (c)).

demagnetization is recommended because some sediments are extremely suscep-
tible to acquiring a spurious ARM during demagnetization (resulting in the "zig-
zagging" in Figure 2.1a). Double demagnetization effectively cancels out the spu-
rious ARM in most cases. There is slight curvature to the demagnetization data
up to about 30 mT evident in the vector end-point diagram shown in Figure 2.1b,
hinting at simultaneous removal of two nearly parallel components. The NRM
intensity remaining after each demagnetization step is plotted in Figure 2.1c.

After demagnetization of the NRM, each specimen is subjected to step-wise
acquisition of ARM in the identical steps as the demagnetization of NRM (filled
squares in Figure 2.1c). At intervals, p-ARMs are also given (cumulative curve
shown by line). *Jackson et al.* [1988] developed the pARM method in order to
obtain discrete ARM contributions, that are unaffected by magnetostatic interac-
tions among the different coercivity fractions. Thus the cumulative pARM should
be somewhat higher (1–5% depending on concentration) than the total ARM.

Following demagnetization of the ARM (open squares), the specimen is sub-
jected to increasing D.C. fields to monitor acquisition of IRM using the same field
steps as the initial demagnetization of the NRM but continuing up to saturation
(filled triangles). This IRM was also demagnetized (open triangles). All specimens
showed a crossing of ARM acquisition and demagnetization curves at about 50%
and a similar crossing for IRM data at about 35%. The ARM data are thus more
stable against demagnetization than the IRM, and are "symmetric". Another way
of looking at this is by plotting the partial remanence gained at a particular peak
field versus the remanence left after demagnetizing the total magnetization to the
same field (see Figure 2.1d and e). This is a similar plot to the so-called "Arai
plot" of *Nagata et al.* [1963]. The Arai plots for the ARM data are rather linear
whereas those for the IRM are markedly curved.

Traditional ways of estimating B^* are shown in Figure 2.2a. $B^*_{A(A.F.)}$ varies
with demagnetizing field as does $B^*_{I(A.F.)}$ although to a lesser extent. The strong
variability of the estimates with demagnetizing field and the differences among
various specimens makes their use difficult to justify, at least for these (rather
well behaved) sediments. The vector difference estimate $B^*_A[^{min}_{max}]$ of all specimens
varies with choice of bounding fields but is generally more stable than the $B^*_{A(A.F.)}$.
The problem is that the optimum bounding fields may vary from specimen to
specimen and must be established anew for each case.

The "pseudo-Thellier" method is illustrated in Figure 2.2b. The data in our
Arai-type plots are not generally linear. Between about 5 mT and 25 or 30 mT,
the data lie along a gentle curve. The associated steps plotted as vector end-points
in Figure 2.1b also are gently curved. We interpret these data as reflecting the
removal of a VRM along with some of the original DRM, assumed to have been
acquired near the sediment/water interface during bioturbation. Data between
about 35 and 95 mT lie along a line (as do the corresponding data in the vector
end-point diagrams).
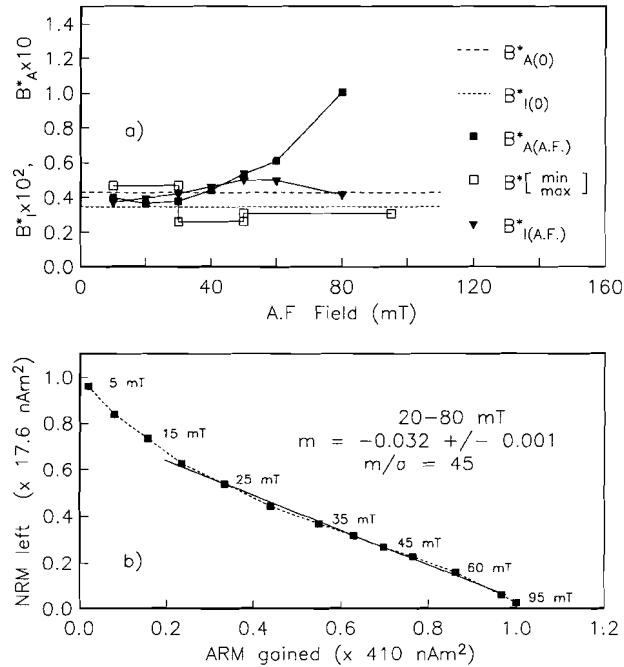
Figure 2.2: *(a) Various paleointensity estimates (see text). (b) Arai plot for the NRM-ARM data shown in Figure 2.1c. ARM gained during magnetization in specified A.F. fields versus NRM left after demagnetization in same field. Data are normalized by values in 2.1c. Also shown is m/σ, the parameter used to optimize the slope calculation.*

The pseudo-Thellier method allows us to treat the data shown in Figure 2.2b in a similar fashion as that developed for Thellier-Thellier data by *Coe et al.* [1978]. The best-fit slope m relating the NRM and ARM (or TRM) between two field steps, can be calculated, taking into account the uncertainty in both (see *Coe et al.* [1978]). We plot the best-fit slope of the NRM-ARM data (m_a). Also shown in the standard deviation σ and a parameter m/σ which estimates the goodness-of-fit of the line to the data. We can therefore objectively choose the portion of NRM-ARM data which maximizes m/σ.
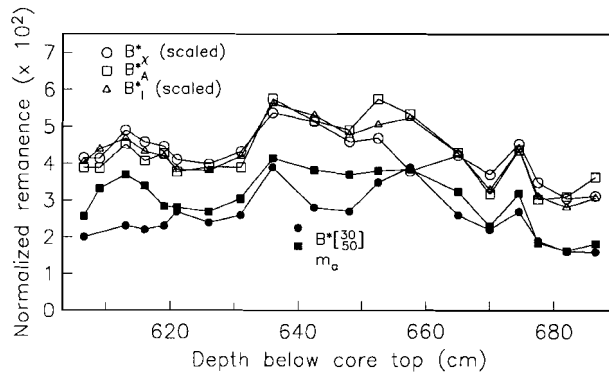
Figure 2.3: *Various relative paleointensity estimates versus depth in core.*

2.4 Discussion

We plot assorted estimates for the 19 specimens versus stratigraphic position in Figure 2.3. Here B_I^* and B_χ^* are scaled based on a linear regression of the respective data to the comparable B_A^* data.

The brute force methods (open symbols) agree with one another quite well as do the best-fit line and vector difference methods (solid symbols). However, as noted before, the brute force methods are generally higher than the best-fit line method. We interpret this as being the result of a pervasive VRM which biases the brute force estimates systematically. Of particular interest is the fact that the degree of offset between the two is not constant, but varies down core. If this is generally true (and we strongly suspect that it is) then there is little justification for using any of the brute force methods and agreement among various brute force methods does not guarantee reliability. When considering data of different polarities, even constant VRM will lead to serious errors (see Part II of this thesis).

We interpret the difference in amplitudes of the normalized remanence data as resulting from differential acquisition of VRM during the Brunhes. In order to test this hypothesis, we tried two approaches. First, it may be that DRM and ARM are never linear on Arai-type plots as IRM gained versus IRM lost is not. However, NRM versus ARM data from freshly made stirred remanences show linear behavior in Arai plots (see Chapter 4). Second, we attempted to assess the potential contribution of VRM to the NRM by observing viscous behavior on short laboratory time scales.

Representative specimens were given a saturation IRM, measured and immediately place in a null magnetic field. The remanence was the measured periodically in order to monitor viscous decay. Typical results are shown in Figure 2.4a. The
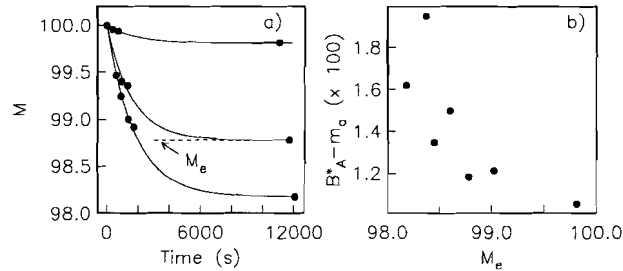
Figure 2.4: *(a) Viscous decay of saturation IRM in zero field. (b) The difference between B_A^* and m_a from Figure 2.3 plotted on M_e (see text).*

magnetization as a function of time $M(t)$ for each specimen was fit with a curve described by the following decay equation:

$$M(t) = M_o + (M_e - M_o)(1 - e^{-t/\tau}) \tag{2.1}$$

where M_o is the initial saturation IRM, M_e is the stable magnetization to which the remanence decays, and τ is the constant controlling the exponential decay. We normalize the magnetization such that M_o is taken as 100%. The decay constant describes the rate at which a stable magnetization is approached and M_e represents the percentage of the magnetization that is stable (over the time span of observation). Thus the higher M_e, the less "viscous" the sample. The τ's of our specimens were remarkably similar.

In Figure 2.4b we plot what we interpreted as the VRM contribution to the normalized remanence $(B_A^* - m_a)$ on M_e. Although the data are scattered, there does seem to be some relationship between the short-term viscous behavior in the laboratory and the inferred long-term viscous behavior in the Brunhes field, supporting our interpretation.

2.5   Conclusions

We present a method for normalizing sedimentary sequences to provide reliable relative paleointensity data, drawing on the most reliable absolute paleointensity method—the Thellier-Thellier method (see *Coe et al.* [1978]), for use with thermally blocked remanences.

We tested the method on 19 specimens from a core from the Ontong-Java Plateau. Comparison with traditional "brute force" methods of normalization suggests that these may be systematically biased by unremoved VRM and that agreement among NRM/ARM, NRM/IRM, and NRM/χ does not constitute a sufficiently rigorous test for reliability.

The principal drawback of the new "pseudo-Thellier" method is that it takes substantially longer than the "brute force" method to make all the measurements necessary. We note that whereas "brute force" methods may work, nearly as much time must be spent on each specimen to establish the fact as is involved in our technique. Because our method allows the removal of unwanted VRM and provides the possibility for internal checks for reliability, we hope it will be possible to gain better core to core agreement for contemporaneous records.

Chapter 3

Jackknife resampling

Abstract We present a method for estimating uncertainties in paleointensity determinations for experiments using Thellier-Thellier (normalization using progressively acquired partial-thermal remanences) or pseudo-Thellier (normalization using partial anhysteretic remanences). For each sample, the best-fit slope for the entire data set is determined. Then, additional best-fit slopes are calculated after removal of each data point. Finally, all possible combinations of two data points are eliminated to provide more best-fit slopes. This jackknife resampling plan produces a distribution of possible paleointensities that allows judging the uncertainty of the original best-fit slope calculation.

3.1 Introduction

In order to obtain paleomagnetic information of the Earth's past from rocks, the first criterion to be met is that the recording medium must contain magnetic material that can retain a representation of the applied field. Next, the question arises whether the magnetization isolated in the laboratory represents the ancient geomagnetic field near to the time of formation of the rock. Secondary components that have obscured the desired primary remanence can often be demagnetized by exposing the rock to either progressively increasing alternating fields or higher temperatures in zero-magnetic field space. When the isolation of the alleged primary component is accomplished, one is able to determine its direction and use the deviation from the expected magnetic direction to deduce characteristics of field features (e.g. polarity reversals or paleosecular variation), or tectonic events. However, the strength of the magnetization is not only dependent on the prevailing field during (or since) formation, but also the amount and type of magnetic material in the specimen. Thus, one needs to adjust the remanent magnetic vector by a 'magnetizability' factor to deduce information about the strength of the

ancient earth magnetic field. These normalizations with bulk magnetic param-
eters, such as susceptibility or anhysteretic remanent magnetization (ARM) can
provide constraints for at least the relative intensity of the paleomagnetic field.
Preferably, a number of determinations of one single specimen is made, either by
dividing the primary remanence by several normalizers or by comparing several
demagnetization steps paired with acquisition of an artificial magnetization. The
last method ought to give rise to a linearity between the two magnetizations of
which the proportion represents the intensity of the ancient magnetic field. We
will refer to it as a multiplex paleointensity (MP) determination.

In this paper, we present a method that allows us to estimate how statistically
robust such an MP estimate is. Instead of using the standard deviation as an
estimate for the uncertainty in the slope, the set is resampled using a jackknife
scheme to obtain a number of estimated slopes. The additional paleointensity
determinations describe a distribution of possible slopes, bounding the original
MP value.

3.2   Experimental paleointensity determinations

3.2.1   Thellier-Thellier method

The Thellier-Thellier method for absolute paleointensities [*Thellier and Thellier*,
1959; *Coe*, 1967] involves a comparison between thermal demagnetization of the
natural remanent magnetization (NRM) and an acquired partial thermoremanent
magnetization (pTRM). In principle, the specimen was originally magnetized by
cooling from temperatures above the Curie temperature (thermoremanent ori-
gin). Recent studies show that not only thermally blocked magnetizations are
suitable for Thellier-Thellier's MP technique, but also deep-sea sediments [*Hartl
and Tauxe*, 1996; *Kok and Tauxe*, 1996b]. Only relative paleointensity estimates
can be obtained from these materials, for depositional NRM is acquired with less
efficiency than thermoremanent magnetization.

3.2.2   Pseudo-Thellier method

Alternating field (AF) demagnetization of NRM takes less laboratory time than
its thermal counterpart. In general, bulk magnetic parameters are used to nor-
malize the NRM intensity after AF cleaning (mostly to 10 or 20 mT) to obtain
relative 'scalar' paleointensity records. When progressive AF demagnetization of
the NRM is compared with progressive acquisition, we have what has been called
a "pseudo-Thellier" normalization [*Tauxe et al.*, 1995]. The pseudo-Thellier ap-
proach turned out to be successful in estimating relative paleointensities from sed-
imentary cores. This MP determination can be more effective than ordinary single

value normalizations, since contributions from different mechanisms of magnetization (e.g. viscous or depositional) can be identified. However, it is tremendously more time consuming than blanket demagnetization and measurement of a single bulk parameter.

3.3 Slope determination and resampling

Ideally, the relation between the demagnetization and acquisition sequences is linear:

$$\frac{\text{NRM}_i}{\text{pTRM}_i} = -\frac{B}{B_{lab}} = \text{constant} \tag{3.1}$$

or

$$\frac{\text{NRM}_i}{\text{ARM}_i} = m_a = \text{constant} \tag{3.2}$$

where B is the paleointensity during the acquisition of the NRM, B_{lab} the laboratory field during the pTRM acquisition, and m_a as in *Tauxe et al.* [1995]. The magnetizations NRM and the laboratory induced are compared in an Arai-plot [*Nagata et al.*, 1963] and, in general, deviations from a linear relation are detected. Often, low treatment steps lie along a slope different than that of the higher treatment steps. This occurs, for example, when the low treatment steps remove a softer viscous remanent magnetization (VRM). Further, the slope for high treatment steps can be erroneous when thermal treatment causes changes in the magnetic properties of the remanence carrying phases. If the magnetic directions clearly show the presence of secondary components, the deviating data can be identified and skipped. In many cases some portion of the data pairs must be rejected, leaving the remaining data for the calculation of the best fit slope, that is, the MP estimate.

The general solution for the slope m of the regression line of a set of k (x, y)–pairs NRM and the artificial remanence [*Coe et al.*, 1978] is:

$$m = \pm\sqrt{\frac{\sum(y_i - \overline{y})^2}{\sum(x_i - \overline{x})^2}} \tag{3.3}$$

where $\overline{x}$ and $\overline{y}$ are the arithmetic means. Information on the reliability of this slope is given by its standard error:

$$\sigma = \sqrt{\frac{2\sum(y_i - \overline{y})^2 - 2m\sum(x_i - \overline{x})(y_i - \overline{y})}{(k - 2)\sum(x_i - \overline{x})^2}} \tag{3.4}$$

As stated by *Coe et al.* [1978] the standard error of the slope 3.4 cannot be attributed strict statistical meaning and must instead be regarded as an *ad hoc* measure of uncertainty. The standard error σ uses all data points in a certain

interval, so one outlying datum biases the result significantly. Another disadvantage is that the uncertainty appears to be symmetrically distributed about the 'best estimate'.

Here we devise a different method for estimating uncertainty using a jackknife resampling technique [*Efron*, 1982], which is a manner of judging the reliability of a data set. The recipe for the multiplex paleointensity determination case is the following:

1. Calculate the best fit slope from at least 4 out of k pairs by minimizing the relative error σ/m (equations 3.3 and 3.4).

2. Perform a "delete-one" jackknife, by systematically skipping each data point and repeating the search for the best slope; one obtains k jackknife estimates for relative paleointensity.

3. Perform a "delete-two" jackknife by skipping every possible combination of two data points; one obtains $\binom{k}{2} = \frac{k \cdot (k-1)}{2}$ jackknife slope estimates.

We now have a distribution of $k + \binom{k}{2}$ additional slope estimates. When plotted in ranked order, they are generally distributed about a central part that has rather consistent values. The extreme values at the low and high end can be truncated by taking a central part of the population (say 68% or 90%), preserving the region of more stable estimates.

3.4   Application

Relative changes of the geomagnetic field strength for the Ontong-Java Plateau have been published by *Tauxe and Shackleton* [1994]. We have resampled piston core RNDB 75p (1–2 cm^3 samples) for further paleointensity research.

Figure 3.1 shows the pseudo-Thellier results of a sample at 222.5 cm depth. The top (Fig. 3.1a) indicates the NRM demagnetization behavior in an orthogonal diagram. Intensities after demagnetization of the NRM and acquisition of the ARM (Fig. 3.1b) are coupled as function of alternating field step in an Arai plot [*Nagata et al.*, 1963] (Fig. 3.1c). The minimum σ/m is found in the interval 35–90 mT, which has a slope m_a of -0.0659. Resampling using the delete-one and delete-two methods gives $11 + \frac{11 \cdot 10}{2} = 66$ jackknife estimates for the slope relating NRM_i and ARM_i (Fig. 3.1d, e). The center 90% of the sorted population eliminates the most extreme values m_a (enclosed by the dashed lines). Thus, for this sample we have obtained a pseudo-Thellier slope m_a with asymmetric jackknife uncertainty bounds.

The results for the entire core are shown in Fig. 3.2. Original paleointensity variations [*Tauxe and Shackleton*, 1994] (dashed line) agree with the conventionally determined NRM_{15}/ARM of this study (open line). The best-fit pseudo-Thellier slopes m_a are plotted together with the jackknife bounds (gray band). In
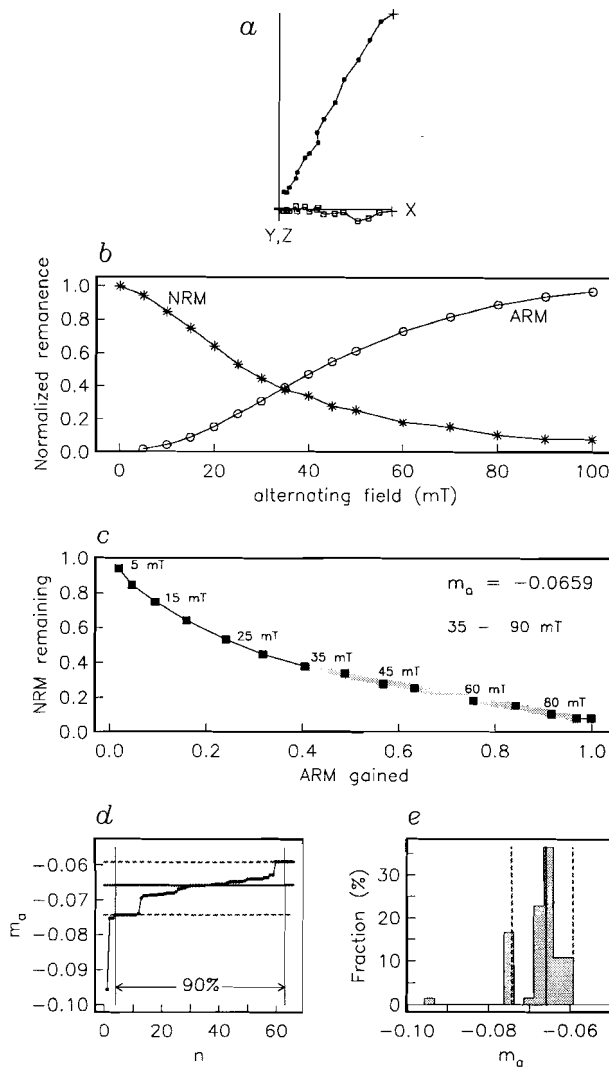
Figure 3.1: *Example of pseudo-Thellier method for a sample of RNDB 75p from the Ontong-Java Plateau. (a) Orthogonal vector end-point diagram of step-wise AF demagnetization. (b) Intensities of NRM demagnetizations and ARM acquisition versus applied alternating field step. (c) Arai plot, pairing the magnetizations NRM and ARM, indicates semi-linear slope. Best-fit slope is found in the 35–90 mT interval. (d) The jackknife resampling gives 66 additional slope determinations. The central 90% of the sorted distribution is enclosed by the dashed lines, and interpreted as jackknife errors of the best-fit slope. (e) Representation of all slopes in a histogram.*

general, the curves are quite similar, except for a few extremities in the original data [*Tauxe and Shackleton*, 1994] that do not appear in the new data set. Already noted was the slight shift within the pseudo-single-domain grain-size range toward super-paramagnetic at about 4 m, that is, in the 375–810 cm interval not only the paleointensity estimates suggest a different character, also the jackknife uncertainty indicates a larger margin. The bounds in the interval 150–350 cm can be interpreted as the envelope containing the 'real' paleointensities, which could have fluctuated less than any of the paleointensity determinations suggest.

We have excluded steps below 25 mT from the slope calculations as these are likely to be dominated by viscous remanence, as opposed to a stable depositional one. If we include these, the number of jackknife estimates would increase; but these would be biased toward steeper slopes which we consider erroneous.
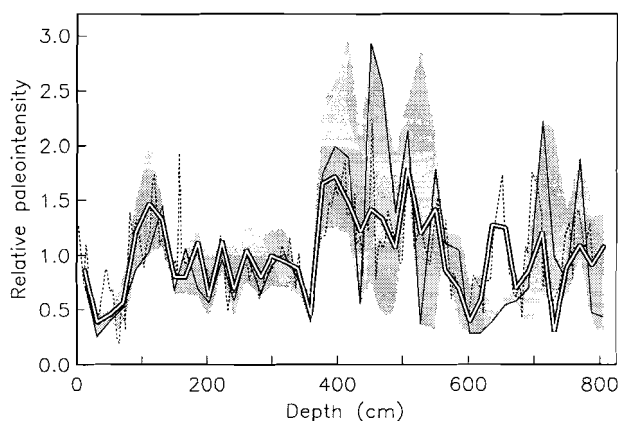
Figure 3.2: *Results of pseudo-Thellier and jackknife resampling on the core RNDB 75p. Original paleointensity determinations (dashed), this study's NRM$_{15}$/ARM (open line), and the best-fit slope according to the pseudo-Thellier method (line). Also indicated the central 90% of the distribution of slopes after the jackknife resampling procedure (gray). Several peaks in the original data correspond to broad distributions. The 150–350 cm interval suggests that the 'real' paleointensities have been more stable within the gray band. Rock-magnetic parameters in the deepest 4 m turned out to be slightly different, which coincides with larger jackknife uncertainties.*

3.5 Conclusion

The most straightforward indication for a reliability in a multiplex paleointensity estimate would be the standard deviation of the slope. However, outlying data can also be included in this estimate; moreover, it is symmetric about the best-fit slope and cannot be attributed strict statistical meaning. We present a technique that yields uncertainty estimates for the slope determinations from the pseudo-Thellier or Thellier-Thellier method. Performing such multiplex paleointensity experiments provides a data set that is usable for this statistical method. The distribution of additional estimates obtained by jackknife resampling often indicates that the original determination was inconclusive. Further, the proposed technique has the advantage of reducing the influence of extreme data points. Possible slopes per sample as a function of depth or age show a band that suggests that paleointensities could have been smoother than individual records indicate.

Chapter 4

Long-τ VRM and relative paleointensity estimates in sediments

4.1 Introduction

In paleomagnetism, the natural remanent magnetization (NRM) of rocks consists of a primary magnetization acquired during formation of the rock, which is often overprinted by secondary magnetizations. The NRM of volcanic rocks is formed by cooling below the Curie temperature of the magnetic material (thermoremanent magnetization or TRM), whereas sedimentary rocks have a more complicated process of magnetization referred to as detrital remanent magnetization (DRM) and/or post-depositional processes (pDRM). We consider the entire continuum of physical processes during deposition, compaction and burial as DRM (see *Tauxe* [1993]).

Viscous remanent magnetization (VRM) is one of the unwanted remanences, which must be eliminated from NRM in order to characterize the properties of the primary remanence. The removal of VRM and other secondary magnetizations is the main purpose of demagnetization methods in use for both directional and intensity studies. Information about the intensity of the primary remanence, and thus an indication of the paleomagnetic field strength, is the most difficult to obtain. For thorough discussions of viscous magnetization we refer to e.g. *Néel* [1949, 1955], *Dunlop* [1973, 1983], or *Dunlop and Özdemir* [1997]. The important aspects of VRM are briefly summarized here.

---

[1]Submitted by Kok and Tauxe to *Earth Planet. Sci. Lett.*

According to *Néel* [1949], any initial remanence M_0 will asymptotically approach its equilibrium magnetization M_e in an exponential fashion with a characteristic constant known as the relaxation time τ, which strongly depends on grain-size, coercivity and temperature. Any naturally occurring assemblage of magnetic particles will have a range of relaxation times. When viewed over a restricted time span, the behavior of VRM can often be reasonably approximated by some $\log t$ relation, where t is time (see e.g., *Néel* [1949], *Lowrie* [1973]). This approximation cannot hold when $t \to \infty$, for that would imply an infinite magnetization. Clearly, the longer a sample stays in a steady non-zero field, the more long-τ VRM is acquired and the closer to M_e its magnetization becomes.

The VRM intensity in paleomagnetic data is also driven by the type of magnetic material present in the rock. Differences in sediment composition inevitably cause changes in the magnetic properties and thus in the type and amount of VRM.

Since relaxation of magnetic remanence is a thermal activation process, elevated temperatures promote viscous behavior, i.e., acquisition or decay of VRM. The principle of thermal demagnetization of rocks rests on the consequence of the logarithmic reduction of the relaxation time on increased temperature. For example, a viscous remanence carried by particles with relaxation times of less than a few million years at room temperature can be erased at 200°C within a few minutes (see *Pullaiah et al.* [1975]). Néel's blocking approximation of this process states that when $t < \tau$ no viscous relaxation has occurred, whereas at $t > \tau$ the equilibrium magnetization is reached. While this is a good approximation on laboratory time scales (grains are either blocked or not), it is a rather poor approximation on geological time scales. It is important to remember that the populations of particles with relaxation times longer than the 'exposure' time t have also undergone some degree of relaxation. Furthermore, when the relaxation time is equal to the exposure time, only 63% of the maximum possible magnetization is reached.

For rocks that have experienced only the present polarity chron, a viscous remanence will be added to the direction of the primary remanence vector. Of course, if the settings of lavas or sediments change, for instance because of tectonics, the secondary component can be in a different direction from the primary vector. Sediments or lavas older than 778 kyr have experienced the two antipodal states of the geomagnetic field, and therefore also have (acquired) VRM in the direction opposite to the primary direction. If such magnetizations are not effectively demagnetized, NRM values spanning a paleomagnetic reversal are expected to be drastically offset. *Kok and Tauxe* [1996a] argued that VRM carried in part by particles with relatively long relaxation times ($\tau > t$) may have caused the asymmetrical saw-toothed pattern observed around polarity reversals in sedimentary paleointensity records [*Valet and Meynadier*, 1993]. More effective demagnetization methods indicated that the saw-toothed pattern in one of the original records

of *Valet and Meynadier* [1993] disappeared [*Kok and Tauxe*, 1996b] (see Part II of this thesis).

We emphasize that here we are mainly concerned with viscous remanent magnetization acquired by populations with long relaxation times over geological time $(\tau > t)$. We refer to this type of VRM as long-τ VRM. Short-τ VRM acquired during collection, transportation or in the laboratory is often easily eliminated, but long-τ VRM is more persistent and may therefore not always be recognized. Moreover, long-relaxation time viscosity applies to *every* grain-size population of magnetic particles, because of thermal activation and is therefore more difficult to remove.

In this study, we put forward a method which yields an estimate for what we interpret as the amount of long-τ VRM. It uses sedimentary data from two cores from the present polarity chron that have been used for paleointensity research. The long-τ VRM is compared with short-τ viscosity effects.

4.2   Paleointensity and VRM

There are two main types of stepwise demagnetization used in paleomagnetic studies: exposure to increasing temperatures or to increasing alternating fields. One standard technique in paleomagnetism involves the measurement of the NRM after a given demagnetization level ("blanket" demagnetization), at which it is assumed that VRM and other secondary magnetizations have been erased. In this way, it is hoped that a primary magnetization has been isolated. In paleointensity studies of sediments, this remanence is subsequently normalized by a bulk magnetic property to account for changes in magnetizability. The blanket normalization procedure assumes magnetic uniformity throughout the record. Changes in the bulk properties through diagenesis or environmental controlled changes can violate the assumption of uniformity, resulting in compromised relative paleointensity estimates. Only when the bulk magnetic parameters (the normalizing factors) account for the primary non-geomagnetic factors that influence the NRM intensity, the ratios (NRM/normalizer) give reliable estimates of variations in the geomagnetic field intensity (see *Tauxe* [1993] for a review on paleointensities).

4.2.1   Pseudo-Thellier and VRM

Conventional relative paleointensity estimates rely on NRM derived from bulk demagnetization at a single step. Often, several normalizers are used to assess magnetic uniformity (see e.g. *King et al.* [1983]), but mostly this is still done for a single NRM measurement. However, the blanket demagnetization step can be insufficient to remove variable amounts of VRM. The problem with using the traditional methods for relative paleointensity estimates is that it is impossible

to assess the contribution of VRM to NRM in which the DRM and VRM are sub-parallel.

For volcanic rocks, a more sophisticated normalization method existed long before sedimentary sequences were used for paleointensity determination [*Thellier and Thellier*, 1959; *Coe*, 1967]. The Thellier-Thellier method uses thermal demagnetization of NRM and compares it with partial thermal remanences acquired in a known laboratory field at the same temperature steps. By plotting NRM remaining against the laboratory TRM, it is possible to separate components dominated by VRM from those that can be considered to be primary components. During the process, one is also able to monitor possible changes in magnetic parameters caused during the laboratory treatment. Absolute paleointensities can only be obtained from this method when the specimen has a thermoremanent (TRM) origin. Deep-sea sediments can also be subjected to the Thellier-Thellier method with promising results (see e.g. *Hartl and Tauxe* [1996]). Although the DRM acquisition process is completely different from thermoremanent magnetization, the Thellier-paleointensities from sediments can at least be considered to be relative measures of the paleomagnetic field.

Recently, a pseudo-Thellier approach was developed for estimating relative paleointensities in sediments [*Tauxe et al.*, 1995]. It uses non-destructive alternating fields (AF) demagnetization and anhysteretic remanent magnetization (ARM) acquisition as opposed to thermal methods in the Thellier-Thellier experiment. They suggested that the pseudo-Thellier technique is capable of separating VRM from DRM. Differences between the two paleointensity estimates were therefore taken to be measures of long-τ viscous effects during the Brunhes. These correlated with viscous behavior on a laboratory time scale [*Tauxe et al.*, 1995].

4.2.2   VRM area model

We explore here the pseudo-Thellier method for detecting and quantifying long-τ VRM contributions parallel to the DRM. A schematic representation of an Arai plot [*Nagata et al.*, 1963] is given in Figure 4.1. NRM (vertical axis) is plotted versus an artificially acquired anhysteretic remanence (ARM) at the same AF peak field (horizontal axis). A linear relation between the two assumes that ARM reasonably mimics DRM. The slope is used as an estimate of relative paleointensity, as is done in the Thellier-Thellier procedure for absolute determinations. If the VRM adds to the DRM, this will result in a higher value for NRM, while the magnetic parameter ARM remains unchanged. The VRM component causes the curve connecting the data to become concave up. After the demagnetization level at which the VRM is eliminated (as well as part of the DRM), only the primary NRM—i.e. DRM—will be further demagnetized. Ideally, the relation between ARM and DRM is linear, however, as *Tauxe et al.* [1995] noted, it may be possible that they will never relate in this way. Please note that only VRM
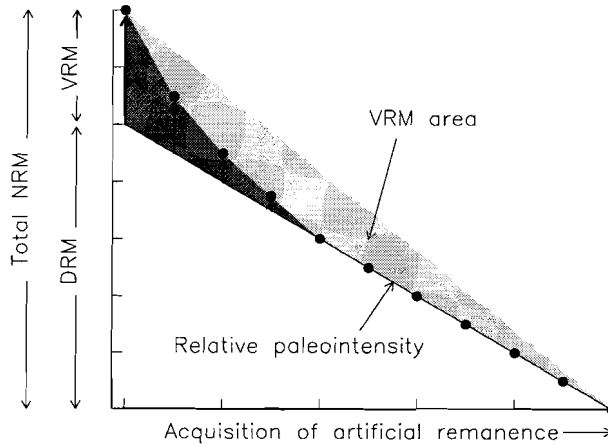
Figure 4.1: *Representation of Arai plot with best-fit slope as a relative measure of paleointensity and the "VRM area"(light gray) as a first-order indication of the amount of VRM. The total NRM comprises DRM and VRM; a separation of the two remanences could ideally be found as the y-intercept of the relative paleointensity slope (see text).*

acquired in the same direction as DRM will behave in this way; when VRM is opposite to DRM the curve in the Arai plot can be concave down. For this study only Brunhes age sediments are used, however.

The vertical axis indicates the sum of DRM and VRM. One way to quantify the relative proportion of VRM to the NRM would be to calculate the slope of the best-fit line through the data and determine the y-intercept on the NRM axis (see Figure 4.1). However, this procedure implicitly requires that the 'real' relative paleointensity has been reliably determined, preferably with a very small error. Thus, the VRM estimate depends on the paleointensity estimate. The dark gray area in Figure 4.1 is also a possible candidate for a VRM estimate. But similar to the y-intercept problems, we first have to know our true 'best-fit line'. Therefore, to calculate the dark gray area strongly depends on what is "forced" to be the paleointensity slope.

To avoid this imposition, we choose to calculate the amount of VRM in a different manner. We determine the so-called "VRM area" (indicated as the light gray area in Figure 4.1), which has the advantage that it does not require that the paleointensity slope be known. The VRM area is the complement of the area under the curve, which is calculated as a Riemann sum (i.e., the sum of the areas of the columns with as widths the difference of two successive acquisition steps, and

Core	Depth	Length	Latitude	Longitude	Age interval
ERDC 89p	1963 m	6.92 m	0°00.2'S	155°51.9'E	123–436 ka
RNDB 75p	3078 m	8.10 m	1°54'N	160°12'E	142–672 ka

Table 4.1: *Characteristics of the records used in this study*

heights the average of two successive NRM demagnetization steps). Because not all specimens have identical volumes, we choose to normalize the VRM area by the area of the right triangle that spans the entire Arai plot (i.e., $\frac{1}{2} \times$ base $\times$ height $= \frac{1}{2} \times \text{NRM}_{max} \times \text{ARM}_{max}$). Thus, the VRM area reflects the proportion of VRM in the NRM and not an absolute value. The VRM area will increase when the VRM contribution becomes more prominent, but this process is non-linear. Therefore, we concede that the VRM area cannot serve as an exact measure of the amount of VRM, nor is it applicable for very inhomogeneous cores. For example, if a record displays an occasional large, but soft, viscous overprint it will disappear early in the demagnetization process, but causes the VRM area to be rather large. Other samples that lack such soft VRMs will give a drastically different answer. Such soft VRM are not very important magnetizations for relative paleointensity studies, because they are routinely removed by storage in magnetically shielded space or low-field demagnetization treatment. What concerns us here is the more resistant long-τ VRM.

4.2.3 Material and methods

Core selection

We have resampled two cores (listed in Table 4.1) which in earlier studies passed the requirements for paleointensity determinations (e.g. *King et al.* [1983]). The first core has been taken during the Eurydice (ERDC) Expedition in 1975 from the Ontong-Java Plateau [*Tauxe and Wu*, 1990]. The remanence is carried by stable pseudo-single domain magnetite and the core is relatively uniform with respect to grain size and concentration. Its normalized record is therefore taken to reflect variations in the intensity of the geomagnetic field. From the same region, a second core was recovered during the Roundabout (RNDB) Expedition in 1988 [*Tauxe and Shackleton*, 1994]. Again, uniformity in the magnetic properties is observed, although a shift to less ideal conditions distinguishes the upper half from the lower half, but the criteria for obtaining paleomagnetic information are still met for the latter. The two cores have been dated by correlating their oxygen isotope records to a standard δ^{18}O curve [*Imbrie et al.*, 1984] (with the Matuyama–Brunhes boundary adjusted to 780 ka [*Shackleton et al.*, 1990]). In this study, the sediments have only witnessed the Brunhes polarity period, and therefore acquired
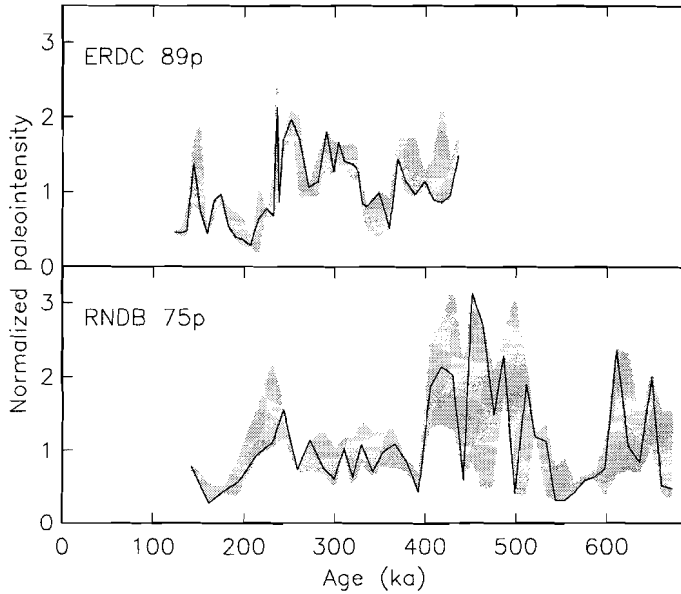
Figure 4.2: *Results of pseudo-Thellier paleointensity determinations on the cores of this study. Gray areas indicate the central 90% of the jackknife estimates for the best-fit slope.*

long-τ VRM in a similar direction as the primary component. Furthermore, all samples were stored in a shielded room prior to measurements.

Paleointensity and error estimates

The pseudo-Thellier experiments took place at Fort Hoofddijk, where the re-manence measurements were done on CTF and 2G cryogenic magnetometers. Alternating field demagnetization and ARM acquisition were performed on an SI-4 single axis instrument (with an optional 50 μT DC field) and the laboratory built AF equipment (with an optional 42 μT background field). Error estimates for the best-fit slope in the Arai-plots were obtained by a jackknife resampling scheme as described in Chapter 3. Relative paleointensity results with 90% confidence bounds for the two cores studied are shown in Figure 4.2.

IRM experiments

Two types of isothermal remanent magnetization (IRM) experiments took place at
Fort Hoofddijk. A PM-4 pulse magnetizer was used to acquire IRM at 1.0 T. For
the first experiment, the samples were bathed in liquid nitrogen ($T = -196°C$)
and immediately put in the PM-4. Directly after imparting IRM, the samples
were transferred to the 2G cryogenic magnetometer and measured while warming
for at least 15 minutes. This so-called IRM warm up experiment (see *Halgedahl
and Jarrard* [1987], *Pick and Tauxe* [1993]) can indicate variable amounts of super-
paramagnetic grains. The second experiment is rather similar to the first, but was
done at room temperature. We monitored the IRM intensity over a time span of
45 days to detect viscous decay in zero-magnetic field on a laboratory time scale.

Epoxy stirred remanence

We have undertaken redeposition experiments (see e.g. *Tucker* [1980, 1981]) on
several samples. After completion of the standard pseudo-Thellier experiment,
the sample was stirred in a thin epoxy and hardened for two weeks in the Earth's
magnetic field. The (very) short-τ VRM was suppressed through storage in the
magnetically shielded room for one day prior to the demagnetization of stirred re-
manent magnetization (StRM). The results for an NRM–StRM example are shown
in Figure 4.3. Normalized StRM and ARM as function of AF demagnetizations
(upper panel) are very similar in the low fields (0–35 mT), whereas StRM and
NRM demagnetization are more alike in interval 40–95 mT. All remanences are
normalized to the highest value. When plotted against each other (middle panel
of Figure 4.3), NRM and StRM show a rather linear relation between 20 and 60
mT, which we interpret to be the DRM part of the original NRM. The curve tails
are ascribed to VRM for low fields, and "spurious" magnetization acquired during
AF demagnetization for high fields. As already expected, the Arai plots (lower
panel) for both curves are rather different. Clearly, the StRM curve has a better
linearity than the NRM. The NRM decreases more at low fields resulting in a
significant VRM area. In addition, from the NRM curve in the Arai plot, it is
clear that determining the best-fit line for the paleointensity estimate is much less
straightforward than for the StRM curve. As a consequence, the y-intercept of the
line through NRM as a possible indicator of VRM (Figure 4.1) cannot be deter-
mined with high certainty. This experiment suggests that sediments exposed to
the Brunhes field for several hundreds of thousands of years can acquire a substan-
tial amount of VRM. Naturally, there is no long-τ VRM when they are redeposited
and exposed for a mere two weeks in the Brunhes field. Stirred remanent magne-
tization is thus an potential method both to normalize NRM data [*Tucker*, 1980;
1981] and to separate long-τ VRM contribution. It requires accurate and repro-
ducible laboratory experiments, if used as paleointensity determinations for a large
set of samples. We found StRM to be highly sensitive to laboratory conditions.
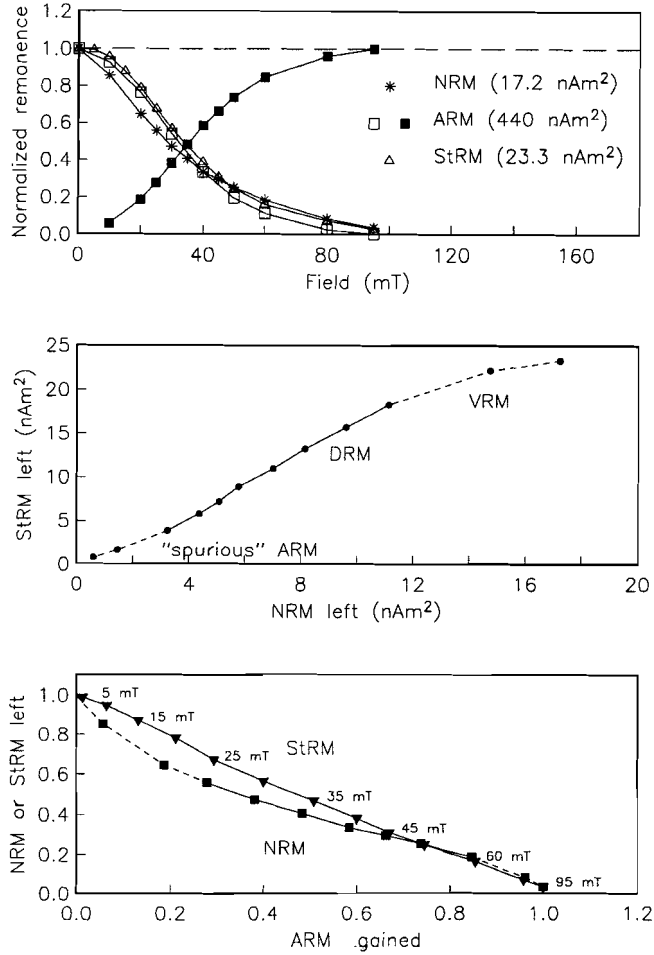
Figure 4.3: *After the pseudo-Thellier procedure of the NRM, the sediment was redeposited by stirring in epoxy in Earth field (StRM). The middle panel indicates that NRM and StRM are linear between 20 and 60 mT. Low demagnetization fields show a deviating part which we label VRM, and at high AF fields there is evidence for acquisition of spurious magnetization. The StRM versus ARM acquisition (lower panel) is much more linear than the NRM counterpart. In other words, the StRM is suggested to be less affected by long-τ VRM.*

4.3 VRM area results

From all our pseudo-Thellier measurements on the two cores we have calculated the VRM area. We begin with two examples that indicate the effects of paleoclimate on our VRM area.

4.3.1 VRM versus climate

Paleoenvironmental conditions can influence magnetic properties and hence also long-τ VRM acquisition. We illustrate this with two samples from core ERDC 89p, one deposited during an interglacial (stage 11) and one during a glacial (stage 12). Figure 4.4a and b indicate rather similar Zijderveld diagrams (because the cores are unoriented, the declinations are not meaningful). Figure 4.4c indicates that the normalized remanences have quite different decay curves, whereas the ARM acquisitions are essentially identical, including their absolute values. Normalization has been done using the maximum NRM and ARM values of the sample deposited in the glacial (cold) stage. The Arai plot (Figure 4.4d) shows the significant difference between the two samples. The 'cold' VRM area is substantially smaller than the 'warm' (interglacial) one, which is the sum of the two gray areas. Thus, these examples indicate a strong variation in the demagnetization characteristics of the NRM, and this variation is expressed in the VRM areas. Possible reasons for these variations must be sought in climate related effects. For instance, paleoproductivity has been shown to influence the remanence carrying grains. *Hartl et al.* [1995] suggested that the differences found between the magnetic properties of Eocene and Oligocene sediments of DSDP Site 522 could be ascribed to a variation in reduction diagenesis caused by increased productivity. Their study of a South Atlantic core indicates that rock magnetics can be sensitive indicators of environmental changes. The productivity estimates are also known for a piston core from the Ontong-Java Plateau, taken quite close to ERDC 89p. *Herguera* [1994] showed that the density of benthic foraminifera preserved in the sediment correlates well with the climatic $\delta^{18}O$ curve. From his reconstruction it was apparent that glacial periods favor higher productivity (i.e., accumulation of benthic foraminifera), at least for the last 250 kyr. It is possible that these variations in paleoproductivity have influenced the magnetic properties at the ocean-floor. It appears that higher productivity intervals are associated with magnetic grain sizes that are more resistant to long-τ VRM, perhaps through dissolution of the finest grains that are most susceptible to VRM. Alternatively, climatically induced factors may be variations in grain-size and provenance of detrital material.
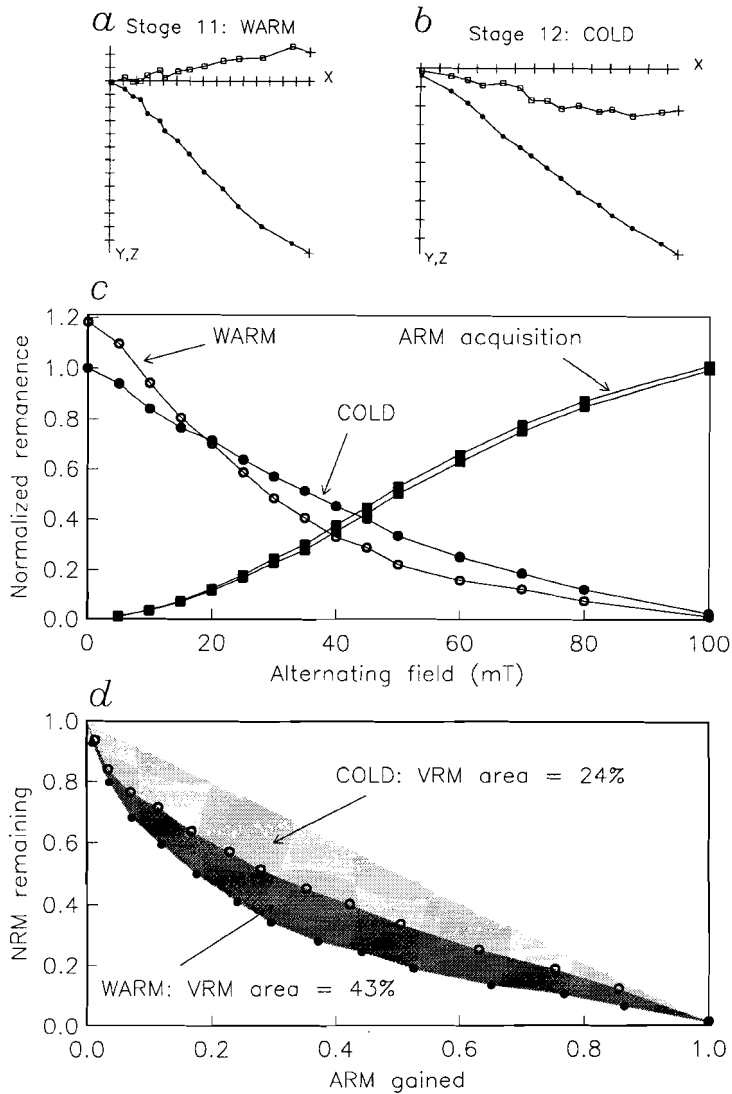
Figure 4.4: *VRM area determination of a sample deposited during an interglacial (warm) (a) and a glacial (cold) (b) stage. The Zijderveld plots indicate a more or less linear decay towards the origin. (c) NRM demagnetization curves are different, whereas ARM acquisition data are similar. (d) The Arai plot of the NRM versus ARM points out the substantial difference between the two samples; the interglacial period corresponds to a much larger VRM area.*
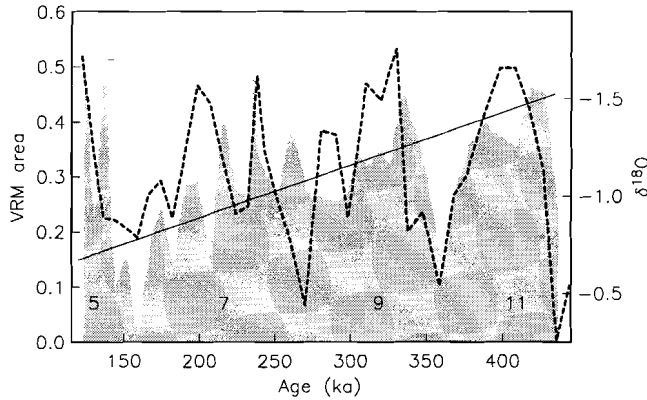
Figure 4.5: *VRM area (gray) versus age for core ERDC-89p. Links between the $\delta^{18}O$ curve (dashed) and the VRM area are suggested, but an age dependence can be suggested as well. Interglacial stages are indicated by odd numbers.*

4.3.2   Core ERDC 89p

Not only the examples shown in Figure 4.4, but data from the entire core ERDC 89p suggest possible links between VRM area and climate as represented by $\delta^{18}O$ (Figure 4.5). Possibly, a superimposed $\delta^{18}O$ pattern on an apparent age-dependent trend is observed in the VRM area.

4.3.3   Core RNDB 75p

The other Ontong-Java Plateau core (RNDB 75p) also shows a trend in the VRM area versus age between 400 and 140 ka (Figure 4.6). As already noted by *Tauxe and Shackleton* [1994], its magnetic properties change abruptly approximately half way down the core (at about 4 m, or 400 ka). The oldest part, which is less ideal for paleointensity research, shows more viscous behavior (significantly larger VRM area data) than the youngest part. Furthermore, some high-frequency components in the oxygen isotope signature correspond well to variations in the VRM area.

The difference between the upper and lower half of this core is evident from the saturation IRM versus susceptibility χ plot of *Tauxe and Shackleton* [1994] (see Figure 4.7). The data fall on two distinct tracks which they ascribed to a change in grain size. To illustrate this, *Tauxe and Shackleton* [1994] calculated a best-fit line through the "upper track". From this they estimated an IRM value from a given χ value. The differences of the expected IRM values with the observed IRM values were called ΔIRM, and are a measure of the influence of grain size. In Figure 4.8 these ΔIRM values are plotted together with the VRM area data.
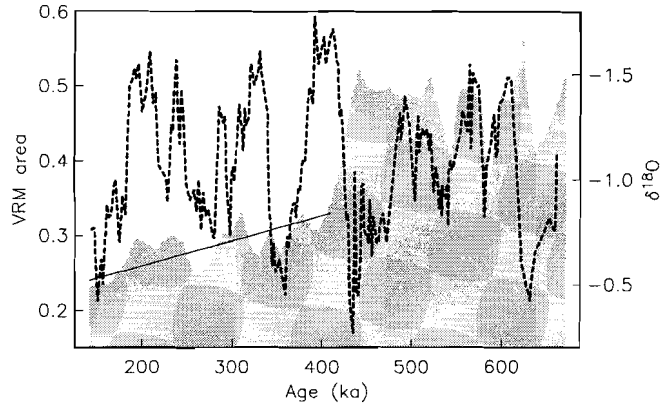
Figure 4.6: *VRM area (gray) versus age for core RNDB 75p. The youngest half shows an age-dependent trend in VRM area data. The oldest part of this record has a slightly different grain size (Tauxe and Shackleton [1994]), which is also evident from the significant difference in VRM area. Correspondence between $\delta^{18}O$ and VRM area are mainly observed in the oldest 150 kyr.*
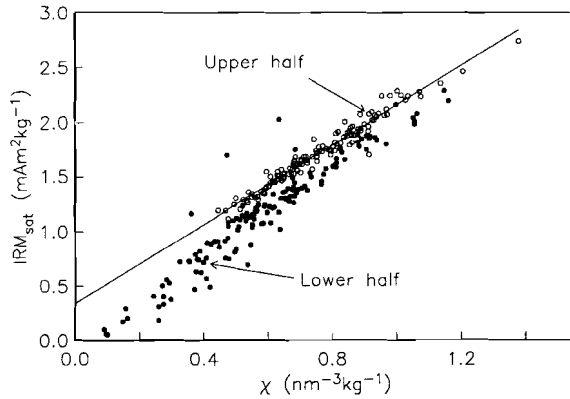
Figure 4.7: *Saturation IRM against low-field magnetic susceptibility. The data fall on two well-defined tracks for samples of either half of the core. (Redrawn from Tauxe and Shackleton [1994].)*
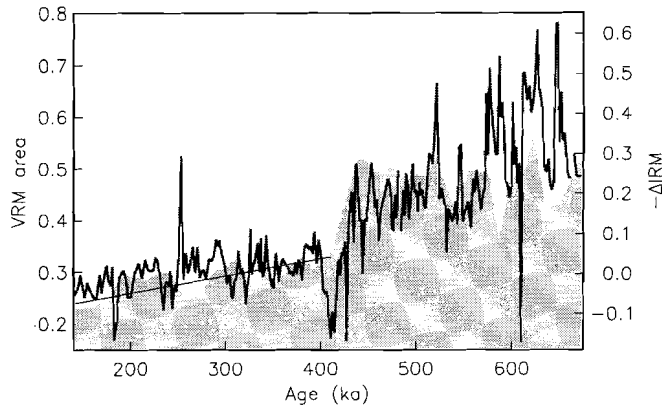
Figure 4.8: *The difference* ΔIRM *between the measured saturation IRM and the value predicted from a given* χ *(Tauxe and Shackleton [1994]) indicates the same behavior as the VRM area for core RNDB 75p.*

The correlation between ΔIRM and VRM area is remarkably good. The trend in the youngest part of the VRM area record seems to correspond to a slight trend in the ΔIRM, which could suggest that this VRM area trend is controlled in part by diagenetic phenomena, as opposed to strictly age-related growth.

The two tracks in the IRM versus χ data [*Tauxe and Shackleton*, 1994] are controlled by enhanced χ in the lower part of the core. This could be the result of either larger grains (multi-domain range), or additional superparamagnetic (SP) particles. SP behavior at room (or ocean) temperature can be detected by IRM warm up experiments (see *Halgedahl and Jarrard* [1987], *Pick and Tauxe* [1993], *Hartl et al.* [1995]). SP grains carry remanence at liquid nitrogen temperature and lose it during warm up to room temperature. An IRM imparted at $T = -196°C$ will show a greater loss of intensity if more SP grains are present. Because the first measurements did not all occur at exactly the same time since the magnetization was acquired, we choose to normalize the IRM intensity with the measured value after 180 s (this does not effect the outcome of this experiment). The results of the IRM warm up experiments are shown in Figure 4.9. It is clear that samples from the oldest part of core RNDB 75p exhibit a greater loss of IRM intensity on warming up, implying that the oldest part of the core has a higher concentration SP grains. We suggest that the enhanced SP concentration in the lower half of the core is accompanied by an enhancement of longer relaxation time grains, leading to an overall higher long-τ VRM contribution.
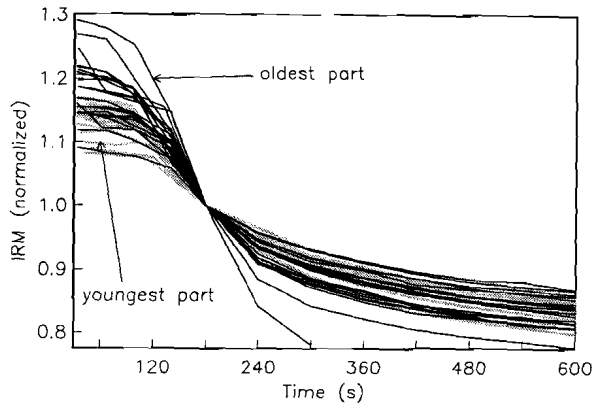
Figure 4.9: *Curves of IRM imparted at liquid nitrogen temperature versus time for core RNDB 75p. The data are normalized to IRM readings after 180 seconds. The oldest part (black) of the record indicates a greater loss of moment than the youngest part (gray), consistent with a greater portion of super-paramagnetic grains.*

4.4 Short-τ VRM

A link between long and short-τ VRM was implied in the pseudo-Thellier approach [*Tauxe et al.*, 1995]. In that study, the long-τ VRM contribution was defined as the difference between the conventional paleointensity estimate (estimated by a blanket demagnetization and normalization) and the slope in the Arai plot. The decay of a saturation IRM intensity in zero field after $3\frac{1}{2}$ hours was taken as the short-τ viscous behavior. Both viscous parameters correlated well (see Figure 2.4), which supported the assumption that the pseudo-Thellier detects VRM. The drawbacks of this approach are that the conventional paleointensity determination depends on a single NRM reading and that the 'real' relative paleointensity must be reliably determined. We now test our improved long-τ VRM estimates—that do not suffer from these objections– against the shorter-term viscous effects. All samples from core RNDB 75p were therefore subjected to an IRM decay experiment.

The first measurements (some 20 s after IRM acquisition) are used to normalize the subsequent measurements after 1, 6, 9, and 45 days. Figure 4.10 shows the behavior of IRM remaining as a function of time for all samples. IRM remaining varies from 99.5% to 91.5% of the initial IRM intensities. The elapsed time is on a logarithmic scale, therefore, the IRM decay are more or less $\log(t)$.

In Figure 4.11 we plot the same IRM-remaining data as function of age, and
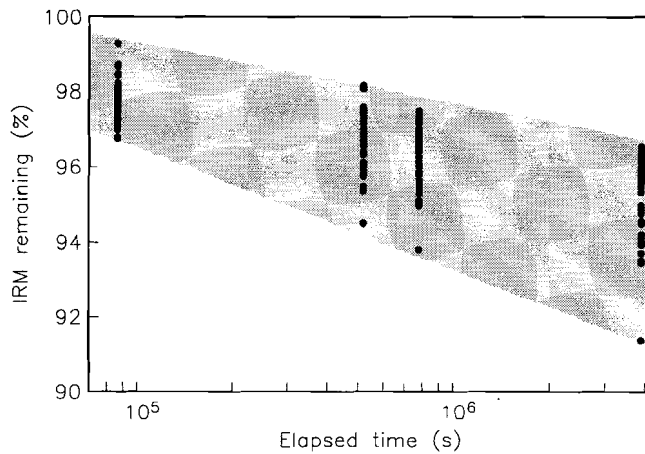
Figure 4.10: *IRM decay in zero field as a function of elapsed time (on logarithmic scale) for samples of RNDB 75p. The values are normalized by the first measurements (100%).*

compare these to the VRM area. After one day, we observe small variations in the percentages of IRM left, that could be correlated to variations in the VRM area. After 6 and 9 days, the correspondence becomes slightly better, but we also note that the oldest part had decayed more than the youngest. The last measurements occurred after 45 days; the separation between upper and lower half is more clear. It supports the contention that short-τ viscous effects of the IRM decay (in the order of weeks) are related to what we think is the long-τ VRM acquisition (in the order of hundreds of thousands of years). In conclusion, the oldest part of RNDB 75p has more VRM, both short-τ and long-τ.

4.5 Conclusions

Acquisition of VRM occurs in all rocks and is—mostly—an unwanted relaxation process of the total NRM. Short-τ VRM contributions are often suppressed by storage in a magnetically shielded space or by rather weak demagnetization levels. On the other hand, viscous remanences acquired over a long time span (several 100 thousand years) are harder to separate from primary magnetizations, also because they are often parallel (or anti-parallel) to DRM. Especially in paleointensity studies, one must be certain to have eliminated VRM as well as other secondary magnetizations before paleointensity can be extracted.
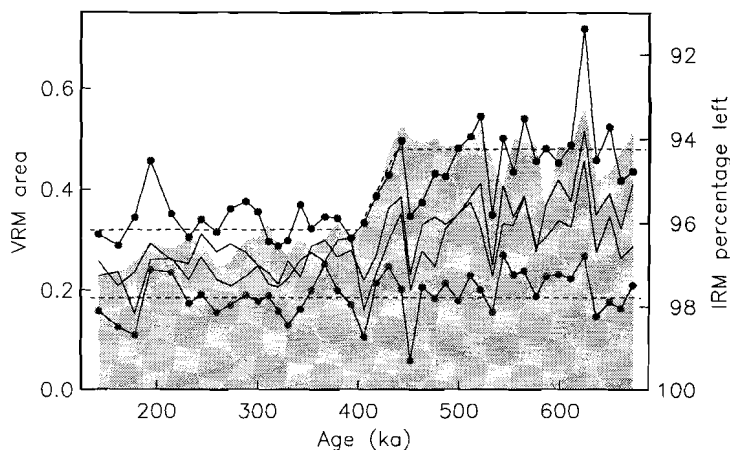
Figure 4.11: *Viscous decay of IRM as function of age, together with the VRM area values for core RNDB 75p. Gray symbols = after 1 day, black symbols = after 45 days, black lines = after 6 and 9 days. Dashed lines suggest that IRM decay after 45 days is linked with long-τ VRM. Note that the IRM percentages are plotted up-side-down.*

We have developed a possible method to characterize long-τ viscous processes of sedimentary natural magnetic remanences. It uses the pseudo-Thellier paleointensity technique described by *Tauxe et al.* [1995] that connects NRM demagnetization with ARM acquisition. When NRM is plotted against ARM, we typically observe a concave-up curve, whose curvature is quantified by the "VRM area" (Figure 4.1). We propose that this VRM area is an indication of long-τ VRM that has built up since deposition.

The VRM area data of the two cores studied here indicate three characteristics: (1) a long-τ decaying trend which is explained as the growth of VRM with time, (2) a link with climate ($\delta^{18}O$ data) where warm periods often correspond to relatively high VRM estimates, and (3) a stronger link with a lithological change—presumably diagenetic in origin—that is confirmed with viscous effects on laboratory time scales.

Part II

Saw-toothed pattern in paleointensity records explained by Cumulative Viscous Remanence

Boulder, July 1995: Jean-Pierre Valet, Lisa Tauxe, Yvo S. Kok and Laure Meynadier.

45

Chapter 5

The Model

Abstract Several studies of relative paleointensity data derived from marine sediments spanning the last four million years display an asymmetrical "saw-toothed" pattern. Polarity reversals of the geomagnetic field are associated with low points in paleofield intensity, preceded by a long-term progressive decay of the field and followed by a rapid post-transitional recovery [*Valet and Meynadier*, 1993; *Valet et al.*, 1994; *Meynadier et al.*, 1994]. Since similar behavior is observed in far-flung sites whose rock magnetic records are different, it is argued, that the world-wide "saw-toothing" represents geomagnetic field behavior [*Meynadier et al.*, 1994]. We present an alternative explanation, calling on the effect of "hard" viscous remanence.

5.1 Introduction

Sedimentary sequences provide the only means of studying the long-term temporal evolution of the geomagnetic field in more or less continuous time series. The intensity of natural remanence (NRM) in sediments is thought to be linearly related to that of the geomagnetic field at the time of deposition [*Kent*, 1973], but it is also affected by the particular magnetic characteristics of the sediment, such as grain-size, concentration, mineralogy (see e.g. *Tauxe* [1993]). A variety of normalization techniques have been tried in order to compensate for changes in the magnetic characteristics within the sedimentary sequence (see *Tauxe* [1993] for recent review). In addition to this changing "magnetic activity" of a sequence, there is also the likelihood that the NRM has been affected by secondary magnetizations such as viscous remanence (VRM). The usual methods

---

for normalization, dividing the NRM by some bulk parameter such as anhysteretic remanence (ARM), both demagnetized to some level (usually by alternating field demagnetization), are rather poor in detecting possible contributions of VRM [*Tauxe et al.*, 1995]. Viscous remanence acquired over long periods (millions of years) might be resistant to the usual demagnetization techniques and could pass unnoticed. Moreover, since VRM is time dependent, sediments from around the globe could well suffer similar VRM contamination, independent of detectable differences in mineralogy. Hence, agreement of various records on a global basis is a necessary, though not sufficient, criterion for reliability of relative paleointensity estimates. In this paper, we explore how unremoved long-term VRM might affect relative paleointensity records and show that it can result in a "saw-toothed" pattern reminiscent of recently published records of paleointensity for the last 4 million years [*Valet and Meynadier*, 1993; *Valet et al.*, 1994; *Meynadier et al.*, 1994].

5.2   VRM model

Theories of magnetic remanence suggest that when a specimen with initial magnetization of M_o is placed in zero field, the magnetization $M(t)$ will approach the equilibrium magnetization of zero by exponential decay [*Richter*, 1937; *Néel*, 1949]

$$M(t) = M_o \cdot e^{-t/\tau} \tag{5.1}$$

where t is time and τ is a decay constant known as the relaxation time, dependent on a variety of factors such as saturation magnetization, grain volume, coercivity and temperature.

If a specimen with zero initial remanence is put into a magnetic field, we expect the magnetization $M(t)$ to grow to the equilibrium magnetization M_e by the complement of equation 5.1, that is

$$M(t) = M_e \cdot (1 - e^{-t/\tau}) \tag{5.2}$$

The more general case in which the initial magnetization of a specimen is nonzero can be written as

$$M(t) = M_o + (M_e - M_o)(1 - e^{-t/\tau}) = M_e + (M_o - M_e) \cdot e^{-t/\tau} \tag{5.3}$$

which grows (or decays) exponentially from $M_o \to M_e$ as $t \to \infty$ and the rate is not only controlled by τ, as well as by the degree to which the initial magnetization is out of equilibrium. We assume, that the initial remanence is a constant fraction of the equilibrium magnetization and depends linearly on the intensity of the paleofield.

In general, the magnetization at a given time will be the sum of a viscous remanence and the original remanence. Depending on the τ chosen, such a VRM
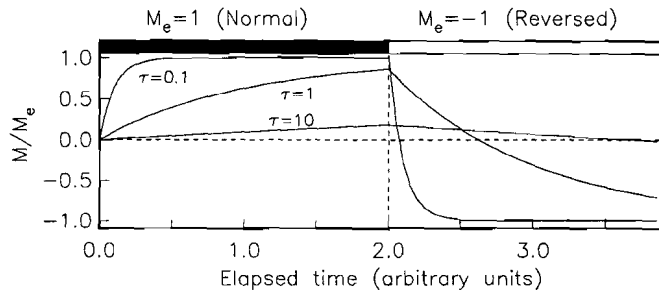
Figure 5.1: *Hypothetical specimens without initial remanence, with relaxation times of respectively 0.1, 1, and 10 arbitrary time units acquire viscous magnetization until $t = 2$. The field then switches polarity, and magnetization grows in opposite direction.*

could be a long term (millions of years) "hard" contamination and would not be reflected in observations on laboratory time-scales.

Some data sets appear to follow the relation $M(t) = S \cdot \log(t)$, but such a relation suggests infinite remanence at $t \to \infty$, so cannot be true. Such behavior can generally only be observed over a restricted time interval and closely spaced, long-term observations only rarely show a strict $\log(t)$-behavior (see e.g. *Lowrie* [1973], *Gee et al.* [1993]). In reality, τ will not be uniform over all magnetic particles in the specimen, but will belong to some distribution $f(\tau)$. Theoretical explanations for the $\log(t)$ observations rely on choosing $f(\tau)$ to be uniform for $log(\tau)$ and limiting the time span of observation (see e.g. *Dunlop* [1973]). We find that equation 5.3 satisfactorily models the viscous behavior of marine sediments typical of those used for paleointensity studies, choosing $f(\tau)$ to be normally or log-normally distributed (unpublished).

5.2.1 Specimen without initial magnetization

Considering for the moment the simplest case of a single τ, we illustrate the effect of varying the value of τ in Figure 5.1. Imaginary specimens with constant M_o $= 0$ are placed in a magnetic field for 2 arbitrary time units. The magnetization approaches M_e according to equation 5.2. Note that relaxation times much longer than the time of observation result in apparently linear behavior. At $t = 2$, the field reverses, so that the equilibrium magnetization becomes $-M_e$. The magnetization acquired at $t = 2$ serves as initial remanence for the second part of the plot to calculate the decreasing $M(t)$ (for $t > 2$, according to equation 5.3). The rate of decay of the magnetization is much faster than the acquisition,

because the magnetization at $t = 2$ is farther out of the equilibrium $(-M_e)$. The parameters that control the rate at which VRM is acquired are thus τ, M_o and the polarity (and intensity) of the magnetic field which in turn controls the sign (and magnitude) of M_e.

5.2.2 Specimen with initial magnetization

We turn now to the case in which a hypothetical specimen has an initial remanence $M_o = 1$. The remanence acquired penecontemporaneously with deposition (M_o) is not in equilibrium with the prevailing field. We believe this to be generally true, because anhysteretic and thermal remanences are more likely to be closer to equilibrium and are several orders of magnitude larger than the (post-)depositional remanence acquired in the same field. Thus, after the physical orientation of the magnetic grains has ceased, the magnetization grows viscously by switching of the magnetic moments within grains and the magnetization approaches M_e. As a zero order approximation, we assume that the equilibrium magnetization (controlled by the mineralogy and the applied field) is of constant magnitude.

In Figure 5.2a we consider the evolution of NRM through time for a specimen which was deposited in the Jaramillo (1.07 Ma) and witnessed two subsequent field reversals. The VRM grows first parallel to M_o until the first field reversal, followed by anti-parallel growth during the reversed Matuyama. During the Brunhes, the magnetization again grows parallel to the initial remanence, increasing to the present. We show curves using several values of τ assuming fixed $M_e = 10$. The NRM (=cumulative VRM plus M_o) at present for $\tau = 10$ Myr is shown as a triangle to the right.

We illustrate the effect of varying M_e while holding τ constant at 10 Myr in Figure 5.2b. In Figure 5.2c we show the evolution of cumulative remanence for a sample deposited 1.5 million years ago (i.e. deposited during a reversed field) . The VRM grows parallel to M_o until the beginning of the Jaramillo at which point it begins to decay. In the reversed field after the Jaramillo, the remanence again grows until the Matuyama/Brunhes boundary. The Brunhes is sufficiently long for the remanence to decay to below M_o and the NRM at present (elapsed time = 1.5 Myr) is shown by a triangle (for $M_e = 10$ and $\tau = 10$ Myr).

5.3 VRM in a reversing field

To calculate the remanence through a series of field reversals, we calculate the cumulative magnetization at present after $(n - 1)$ polarity reversals, as the last term (M_n) of the sequence

$$M_k = \left\{ \pm M_e + (M_{k-1} \mp M_e) \cdot e^{-\Delta t_k/\tau} \right\}_{k=1}^{n} \tag{5.4}$$
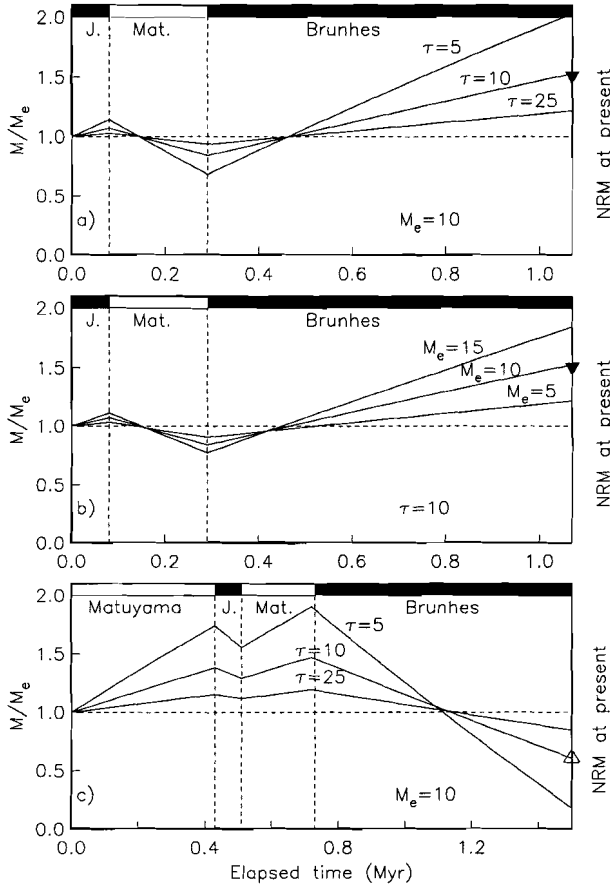
Figure 5.2: (a) Relative paleointensities calculated for three values of τ and M_e = 10. Triangle indicates cumulative remanence at present for M_e = 10 and τ = 10 Myr (M_o = 1 for all simulations). (b) Same as a) but now varying M_e with constant τ = 10 Myr. (c) Same as a) but deposited at 1.5 Ma in a reversed field.

where term M_k is the magnetization acquired during the k-th polarity interval with duration Δt_k, and M_o is the initial magnetization. The $\pm$ and $\mp$ signs indicate the switching paleofield.

Now we wish to calculate the NRM at present for a hypothetical sequence spanning the last 4 Ma (Figure 5.3a). We take $M_o = 1, M_e = 10$ and $\tau = 10$ Myr, and use the time scale of reversals of *Valet and Meynadier* [1993] (see Table 5.1).
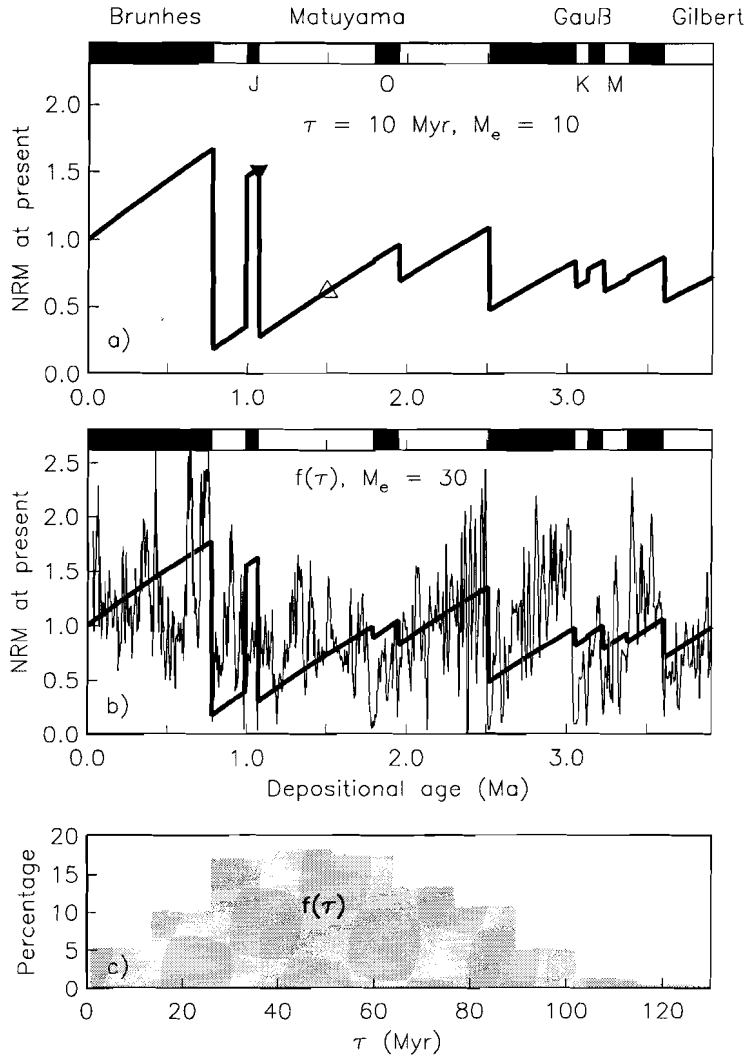
Figure 5.3: *(a) NRM at present as a function of depositional age using the ge-
omagnetic reversal time scale of Table 5.1. J = Jaramillo, O = Olduvai, K =
Kaena, and M = Mammoth. The values shown as triangles Figure 5.2 are also
included. (b) Model a normal distribution of τ with a mean of 50 Myr, and a
standard deviation of 25 Myr (N=500) (heavy line). Also shown are the original
sedimentary data normalized by their mean value. (c) Histogram of τ values used.*

EVENT	Age (Ma)
Matuyama–Brunhes	0.780
Upper Jaramillo	0.990
Lower Jaramillo	1.070
Upper Olduvai	1.790
Lower Olduvai	1.950
Gauss–Matuyama	2.510
Upper Kaena	3.050
Lower Kaena	3.125
Upper Mammoth	3.225
Lower Mammoth	3.375
Gilbert–Gauß	3.600

Table 5.1: *Estimates of ages of reversals used in this study*

The triangles indicate the points from Figure 5.2b and c (deposited 1.07 Ma and 1.5 Ma respectively). Please note that the cumulative viscous remanence described here will "demagnetize" itself by the alternating paleofield [*Denham*, 1981], and, given sufficient time, stabilize to some constant value.

5.4 Distribution of τ

As already mentioned, any real specimen will have a range of values of τ. Because of the exponential dependence of τ on grain volume and coercivity, small changes in these parameters can lead to enormous variations in τ [*Néel*, 1949]. These relaxation times will belong to some distribution $f(\tau)$, spanning perhaps from milli-seconds to billions of years. So, with N values of τ_i for the relaxation times, equations 5.3 and 5.4 become

$$M(t) = M_e + \frac{M_o - M_e}{N} \sum_{i=1}^{N} e^{-t/\tau_i} \qquad (5.5)$$

and

$$M_k = \left\{ \pm M_e + \frac{M_{k-1} \mp M_e}{N} \sum_{i=1}^{N} e^{-\Delta t_k/\tau_i} \right\}_{k=1}^{n} \qquad (5.6)$$

We have no *a priori* knowledge of $f(\tau)$. In fact, the conclusions drawn here do not depend on any particular type of distribution of τ and are valid for all those we considered (uniform, log-uniform, normal and log-normal). All that appears to be required is to have τ values in the range between about 1 and 100 Myr. Relaxation

times shorter than about 1 Myr saturate quickly, generate square waves, and are also most likely to be demagnetized by normal laboratory cleaning fields (e.g. AF demagnetization to 20 mT), while the magnetization of grains with very long τ's remain close to M_o (see Figure 5.1).

In Figure 5.3b, we show a representative curve using a normal distribution of τ (shown in Figure 5.3c). We compare our synthetic cumulative remanence model with patterns of relative paleointensity observed in sedimentary sequences from the equatorial Pacific taken during Leg 138 of the Ocean Drilling Program [*Valet and Meynadier*, 1993]. The cumulative remanence models do a fair job in duplicating global trend of the long-term "saw-toothing" of the sedimentary data (normalized by the mean), particularly for the period 2–4 Ma. The fit for the period 0 to 2 is less good, but the saw-toothed behavior is also less well expressed in the sedimentary data.

5.5   Discussion

Valet and Meynadier [1993] pointed out that in their relative paleointensity data, the "jump" associated with reversal boundaries (the magnitude of the recovery in intensity after a polarity reversal) was proportional to the duration of the subsequent polarity interval. Therefore, according to the authors, the Earth's magnetic field might have some "memory" of a powerful jump and resulting in a long interval of stable polarity. Since our models, with M_o and M_e constant, show similar jumps, we argue that jumps in the measured data could be the result of the cumulative VRM acquired and lost over the subsequent parallel and anti-parallel polarity intervals.

The geomagnetic field intensity has not been of constant intensity over the last 4 million years, nor can the distribution τ_i be assumed constant throughout such a period. On the other hand, since we are dealing with deep sea sediments, the particles are essentially of similar origin and volume, so a rather constant and narrow distribution around an unknown mean τ is expected. The success of our model lies in the fact that

1. the *average* field intensity has been approximately constant [*Prévot and Perrin*, 1992],

2. a constant distribution of τ probably sufficiently well characterizes the entire record (magnetic uniformity is a necessary criterion for acceptable sedimentary material in relative paleointensity studies [*Tauxe*, 1993] and the Leg 138 sediments were screened for this),

3. the contribution of grains with short τ's has been erased by demagnetization to $\sim$20 mT (as was done by *Valet and Meynadier* [1993]), and very long τ's hardly contribute to a magnetization acquired in a few million years.

Naturally, if we allow M_o and M_e to vary freely through time, we could model the trend of the observed data exactly. What impresses us, however, is the degree to which a rather simple model can explain the major features of the data.

5.6 Conclusion

In conclusion, we have a presented a plausible mechanism by which saw-toothed patterns in relative paleointensity records result from unremoved contributions from viscous remanence. The model calls on acquisition of cumulative viscous remanence and explains saw-toothing at reversal boundaries. Whereas we have not proved that saw-toothing is in fact caused by "hard" long-term VRM as opposed to being of geomagnetic origin, we have certainly provided grounds for suspicion.

Chapter 6

The Data

Abstract The relative paleointensity of the earth's magnetic field from ODP Site 851 has been characterized by progressive decay towards polarity reversals, followed by sharp recovery of pre-reversal values [*Valet and Meynadier*, 1993]. We resampled the Gilbert-Gauß reversal boundary of this deep-sea core, and show that during demagnetization this "saw-toothed" pattern disappears. Further, the recently published Cumulative Viscous Remanence model [*Kok and Tauxe*, 1996a] using the herewith obtained paleointensity record and constraints from thermal treatment replicates the saw-tooth of *Valet and Meynadier* [1993], implying that it is of non-geomagnetic origin.

6.1   Introduction

Detrital remanence (DRM) of sediments is thought to be linearly related to the ambient field during deposition [*Kent*, 1973], hence accurate analyses of their magnetic characteristics could provide us with the long-term behavior of the geomagnetic field. To compensate for both contaminations as well as 'magnetizability' of the sedimentary rocks, several normalization techniques are available, using either division of the remanence after a certain demagnetization step by some bulk parameter [*Tauxe*, 1993], or the comparison of an interval of demagnetization treatments with the acquisition of remanence in the laboratory (see e.g. *Tauxe et al.* [1995]). Several sedimentary paleointensity records of the earth's magnetic field show a distinct saw-toothed pattern [*Valet and Meynadier*, 1993; *Valet et al.*, 1994; *Verosub et al.*, 1996], in which a progressive decay of the field

---

[1]Apart from slight modifications, this chapter has been published by Y.S. Kok and L. Tauxe as "Saw-toothed pattern of sedimentary paleointensity records explained by cumulative viscous remanence " in *Earth Planet. Sci. Lett.*, 144, E9–E14, 1996 (reprinted with permission from Elsevier Science).

leading to reversals is followed by rapid post-reversal recovery. Supposing this observation to be a common characteristic of geomagnetic field behavior, severe implications on processes within the interior of our planet are imposed. Doubt was raised when a ^{10}Be/^{9}Be record across the youngest reversal indicated no offset in pre- and post-transitional geomagnetic field strengths [*Raisbeck et al.*, 1994]. Recently, we published an alternative explanation for the saw-toothed pattern, which explained the effect by a long-term Cumulative Viscous Remanence model (CVR) [*Kok and Tauxe*, 1996a]. The saw-tooth has also been explained by a comparable model with delayed acquisition of the natural remanence (NRM) [*Mazaud*, 1996]. The purpose of our study is to re-analyze some of the deep-sea sediments used in the pioneer study by *Valet and Meynadier* [1993]. Increased thermal and alternating field demagnetizations show that the saw-tooth disappears. Further, we show that the experimentally derived parameters for CVR are appropriate to explain the artificial nature of the saw-tooth.

6.2   Samples and methods

Valet and Meynadier [1993] constructed a last four million years paleointensity record by alternating field demagnetization to 15 or 20 mT of deep-sea sediments retrieved in the Eastern Equatorial Pacific during ODP Leg 138 [*Valet and Meynadier*, 1993]. In this study we will focus on the Gilbert-Gauß transition (3.6 Ma), which showed a substantial post-reversal recovery in *Valet and Meynadier* [1993]. Discrete samples in small glass tubes were taken from Holes 851B and E drilled at 2°46' N, 110°34' W, and 3760 m water depth. The typical sampling strategy was ~1 cm^3 every ~3 cm. The depth-age model for Site 851 is the one of *Shackleton et al.* [1995]. We thermally demagnetized specimens of Hole 851E in the magnetically shielded room of Scripps Institution of Oceanography. The wet specimens were placed in elevated temperatures for 45 minutes from set point, followed by *in situ* cooling to room temperature enhanced by forced air. Partial thermal remanence (p-TRM) was induced by applying an axial field of 40.0 μT. This Thellier-Thellier type method has shown to be successful for relative paleointensity estimates of ODP Leg 130 sediments [*Hartl and Tauxe*, 1996].

Additional alternating field demagnetization of sediments from Hole 851B took place at Fort Hoofddijk. The acquisition of anhysteretic remanence (ARM) was imparted in a vertical field of 42 μT.

Total magnetic susceptibilities χ were measured on a Jelinek susceptibility bridge type KLY-2.02 before demagnetization. Thermomagnetic runs on the modified Curie balance [*Mullender et al.*, 1993] at Fort Hoofddijk indicated that alterations occur above 400°C, probably caused by magnetite formed through breakdown of sulfides (Figure 6.1).
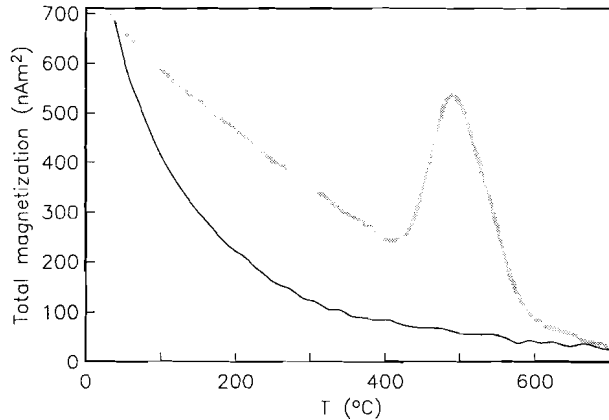
Figure 6.1: *Thermomagnetic curve that indicates creation of magnetic material above circa 400°C, which could be an influence on NRM behavior at elevated temperatures.*

6.3   Demagnetization results

Figure 6.2 displays NRM directions and intensities of Hole 851E after demagnetization to various temperature steps normalized by total susceptibility. Before demagnetization, the Gauß part of this normalized intensity record shows remarkably higher values than the Gilbert, producing the characteristic offset of the saw-tooth. The effect of increased temperature results in a dramatically greater decay in the post-transitional Gauß than in the pre-transitional Gilbert. In the 250–400°C interval, the post-reversal jump towards higher values has disappeared entirely. Temperature treatments higher than 400°C should be viewed with caution, because of the possibility of alteration suggested by the thermomagnetic data. The normalizer χ_{total} (not weight corrected) is shown for completeness.

Alternating field demagnetizations were performed on samples of the parallel section Hole 851B. Figure 6.3 shows the decay of the NRM intensities normalized by the anhysteretic remanence acquired at 100 mT alternating field (ARM_{max}). Like the thermal results, the intensity decay of the youngest part of the record is clearly larger. However, a minor offset after some 70 mT is still present and demagnetizations to higher AF fields give rise to unstable intensities and directions. Since the offset disappears completely on thermal cleaning, we assume the alternating field demagnetizations to be of lower fidelity, also there the mechanism of AF demagnetization is never fully understood. Moreover, it will not provide constraints for our thermal activation model.
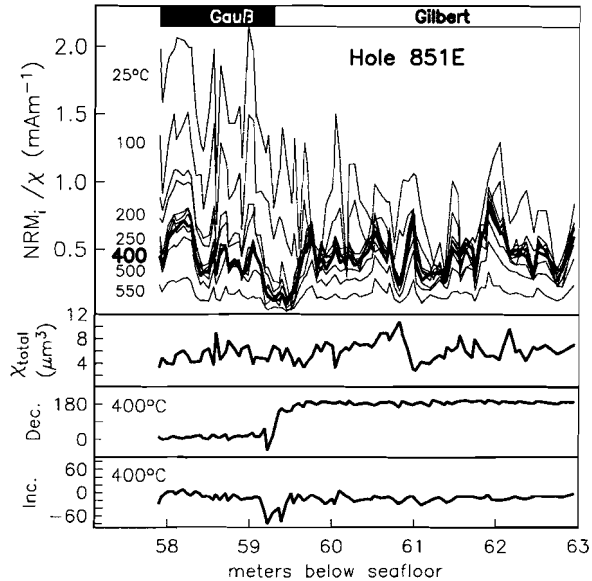
Figure 6.2: *NRM intensities of ODP 138-851E-7H after thermal demagnetization treatments (every 50° C starting at 100° C) normalized by χ. Low temperatures have not removed overprints and show post-transitional recovery above 59.3 meters below sea-floor (mbsf). From 250° C and up an "even-shouldered" pattern around the transition is evident. The normalizer χ_{total} before thermal procedure and characteristic directions after demagnetization to 400° C are shown in lower panels.*

6.4   Alternative explanations for the saw-tooth

A model calling on long-term cumulative viscous effects of the magnetic remanence gives an alternative explanation for the saw-toothed patterns in paleointensity records [*Kok and Tauxe*, 1996a]. We argued that the initial detrital magnetization after deposition M_o is not in equilibrium with the external earth magnetic field, inducing a relaxation process towards an unknown equilibrium remanence M_e. The rate of the growth is not only controlled by the relaxation time τ, but also by the degree to which the initial magnetization is out of equilibrium. Since its deposition the sample has witnessed varying paleofields with either parallel or anti-parallel polarities, which could have significant consequences for the evolution of the total remanence. We calculate the cumulative magnetization at present after
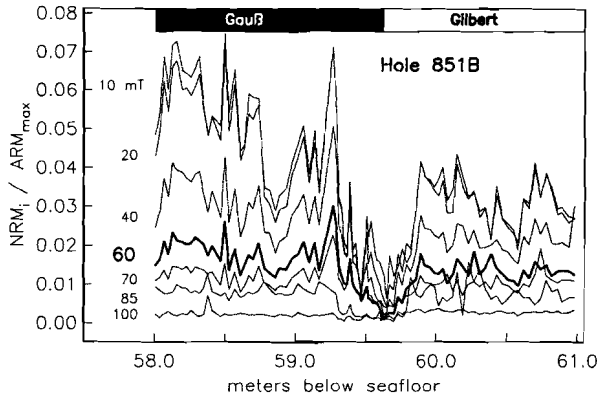
Figure 6.3: *Several NRM intensities of ODP 138-851B-7H after alternating field demagnetization treatments normalized by the ARM acquired at 100 mT. Low AF fields still indicate the offset of the saw-toothed pattern, whereas increased AF fields show a larger decay in the the youngest part (above 59.6 mbsf). However, a reliable symmetric pattern around the transition is not established.*

$(n\text{-}1)$ polarity reversals, as the last term (M_n) of the sequence

$$M_k = \left\{ (-1)^{k+1} M_e + \frac{M_{k-1} + (-1)^k M_e}{N} \sum_{i=1}^{N} e^{-\Delta t_k / \tau_i} \right\}_{k=1}^{n} \qquad (6.1)$$

where term M_k is the magnetization acquired during the kth polarity interval with duration Δt_k, and N the number of values τ_i. The Cumulative Viscous Remanence model (CVR) used $M_o = 1$ (arbitrary unit), typical values between 5 to 100 Myr for $f(\tau)$ and 5 to 30 for the constant M_e [*Kok and Tauxe*, 1996a].

Another alternative explanation for the saw-tooth in paleointensity records is given by *Mazaud* [1996]. Again, a softer magnetic component is acquired after deposition. A large fraction (X) of the magnetic grains acquires NRM at deposition time, while remaining grains reorientate or acquire magnetization after deposition. The difference between the two alternatives is that in the latter model the secondary magnetization is locked in physically, whereas in the former it always relaxes to the varying equilibrium magnetizations. It is difficult to obtain experimental constraints for the parameters X and lock-in time. On the other hand, we are able to constrain M_e and the distribution of relaxation times $f(\tau)$ existing in the specimen using thermal experiments.

6.4.1   Equilibrium magnetization M_e

We suspect an induced thermal remanence (TRM) will be in equilibrium with the applied field, and would be an estimate for M_e. Because of the alteration of the samples above 400°C we cannot simply impart a total TRM to determine the value of M_e. For this reason, we subjected each specimen to a Thellier-Thellier type experiment [*Thellier and Thellier*, 1959; *Hartl and Tauxe*, 1996]. Zijderveld diagrams of thermal demagnetization of a Gauß and a Gilbert specimen are shown in the insets of Figure 6.4a and b respectively. After circa 250°C a soft component has been removed and more or less stable vectors are encountered (see also Figure 6.2). The Arai plots [*Nagata et al.*, 1963] of NRM remaining versus p-TRM acquired show distinct segments:

- a soft interval up to 250°C

- a more stable segment from 250–400°C

- the higher temperature steps that were expected have suffered from magnetic alterations, although intensities of both NRM and TRM do not appear to be wildly deviant even up to 500°C

The slopes of the middle segment vary from -0.02 to -0.10; in other words, the p-TRM acquisition is 10 to 50 times more efficient than the DRM. This range is the effect of the paleofield variations (± 60%) around a certain mean. If the average ancient field would have been equal to the laboratory field (40.0 μT), M_e would be constrained to be the mean of this range of approximately 30 (i.e. ∼30 times more efficient than $M_o = 1$). Naturally, we do not know the ancient field strength. However, *Constable and Tauxe* [1996] provide a possible means for a quantitative calibration. They suggest that if the axial dipole term is assumed zero at the midpoint of the transition and the average non-axial dipole field is assumed to have the present-day average value of 7.5 μT everywhere, then the relative intensity records can be transformed into quasi-absolute values. In this way, the non-transitional average paleofield intensity for our Gilbert-Gauß data is 32 μT. Noteworthy, the IGRF value at Site 851 is also 32 μT. Presuming linearity, an estimate for the equilibrium magnetization is $M_e = \frac{32}{40} \times {\sim}30 = {\sim}24$.

6.4.2   Relaxation times τ_i

In Figure 6.4c and d the intensity decay data of the samples shown in Figure 6.4a and b are plotted as a heavy line. Also shown is the sum of the norms of the vector differences which takes care of anti-parallel directions (thin line). The unblocking spectrum of this monotonic decay is plotted as a function of temperature on the lower horizontal axis. In our thermal demagnetization experiment, the specimen must have been exposed to temperature T_{lab} for at least some 5 minutes ($t_{ub} =$
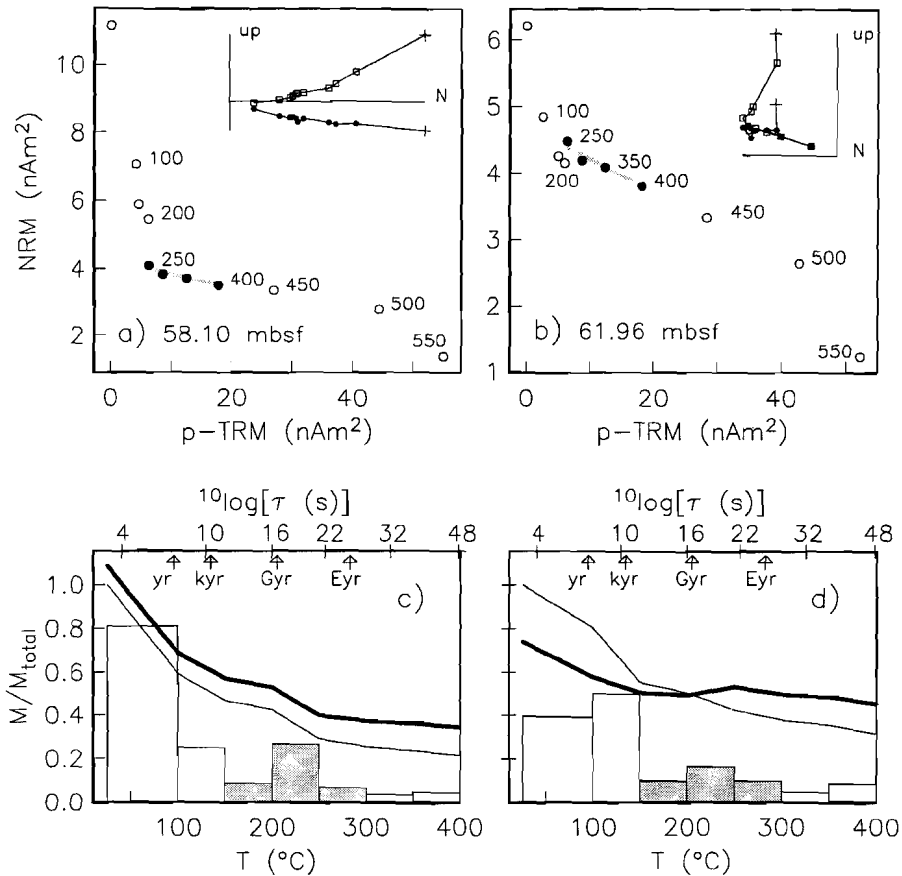
Figure 6.4: *Typical results for thermal demagnetization and acquisition from Hole 851E for a Gauß sample (left), and a Gilbert sample (right). (a)(b) Arai plots indicate segmented line (see text). Insets represent Zijderveld diagrams of stepwise thermal demagnetizations. (c)(d) The decay curves as function of temperature for the intensity (heavy line) and for the sum of the norms of the vector differences intensity (thin) tied to 550° C. The unblocking spectra of the latter are indicated by bins. Conversion from unblocking temperature to relaxation times τ at the ocean floor $(T = 2°C)$ results in upper logarithmic scale (see text). Shaded areas indicate the unblocking of particles argued to give rise to long-term viscous effects.*

300 s). If the magnetization has unblocked to 5% of its initial value (i.e., $e^{-t_{ub}/\tau_{lab}}$ = .05), then the unblocking time t_{ub} will be 3 times the 'effective' relaxation time in the laboratory τ_{lab}. Therefore, we estimate this relaxation time in our thermal experiments to be 100 seconds. Following *Pullaiah et al.* [1975], we assume that the coercivity of the magnetic grains is shape dominated, hence $H_c(T)$ is proportional to $J_s(T)$. By rearranging their equation (2) we have

$$ln(C\tau_{ocean}) = \frac{T_{lab}}{T_{ocean}} \frac{ln(C\tau_{lab})}{J_s^2(T_{lab})} \tag{6.2}$$

where C is the characteristic frequency of thermal fluctuation ($\sim 10^{10}$ Hz), T_{ocean} the temperature at the ocean floor (2°C = 275 K), and $J_s(T)$ the spontaneous magnetization as function of temperature of Ward's standard magnetite (data courtesy J. Gee), assuming $J_s(T_{ocean}) = 1$ (arbitrary unit). By using equation 6.2 the laboratory induced unblocking temperatures are converted to relaxation times under ocean floor conditions on the logarithmic upper scale in Figure 6.4c and d. For example, at $T_{lab} = 200°C$, equation 6.2 reduces to $\tau_{ocean} = C^{1.17} \times \tau_{lab}^{2.17}$. Using $\tau_{lab} = 100$ s, one obtains a τ_{ocean} of circa 350 Myr ($\sim 10^{16}$ s). Small variations in the adopted τ_{lab} have no drastic influences on the calculation, keeping in mind that the exposure time at the ocean floor is two orders of magnitude shorter (10^{14} s ≈ 3.5 Myr) than τ_{ocean}.

The large peaks in the unblocking spectra at low temperatures indicate the unblocking of those particles that contribute only to the short-term viscous effects (10^8 s ≈ 3 years). We suppose that the long-term viscous effects are caused by grains that are unblocked in the secondary peak [150–300°C] (shaded intervals), implying that the mean of the relaxation time distribution τ_i will be between 10^{16} s ($\sim 200°C$) and 10^{22} s ($\sim 250°C$).

It appears that the logarithm of the distribution of relaxation times is consistent with a Gauß-Laplace distribution with a mean of circa 16.5 and standard deviation of 5.5, i.e., $f(\tau) = 10^{16.5 \pm 5.5}$ s. At $T_{lab} = 400°C$, grains with astronomical τ_{ocean}'s of 10^{48} s are unblocked; these will not contribute to the CVR in a few million years and presumably carry the "stable" magnetic information. To exclude as many viscously behaving components as possible from the usual paleointensity calculation (slope of the stable 250–400°C interval in the Arai plot), we use only the 400°C step for the paleointensity estimates.
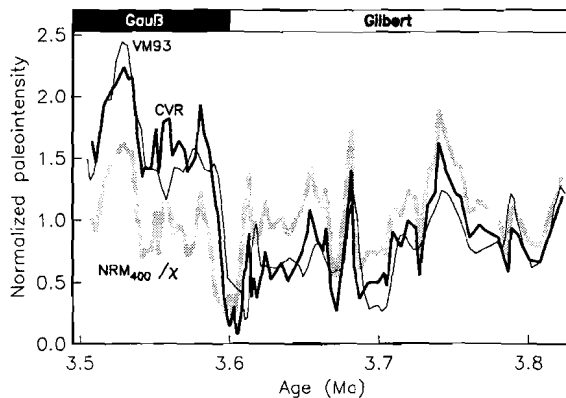
Figure 6.5: *Paleointensity records normalized by their means as function of depositional age. Gray line represents the NRM_{400}/χ paleointensities fed to the Cumulative Viscous Remanence model with parameters $M_e = 24$ and $\tau_i = 10^{16.5 \pm 5.5}$ s (N = 1000), resulting in CVR curve. Also shown are typical "saw-toothed" data (20 mT alternating field demagnetization) from the same Site normalized by their mean value by Valet and Meynadier (VM93). CVR displays strong similarities with VM93, advocating the artificial origin of saw-toothed patterns in paleointensity records.*

6.5   Remodeling the saw-tooth

For simplicity, we assumed a constant initial remanence $M_o = 1$ in our first modeling attempts [Kok and Tauxe, 1996a]. If one interprets the NRM_{400}/χ record to represent the real paleointensity fluctuations, it can be used as input for the described CVR model (normalized by the mean of the record). Together with its experimentally constrained parameters $f(\tau)$ and M_e, it results in the NRM at present as plotted in Figure 6.5. The gray curve represents the alleged paleointensity (NRM_{400}/χ), the heavy line is the calculated NRM at present (CVR) which agrees remarkably well with the thin Valet & Meynadier curve (VM93). Dating discrepancies between CVR and VM93 stem from the ambiguous conversion and interpolations from meters below sea floor (Hole 851E) via meters composite depth (Site 851) to depositional age [Shackleton et al., 1995]. Small amplitude differences can be explained by the fact that we characterized our 5 meter record by a constant set of parameters. We note that the corresponding finer-scale features appear in all records, wholly contradicting the rationalization that VRM would erase or obscure these properties [Verosub et al., 1996].

6.6   Conclusion

The occasionally detected saw-toothed pattern in sedimentary relative paleointensity records [*Valet and Meynadier*, 1993; *Valet et al.*, 1994; *Verosub et al.*, 1996] can be explained by unremoved remanence acquired since deposition. Thermal demagnetization of the reexamined Gilbert-Gauß reversal causes the large post-transitional recovery of the paleofield intensity to disappear entirely. Using our NRM_{400}/χ paleointensity estimates as well as model parameters derived from Thellier-Thellier type experiments, the Cumulative Viscous Remanence model [*Kok and Tauxe*, 1996a] calculates an NRM at present that is virtually identical with previous results of *Valet and Meynadier* [1993]. Thus, the likelihood that the contamination is of long-term viscous origin is considerable.

Chapter 7

The Comment

7.1 Introduction

Valet and Meynadier [1993] presented a sedimentary record of relative paleoin-
tensities spanning the last 4 million years. In this record, there was an apparent
long-term decrease of magnetic field strength prior to polarity reversals, followed
by a vigorous recovery of the field after the reversal. This behavior resulted in a
"saw-toothed" pattern in intensity variations. If the saw-tooth is a genuine feature
of the geomagnetic field, it suggests a different mechanism of generation of geody-
namo than is currently considered likely (see e.g. *McFadden and Merrill* [1998]).

7.2 Cumulative Viscous Remanence Model

Because of the importance of the saw-tooth behavior to our understanding of the
geodynamo, *Kok and Tauxe* [1996a] pointed out a possible source of contamina-
tion that could also result in saw-toothed behavior similar to that observed by
Valet and Meynadier [1993] : Cumulative Viscous Remanence (CVR). The prin-
ciples of the CVR model are quite simple. A sedimentary rock with a given initial
magnetization M_o experiences subsequent normal and reversed fields. Its magne-
tization is not an equilibrium magnetization M_e in the ambient field because of
two factors. First, DRM is a relatively inefficient process, it differs by a factor
of at least an order of magnitude from thermally blocked remanences acquired in
the same field, which are more likely to be equilibrium magnetizations. Second,
the geomagnetic field changes sign frequently, so the equilibrium magnetization is

---

[1]This chapter is a response to the paper by L. Meynadier, J.-P. Valet, Y. Guyodo and
C. Richter entitled "Saw-toothed variations of relative paleointensity and cumulative viscous
remanence: Testing the records and the model" in *J. Geoph. Res.*, 103, 7095–7105, 1998. It has
been submitted to this journal by Y.S. Kok and L. Tauxe.

from time to time antipodal to the direction of M_o. Thus, there is a tendency for sedimentary rocks to acquire viscous remanence when their magnetic moments "relax" into the prevailing field direction.

Viscous relaxation is a thermally driven phenomenon and is governed by exponential growth or decay. Furthermore, the rate at which the viscous remanence is acquired depends on the distribution of relaxation times $f(\tau)$ in the specimen [*Néel*, 1949; 1955]. Following our derivation [*Kok and Tauxe*, 1996a], the evolution of the magnetic remanence is a function of time t, relaxation times τ_i, and magnetizations M_e and M_o. After the kth polarity interval of duration Δt_k the magnetization M_k is

$$M_k = (-1)^{k+1} M_e + \frac{M_{k-1} + (-1)^k M_e}{N} \sum_{i=1}^{N} e^{-\Delta t_k / \tau_i} \qquad (7.1)$$

where τ_i is the relaxation time for the ith fraction in a sample with N relaxation time fractions. The cumulative effect of equation 7.1 gives the remanence at present, which includes information from the time that the sediment was deposited onwards. The main conclusion of *Kok and Tauxe* [1996a] was that CVR produces paleointensity offsets around reversal boundaries, mostly depressed values prior to and enhanced values after the polarity switch.

The choice of M_e/M_o and $f(\tau)$ is not unique; a given pattern can be modeled by many different fitted parameters. *Kok and Tauxe* [1996a] investigated a few examples that yielded slopes similar to those displayed by the VM93 data. In the second paper, *Kok and Tauxe* [1996b] sought to constrain the parameters M_e/M_o and $f(\tau)$ for the sediments in question, i.e. those from Site 851 drilled during Leg 138 of the Ocean Drilling Program and investigated earlier by *Valet and Meynadier* [1993]. We sampled a five-meter interval spanning the Gilbert–Gauß polarity reversal with a sample spacing of some 3 to 4 cm (i.e. approximately the spatial resolution of the continuous measurements on U-channels). We performed extensive thermal demagnetization experiments and used the blocking temperature spectrum to calculate the equivalent relaxation time spectrum. The blocking temperature spectra between 150 and 300°C were associated with the long-term viscous effects, and were parameterized as a distribution of relaxation times $f(\tau)$. The M_e/M_o ratio was estimated using thermal remanences acquired during a *Thellier and Thellier* [1959] type experiment. This latter approach was imitated by *Meynadier et al.* [1998]. Using the empirically determined parameters derived from the rock-magnetic properties of the Site 851 sediments, equation 7.1, and the thermally "cleaned" paleointensity record, *Kok and Tauxe* [1996b] calculated the theoretical total remanence observed at present (see Figure 6.5). Figure 6.5 suggests that (1) the VM93 saw-tooth can be demagnetized with thermal techniques and (2) the parameters M_e/M_o and $f(\tau)$ derived from thermal experiments model the original VM93 curve is remarkably well.

7.3 Discussion

We appreciate the efforts of *Meynadier et al.* [1998] to test our model theoretically and experimentally. Within in the compass of this commentary we will not focus on the different experimental methods used by the two groups, but we point out where we have major problems with the theoretical refutation of our alternative model.

7.3.1 Relaxation times present in sediment and model

If the single-domain theory of Néel applies [*Néel*, 1949; 1955], relaxation time τ can be converted to expected blocking temperatures and vice versa. This was in fact done by *Kok and Tauxe* [1996b] who converted laboratory blocking temperatures, the temperature at which a given population of grains has relaxation times of the order of 10^2 seconds, into expected relaxation times at ocean floor temperatures (2°C). Most of the alleged long-term VRM contributions were demagnetized in the interval 150–300°C, which is equivalent to circa $f(\tau){=}10^{16.5\pm5.5}$ s. This is a sub-distribution of all relaxation times present in Leg 138 sediments that contains values of τ from years to many trillions of years, as shown by *Kok and Tauxe* [1996b].

> *Meynadier et al.* [1998] follow a comparable approach, although with an incorrect T_{ocean} of 20°C and an unrealistic 1-second experiment, and convert one of the hypothetical models used in *Kok and Tauxe* [1996a], i.e. 50±25 Myr, into equivalent blocking temperatures with a maximum of circa 250°C. This hypothetical distribution is compared with equivalent blocking temperatures up to 580°C obtained from Site 851 sediments: they find the model wanting. This is the crux of the matter, since *Kok and Tauxe* [1996a], *Kok and Tauxe* [1996b] specifically mention the non-uniqueness of the solution and the presence of much longer τ's. The label in their Figure 3b of "Model Kok and Tauxe" is therefore highly misleading. Surprisingly, the much broader distribution of relaxation times from *Kok and Tauxe* [1996b] is completely ignored by *Meynadier et al.* [1998]. We note that even this $f(\tau)$ will not convert to a 'proper' thermoremanent acquisition curve since it is merely the subset of the τ distribution most likely to contribute to VRM. It will, of course, convert to the maximum blocking temperatures of 300°C. Also mentioned [*Kok and Tauxe*, 1996b] (and apparently missed by *Meynadier et al.* [1998]) is the statement that at $T_{lab}{=}400$°C and higher, grains with astronomical τ_{ocean}'s of 10^{48} s are unblocked which will not contribute to CVR in a few million years and presumably carry the "stable" magnetic information. The thermoremanent acquisition data of *Kok and Tauxe* [1996b] (Figure 6.4a and b) clearly suggest a blocking temperature spectrum similar to the one labeled "Sediment ODP Hole 851E". It is noteworthy that *Meynadier et al.* [1998] do not attempt to estimate what CVR would result from their own blocking temperature spectrum.

We would like to point out that the fact that one is able to explain the saw-tooth with a subset of all relaxation times does not justify its equivalent thermal blocking spectrum to be compared with actual blocking temperature curve.

7.3.2   Mathematical approximation

Of minor importance, but still significant, is a problem with the rather redundant mathematical section in *Meynadier et al.* [1998] (see also Appendix). By restricting the relaxation times to greater than 8 million years, *Meynadier et al.* [1998] approximate the cumulative viscous remanence equation. As noted in the above, *Kok and Tauxe* [1996a] and KT96b used distributions of τ that included values much shorter than 8 Myr. The very short relaxation times, up to 1 Myr, saturate quickly, are easily demagnetized, and do not contribute significantly to the saw-toothed pattern. The portion 1–8 Myr, however, cannot be discarded from the calculations, therefore their approximation is not appropriate.

7.3.3   Stability of the saw-toothed signal

Finally, *Meynadier et al.* [1998] imitate our efforts [*Kok and Tauxe*, 1996b] by performing Thellier experiments on Site 851 sediments across several reversal boundaries. They claim that their results substantiate the saw-tooth signal. However, close examination of their Figure 7 shows that the post-reversal thermal results are in fact lower than the alternating field results and the pre-reversal thermal results are higher, reminiscent of the experience of KT96b.

7.4   Conclusion

The contention of *Meynadier et al.* [1998] that "...cumulative long-term viscous effects do not account for the saw-tooth patterns observed so far in paleointensity records covering the last 4 Ma" relies on a myopic reading of our work. They convert one single hypothetical distribution of relaxation times discussed by KT96a to equivalent blocking temperatures. Obviously, it does not represent all relaxation times present in the sediment, merely a part that behaves viscously if the tooth of time has worked on it for just a few million years. This is explained in both our papers and reinforced here.

We conclude that our colleagues [*Meynadier et al.*, 1998] missed the major point of the Cumulative Viscous Remanence model which was that it can explain the saw-toothed patterns observed by *Valet and Meynadier* [1993]. Any distribution of relaxation times that contains a subset spanning from one to several dozens of Myr can viscously relax to a saw-toothed pattern as observed in VM93.

7.5 Appendix: Slope approximation

Although we think the mathematics section is redundant, we give here an outline of an approximation of the slopes that are calculated by CVR. The sequence in equation 5.4 [*Kok and Tauxe*, 1996a] can be written as

$$M_k = \left\{ M_{k-1} + ((-1)^{k+1} M_e - M_{k-1})(1 - e^{-\Delta t_k/\tau}) \right\}_{k=1}^n \qquad (7.2)$$

where term M_k is the magnetization acquired during the kth polarity interval with duration Δt_k, and the magnetization at present is the last term M_n. If $\Delta t_k \ll \tau$, then $(1 - e^{-\Delta t_k/\tau}) \approx \frac{\Delta t_k}{\tau}$, and (7.2) is approximated by

$$M_k \approx \left\{ M_{k-1} + ((-1)^{k+1} M_e - M_{k-1}) \frac{\Delta t_k}{\tau} \right\}_{k=1}^n \qquad (7.3)$$

Instead of writing M as a function of time (or age) [*Meynadier et al.*, 1998], we simply use the terms of equation (7.3) to approximate the slope in the saw-tooth by taking the difference of two points.

Let us consider a sample born infinitely close before present, this means $\Delta t_1 \to 0$ and thus $M_{1,0} = M_o + (M_e - M_o) \frac{\Delta t_1}{\tau} \approx M_o$, or, the magnetization is identical to the initial remanence M_o. When we compare it with an older ($\Delta t_1 \neq 0$) brother with magnetization $M_1 = M_o + (M_e - M_o) \frac{\Delta t_1}{\tau}$, the slope connecting these specimen of becomes

$$S_1 = \frac{M_1 - M_{1,0}}{\Delta t_1} \approx \frac{M_e - M_o}{\tau} \qquad (7.4)$$

Of course, we crudely assume that the polarity has remained constant throughout the Brunhes.

Going further back in time, a sample born just before the Matuyama–Brunhes reversal (again $\Delta t_1 \to 0$) has experienced two polarity intervals. The first magnetization term M_1 from the Matuyama equals $M_o + (M_e - M_o) \frac{\Delta t_1}{\tau} \approx M_o$, and the second term—for the Brunhes Chron with length Δt_2—includes term M_1, that is,

$$M_{2,0} \approx \overbrace{M_o}^{M_1} + (-M_e - \underbrace{M_o}_{M_1}) \frac{\Delta t_2}{\tau} \qquad (7.5)$$

An older sample from the Matuyama polarity interval renders

$$M_2 \approx \overbrace{M_o + (M_e - M_o) \frac{\Delta t_1}{\tau}}^{M_1} + $$
$$+ (-M_e - \underbrace{(M_o + (M_e - M_o)) \frac{\Delta t_1}{\tau}}_{M_1}) \frac{\Delta t_2}{\tau} \qquad (7.6)$$

and the slope between these two becomes

$$S_2 = \frac{M_2 - M_{2,0}}{\Delta t_1} \approx \frac{M_e - M_o}{\tau}(1 - \frac{\Delta t_2}{\tau}) \qquad (7.7)$$

This shows again a constant slope that is slightly shallower than S_1 from equation (7.4). The generalized case after n polarity intervals is

$$S_n \approx \frac{M_e - M_o}{\tau} \prod_{k=2}^{n}(1 - \frac{\Delta t_k}{\tau}) \approx \frac{M_e - M_o}{\tau}(1 - \frac{t^*}{\tau}) \qquad (7.8)$$

with $t^* = \sum_{k=2}^{n} \Delta t_k$, that is, the *age* of the first experienced reversal.

Every segment of a saw-toothed record has a different number of experienced polarity intervals n, thus according to equation (7.8) a slightly different slope S_n. After many polarity intervals S_n becomes very shallow, eventually a flat-liner. Still, if $t^* \ll \tau$, then equation (7.8) is similar to (7.4), or, the slope after any number of polarity intervals is approximated by $\frac{M_e - M_o}{\tau}$. Intuitively, this estimate for S_n can be directly deduced from (7.3), therefore most of the equations could be skipped in both this manuscript as well as in *Meynadier et al.* [1998].

In order to arrive at a slope of circa 1 per million year—as the saw-toothing paleointensity records suggest, the value M_e (in arbitrary units) needs to be comparable to τ in millions years (choosing $M_o = 1$ a.u.).

In our opinion the reader will feel more at ease with this derivation, rather than with the one in *Meynadier et al.* [1998] with confusing $\pm\epsilon, A$ and absolute values of both M_e and M_o.

Part III

Stacks
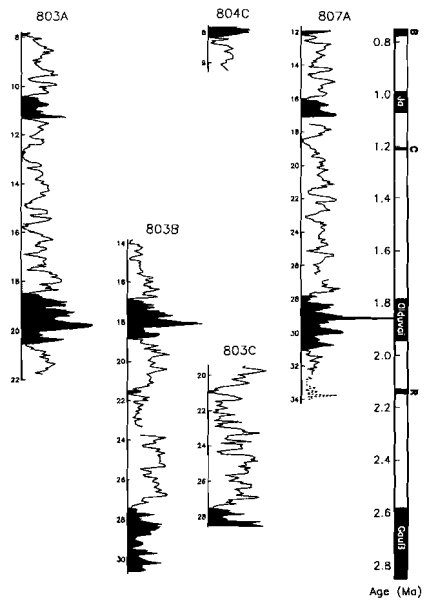
Chapter 8

Climatic influence in NRM and ^{10}Be derived geomagnetic paleointensity data

Abstract One can determine geomagnetic paleointensities from natural rema-
nent magnetizations (NRM) and by inverting cosmogenic ^{10}Be production rates.
Recently, two independently derived 200-kyr paleointensity stacks [*Guyodo and
Valet*, 1996; *Frank et al.*, 1997] were compared and the good agreement could val-
idate the use of sedimentary cores for paleointensity studies. Both compilations
use mainly a climatically controlled oxygen isotope profile to date and synchronize
the sedimentary records, while this very curve has several coherent features with
the supposedly pure geomagnetic records. A conventionally determined relative
paleointensity record, included in the conventional paleointensity stack [*Guyodo
and Valet*, 1996], shows correspondence with climatic features, which is explained
by an inadequacy in the normalization technique. Therefore, it is possible that
the extraction of pure paleointensity from sediments has not always been accom-
plished.

8.1   Introduction

The records of variations of the paleomagnetic field of the Earth registered in rocks
provide information on geophysical processes, for instance those related to the
long-term history of its core. In general, lavas record most reliably information on
the prevailing magnetic field by recording magnetic vectors during cooling. These

---

[1]Submitted by Y.S. Kok to *Earth Planet. Sci. Lett.*

spot-readings of absolute paleointensity have a more continuous equivalence in relative paleointensity records reconstructed from sediments, which have proved to be able to register both directions and intensities of the ancient geomagnetic field (see review [*Tauxe*, 1993]). However, the mechanism of sedimentary remanence acquisition is still not fully understood, thus the inversion from sedimentary magnetizations to geomagnetic information remains ambiguous. A recent compilation of several globally distributed sedimentary records provides a coherent Synthetic intensity curve for the last 200 kyr (Sint-200) [*Guyodo and Valet*, 1996]. However, worldwide agreement of variations in various sedimentary paleointensity records is a necessity, though not a sufficient proof that the evolution of the strength of the geomagnetic dipole field has been recorded.

Many problems with sediments as recorders of geomagnetic field strength have been suggested, e.g. by *Kent* [1982]. He reminds us that Pleistocene NRM intensity records correlate well with lithological parameters driven by the same climatic forcing as $\delta^{18}O$ (oxygen isotopes) or carbonate content. It is likely that the intensity of NRM co-varies with climate, but also with the geomagnetic field. Normalization of such NRM intensities by magnetic susceptibilities χ or laboratory induced magnetizations gives relative paleointensity estimates. In principle, these normalized records should not correlate with climatic features, unless the geomagnetic field genuinely co-varies with climate. When a normalized remanence record still correlates with for instance carbonate content, either some geomagnetic–climatic dependency or—more likely—an inadequacy in the normalization must exist.

The alternative to the explanation that sediments have registered additional climatic behavior instead of pure relative paleointensity, is an actual link between the Earth's magnetic intensity and its orbital parameters. Twenty years ago, *Wollin et al.* [1978] suggested a relationship between climate, intensity of the geomagnetic field and the eccentricity of the Earth's orbit. Somewhat later, *Chave and Denham* [1979] and *Kent* [1982] maintained that no connection is evident and that the previous results are due to a failure—or an omission—to remove the effect of varying magnetic material input, which is largely climatically controlled.

More recent studies cast additional doubt on the fidelity of sedimentary paleointensities. *Schwartz et al.* [1996] suggest that about 25% of the low-frequency variation in their normalized paleointensity record can be biased by climatic or other environmental factors. The authors caution that extreme care must be taken to remove such influences from sedimentary paleointensity records, and they are concerned that other records are similarly affected. *Worm* [1997] suggests a link between reversals, events, paleointensities and glaciations. The apparent correlations of normalized NRM intensity and $\delta^{18}O$ records are thought to stem from normalizing problems.

Not only time-domain records are tested, but also the frequency analyses give interesting results regarding paleointensity data. *Kent and Opdyke* [1977]

found spectral power around 43 kyr in a western Pacific sedimentary paleointensity record. They suggested that perhaps the Earth's obliquity could influence the geodynamo. Dominant periods between 30 and 40 kyr for relative paleointensity variations are also found in records from the Ontong-Java Plateau, and are argued not to be an artifact of lithologic variability [*Tauxe and Wu*, 1990; *Tauxe and Shackleton*, 1994]. Some correspondence with periods describing the Earth's orbit appears, but the stacked records are too short for a meaningful discussion on geomagnetic–climatic dependency.

An independent estimate for geomagnetic field intensity variations is deduced from the recently published stack of beryllium-10 (^{10}Be) deposition rates for the last 200 kyr [*Frank et al.*, 1997]. The normalized ^{10}Be stack is interpreted as a record of cosmogenic radionuclide production rates which are translated into relative geomagnetic field intensity changes (following *Lal* [1988]). These paleointensity variations correspond well with those from the conventionally determined paleointensity stack Sint-200 [*Guyodo and Valet*, 1996]. However, several studies hint that the ^{10}Be deposition rates can be controlled by climatic factors, such as advection of different water masses on glacial–interglacial time scales [*Von Blanckenburg et al.*, 1996], enhanced scavenging due to increased productivity [*Kumar et al.*, 1993], or increased glacial terrigenous particle flux [*Frank*, 1996]. Therefore, one may fear that the translation from ^{10}Be production rates to 100% variations of geomagnetic field intensity—as done by *Frank et al.* [1997]—is not always valid.

In this paper it will be shown that both recently published 200-kyr stacks, which mainly use the δ^{18}O chronology [*Imbrie et al.*, 1984] to construct the age models, have coherent features with the oxygen isotope record itself. Different material and/or techniques are needed to obtain more reliable paleointensities from the sediments if persistent climatic contaminations are added to the geomagnetic signal. New data from an individual core included in Sint-200 suggest that more sophisticated normalization techniques can reduce the coherence with environmental factors.

8.2 Stacks for the last 200 kyr

Shown in Figure 8.1 are the stacked profiles of sedimentary records for oxygen isotopes [*Imbrie et al.*, 1984] (δ^{18}O), conventional sedimentary paleointensities [*Guyodo and Valet*, 1996] (Sint-200), and the expected geomagnetic field intensities derived from beryllium isotopes [*Frank et al.*, 1997] (for brevity I refer to this Synthetic geomagnetic intensity stack as Sint-Be). The δ^{18}O record has a very smooth ("over-stacked") character and conforms to the convention depicting 'warm climate' (small global ice volume) up and 'cold climate' (large global ice volume) down.

Frank et al. [1997] point out the impressive agreement between Sint-Be (Figure 8.1a) and Sint-200 (Figure 8.1b). However, upon close inspection, it is noticeable
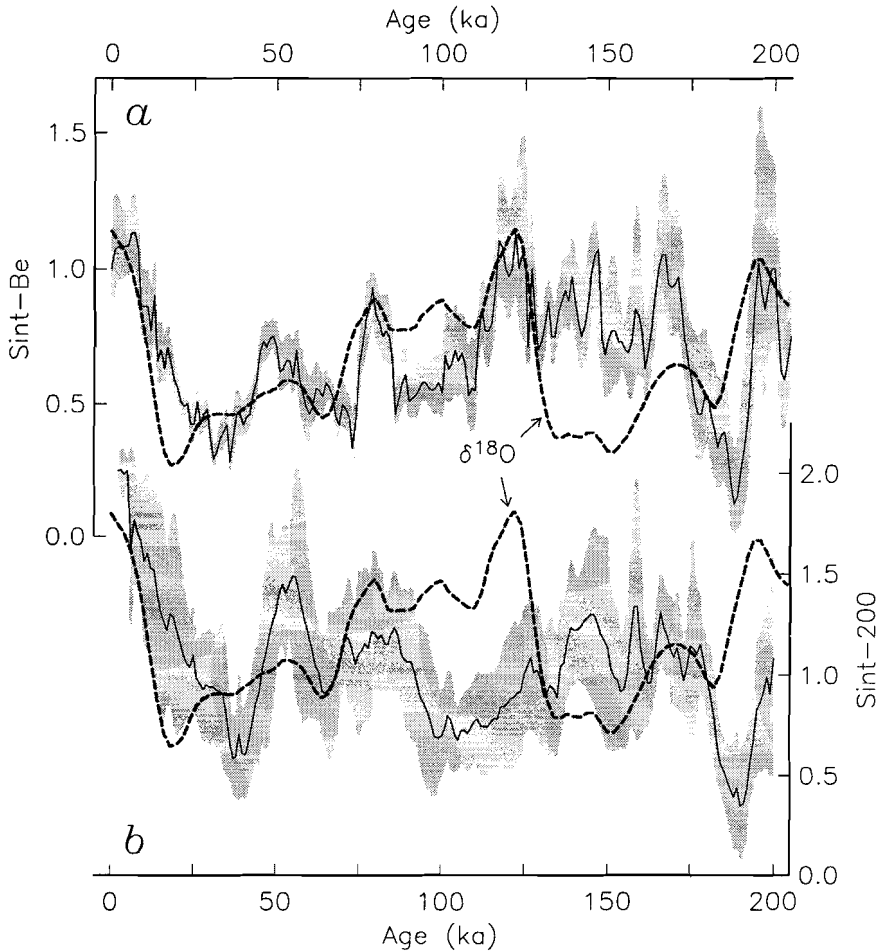
Figure 8.1: *Independent paleointensity records for the last 200 kyr with error estimates (gray) and the $\delta^{18}O$ curve (dashed) indicating global climate. (a) Stack of ^{10}Be production rates inverted to geomagnetic field strength [Frank et al., 1997]. (b) Stack of relative paleointensities determined the conventional way [Guyodo and Valet, 1996]. Fluctuations in both (a) and (b) are compared to the oxygen isotope signature.*

that a slight shift of Sint-200 to younger ages would improve the fit. More impor-
tantly, the $\delta^{18}O$ curve contains many features that are present in both relative

paleointensity records. In particular, the strong correspondence of $\delta^{18}O$ with Sint-Be seems to contradict the assumption of *Frank et al.* [1997] that climatic influences are averaged out in the ^{10}Be compilation, even though the agreement is not evident in the 160–130 ka interval (Figure 8.1a). One must keep in mind that other factors have influenced the beryllium stack as well, and it is assumed that for the *entire* 200-kyr period no link between paleomagnetic field strength and $\delta^{18}O$ exists. Comparing the ^{10}Be-based record to Sint-200, an inconsistency in the 125–115 ka interval is mentioned [*Frank et al.*, 1997] which seems now to correspond extremely well to oxygen isotope stage 5.5 ($\sim$120 ka). *Frank et al.* [1997] argue that, by coincidence, it can be an interval with uniformly reduced local ^{10}Be rain rates. It is also possible that this Eemian interval is hampered by sediment cores with relatively high $^{230}Th_{ex}$ concentrations that are used to normalize the ^{10}Be data [*Mangini et al.*, 1990].

8.2.1 Cross-spectral analysis

To investigate the correspondence between two time series, one can calculate correlation coefficients. However, their significances strongly depend on the amount of data. The data also need to be Gauß-Laplace distributed, which is not always the case and is rarely checked for paleointensity data. A more quantitative means of determining the degree of resemblance of two data sets is cross-analysis of spectral power. This technique, first described for paleointensity data by *Tauxe and Wu* [1990], and more recently by *Constable et al.* [1998] (whose code is used in this manuscript), can reveal potentially important relationships. When the squared coherence γ^2 lies above the zero-coherence level, two time series are similar for the specific frequency at a certain confidence level. *Constable et al.* [1998] recommend that the phase spectrum of squared coherence γ^2 should be used as an additional diagnostic.

Frequency analyses of the Earth's climate exhibits the Milanković periods of circa 100 kyr for eccentricity, 41 kyr for obliquity, and 23 and 19 kyr for precession (see e.g. *Imbrie et al.* [1984]). It is therefore interesting to test the power spectrum of the paleointensity stacks for coherence with these orbital components. The stacked $\delta^{18}O$ curve shows spectral power at the Milanković frequencies (Figure 8.2a). It is important to note that both paleointensity data sets have power spectrum density (PSD) concentrations at and near the orbital frequencies as well. Figure 8.2b shows the squared coherence as function of frequency for the three curves. When γ^2 is higher than the zero-coherence criterion (circa 0.21), frequencies are considered significantly coherent at a 95% confidence level. Although the coherences between the conventional Sint-200 paleointensity stack [*Guyodo and Valet*, 1996] and the beryllium based Sint-Be stack [*Frank et al.*, 1997] (Sint-200 & Sint-Be) are clearly the most prominent, significant coherences at or near some of the Milanković frequencies are present for the other combinations as well. The
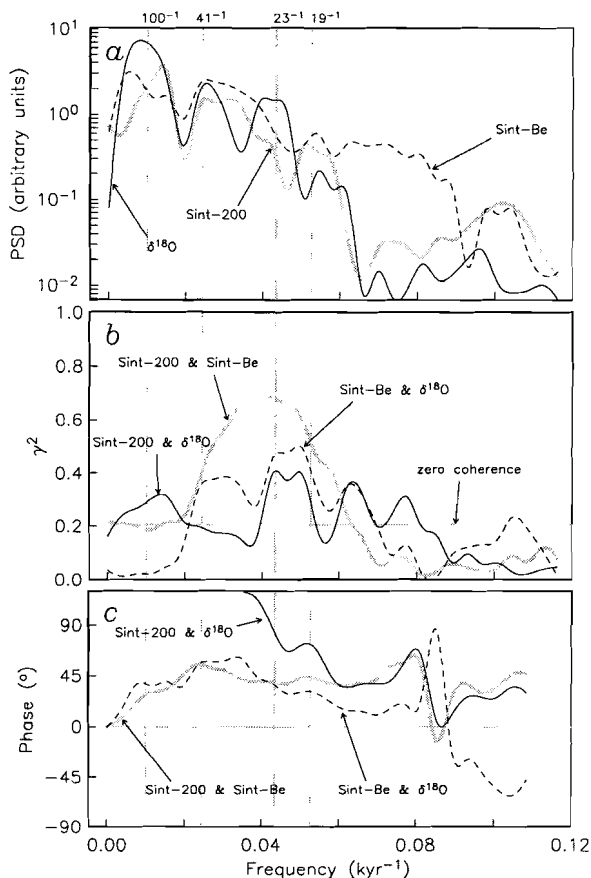
Figure 8.2: *Spectral analysis results for the three stacks of previous figure. (a) All records contain power spectrum density (PSD) at Milankovic frequencies. (b) Squared coherences γ^2 above zero-coherence are significant (95% confidence level) at several frequencies. The resemblance of Sint-200 and Sint-Be is most prominent, though other combinations show cross-spectral coherence as well. Note that the $\delta^{18}O$ stack contains relatively little power at the frequencies where γ^2 peaks in Sint-200 & Sint-Be. (c) Phase of squared coherences of (b) (Code courtesy B. Parker)*

phase diagram for the coherence of all combinations is indicated in Figure 8.2c. It suggests that all records are not in phase with each other, but that small and consistent delays are present. A phase shift of 45° (i.e., $\frac{1}{8}$ of a cycle) in the precessional band corresponds to a delay of circa 2.5 kyr. The shift at the obliquity

frequency is approximately 7 kyr. The 100-kyr component lacks in Sint-Be & δ^{18}O (and Sint-200 & Sint-Be), but this eccentricity component could be ignored because the records are only twice its cycle length. Also the phase diagram indicates non-uniform behavior in the left part of the spectrum (i.e., in the interval 0.00–0.02 kyr^{-1}). Furthermore, the 41-kyr component is missing in Sint-200 & δ^{18}O, but present in ^{10}Be & δ^{18}O, whereas Figure 8.2a suggests that the paleointensity curves have rather similar power spectral density. Although the Nyquist frequency of the paleointensity records with 1-kyr data spacing would be 0.5 kyr^{-1}, *Guyodo and Valet* [1996] warn that paleointensity variations shorter than 5 kyr cannot be extracted from their record, since the sample frequency of the original records in Sint-200 much lower than 1 per kyr. Therefore, frequencies higher than 0.08 kyr^{-1} are not meaningful; note also that the phase data become unstable.

The above mentioned problems illustrate the limitations of squared coherence analysis on these rather short stacked records. Still, the benefits of of working in the frequency domain, rather than a correlation coefficient of the time series, are clear. Just for the record, the correlation coefficient for the two Sint records is 0.492, for Sint-Be & δ^{18}O 0.298, and for Sint-200 & δ^{18}O 0.079. One should consider that the 5% and 1% significance levels for 198 degrees of freedom are respectively 0.138 and 0.181, implying that Sint-Be and δ^{18}O are significantly correlated.

8.3 Individual record

Compilations that include a number of globally distributed records from different environments will not perfectly represent the behavior of magnetic paleointensity or δ^{18}O. In the previous section, exact one-to-one matches between the records of magnetics and climate may be obscured. Consequently, one turns to a high-resolution record that has detailed oxygen isotope and paleomagnetic data. The piston core SU-92-18 from the Açores area with sedimentation rate circa 3.6 cm/kyr [*Lehman et al.*, 1996] is selected from the Sint-200 stack because it is one of the few records that span the entire interval of 200 kyr. It appears that the NRM (demagnetized to 25 mT) agrees well with the δ^{18}O of this core (Figure 8.3a), and it is therefore corrected by an estimate of 'magnetizability': anhysteretic remanent magnetization (ARM). Note that the upper axes of the magnetizations are shifted 5 kyr ($\approx$18 cm) to younger ages with respect to the lower ones of oxygen isotopes to improve the fit. The correspondence between the ratio NRM/ARM (Figure 8.3b) and the oxygen isotopes for this individual core is more evident than the one between the stacks Sint-200 and δ^{18}O (Figure 8.1b). In this Atlantic record, characteristic signatures in paleointensity often correlate with variations in the oxygen isotope curve, in spite of the normalization to obtain a cleaner record. Examples are the paleointensity high at ~125 ka (isotopic stage 5.5), the low at ~180 ka (isotopic stage 6.6), and, despite the offset in amplitude,

the pattern from circa 115 to 80 ka can be matched to isotopic stages 5.4–5.2. When compared to the Sint-200 curve (dotted), the NRM/ARM paleointensity estimate has similarities, but interesting discrepancies are present as well (Figure 8.3b). A usual characteristic for stacks like Sint-200 is that high-amplitude and high-frequency features are filtered. Core SU-92-18 has a 'rather high' coefficient
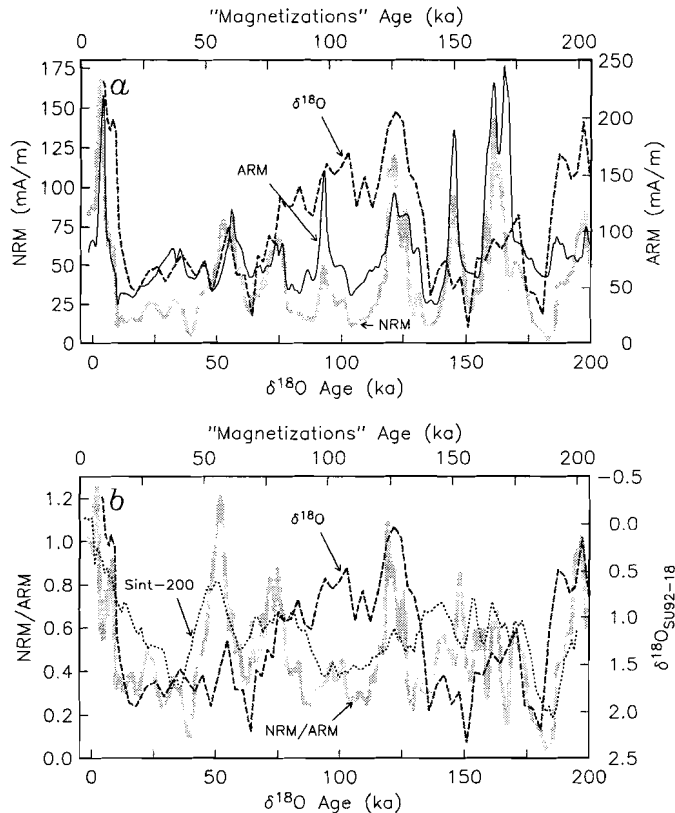
Figure 8.3: (a) Natural remanent magnetization NRM of core SU-92-18 [Lehman et al., 1996] (gray) depicts strong correlations with the oxygen isotopes (dashed), the normalizer ARM (black) is concordant. Both remanences have been demagnetized at 25 mT. (b) The NRM/ARM ratio (gray) contains several features that correlate with the $\delta^{18}O$ curve (dashed); in other words, this relative paleointensity estimate does not seem to be sufficiently free of climatic influences. Please note the 5-kyr shift of the magnetizations to 'younger ages' (upper axes). Sint-200 (dotted) shows good correlation with NRM/ARM, but often lacks the specific signatures of the $\delta^{18}O$ curve of this core.

of correlation with Sint-200 (0.64, calculated by *Guyodo and Valet* [1996]), but such a coefficient only has strict statistical meaning if both records are normally distributed.

8.3.1 Thellier-Thellier paleointensity estimates

Because there is reason to suspect that the NRM/ARM ratio is not a perfect determination of the paleointensity, the core has been resampled and discrete samples were subjected to more sophisticated paleointensity methods. Thermal methods have been performed on part of the resampled collection. This took place in the shielded room of Scripps Institution of Oceanography, in an identical manner as earlier encouraging studies on deep-sea sediments [*Hartl and Tauxe*, 1996; *Kok and Tauxe*, 1996b]. Although thermal paleointensity techniques on sediments are increasingly used, the mechanism of detrital remanent magnetization (DRM) is fundamentally different from thermoremanent origin. Therefore, absolute paleointensity estimates will be difficult to obtain from sediments, whereas volcanics do give rise to absolute values. An example of sedimentary Thellier-Thellier experiment is shown in Figure 8.4 for a sample with age 77 ka. The NRM demagnetization shows a gradual decrease of the magnetic vector. The pTRM acquisition shows a very typical change after 275°C, which might be explained by magnetic alteration caused by repetitive heating. Thermomagnetic runs on these sediments suggest that after temperatures as high as 325–350°C the magnetic phases slightly change. In any case, the Arai plot (lower panel), which ties NRM to corresponding pTRM, can only be used up to 275°C. For this example, the best-fit slope through at least 3 data points is −0.056, which is found between 175–250°C.

The crucial information about the uncertainty in the best-fit line is obtained by the method described in Chapter 3. On all samples, jackknife resampling of the NRM–TRM pairs in the interval 150–275°C was performed to obtain additional estimates for the best-fit slope. The central 90% of the distribution of 21 extra paleointensity estimates comprises the original slope and slightly steeper slopes up to −0.073 (see Figure 8.4d). This error indication is not symmetrically distributed around the best-fit slope, contrary to the standard deviation. Also measurement errors that result in deviating data in the Arai plot can be suppressed by this technique. Figure 8.5a depicts the best-fit slopes picked between 150 and 275°C (filled circles) and jackknife error estimates as a gray band. These thermal data suggest a rather constant paleointensity pattern for the last 200 kyr, with a distinct decrease in paleointensity between circa 190 and 180 ka. However, the amount of samples is small and it is likely that aliasing has occurred.

The absolute paleointensity data set has recently been extended with a record from Hawaiian lava flows, and has been compared with the sedimentary stack Sint-200 by *Brassart et al.* [1997]. The two records are not inconsistent, but an alternative interpretation of the virtual axial dipole moments (VADM) of the 8 lava
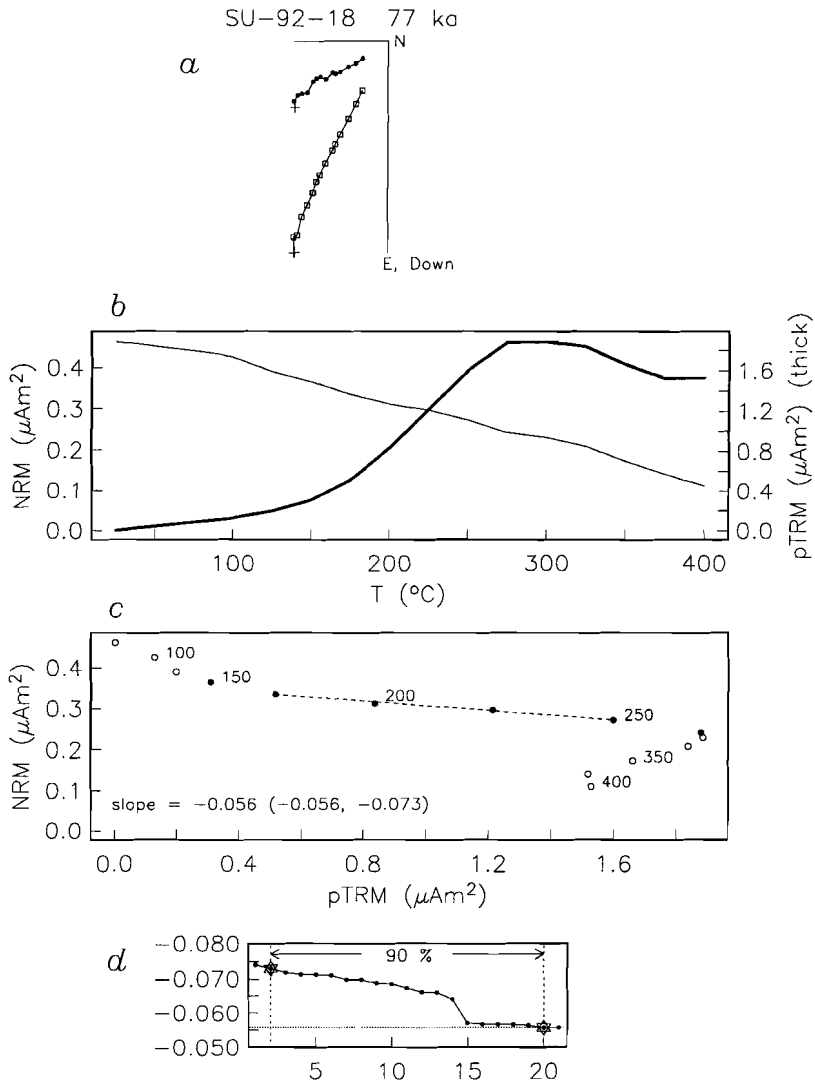
Figure 8.4: *An example of Thellier-Thellier paleointensity determination on sediment of SU-92-18. (a) Zijderveld diagram depicts step-wise destruction of the net magnetic moment. (b) The NRM intensity gradually decays on higher temperature steps. Peculiar behavior in the pTRM acquisition is observed after 275°C. This temperature step is therefore the highest to be used in the Arai plot (c). A relative estimate for the geomagnetic paleointensity is given by the slope determined between 175 and 250°C. (d) Representation of the 21 additional jackknife slopes in ranked order. The central 90% excludes the two most extreme data.*
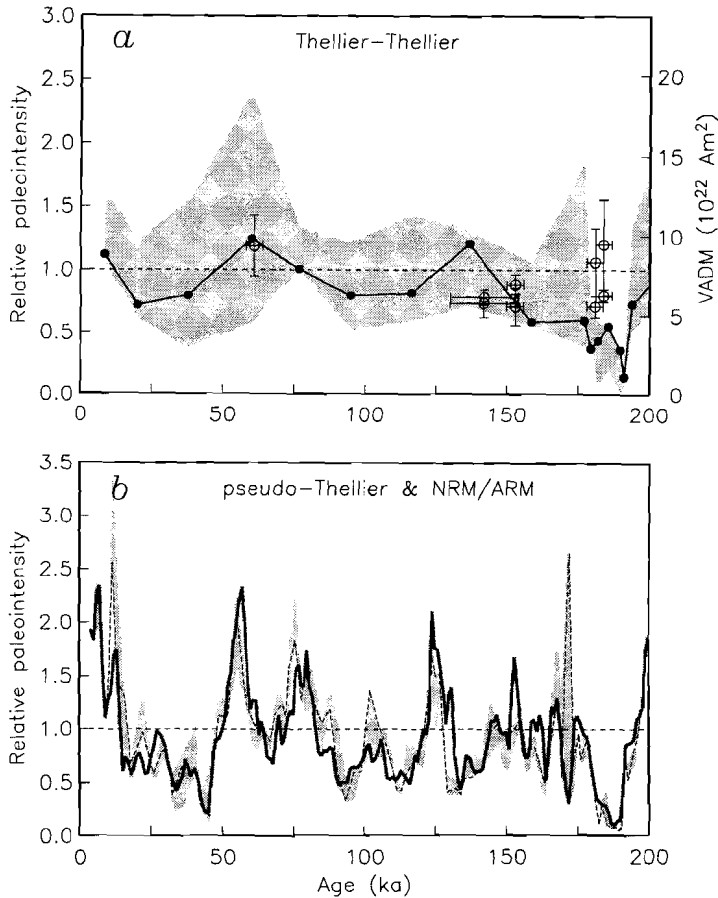
Figure 8.5: *Paleointensity estimates as function of age for SU-92-18. (a) Best-fit slope results from Thellier-Thellier for sediments indicated by filled circles with their jackknife error estimate in gray, show a rather constant paleointensity behavior for the last 175 kyr. Absolute determinations in VADMs (open symbols) from a recent study by Brassart et al. [1997] do not contradict the sedimentary data. The horizontal dashed line indicates the present-day dipole moment of 8 × 10²² Am². (b) Alternating field results of this core by Kruiver et al. [1998]. Thick line represents the original NRM/ARM data [Lehman et al., 1996]. In principle, the data are rather similar to the more sophisticated pseudo-Thellier slope (dashed curve) and jackknife error bounds (gray), though second order differences are present The horizontal dashed line indicates the mean of the record.*

flows (circa 400–60 ka) is that the paleointensity has varied less than sedimentary records suggest. Figure 8.5a also includes the new results [*Brassart et al.*, 1997] (symbols with error bars) for the last 200 kyr, and the fit with the new thermal paleointensities of SU-92-18 is acceptable.

8.3.2 Pseudo-Thellier paleointensity estimates

A pseudo-Thellier approach [*Tauxe et al.*, 1995] on the resampled collection of SU-92-18 sediments shows, to first order, similar results as the NRM/ARM paleointensity estimates [*Kruiver et al.*, 1998]. Figure 8.5b indicates pseudo-Thellier slopes m_a (dashed line) and corresponding jackknife uncertainty bounds (gray). The trend of this pseudo-Thellier record is similar to the one of the Thellier-Thellier data (Figure 8.5a versus b). One could argue that the paleointensities have been more stable than the alternating field results of Figure 8.3b (and 8.5b) indicate. Then again, the thermal results of SU-92-18 can be hampered by undersampling. As already mentioned by *Brassart et al.* [1997], the possibly too broad intensity low from sediments in 190–175 ka—in Sint-200, but also all three records of SU-92-18—could be caused by other factors than the geomagnetic field behavior.

8.3.3 Cross-spectral analysis

Since there now are different data from one single core, we can perform more detailed and appropriate squared coherences tests. Although in the interval 0–200 ka the thermally derived paleointensity estimates outnumber the absolute paleointensity determinations of *Brassart et al.* [1997], their sample density is still far too low to be used in frequency analyses. Just the pseudo-Thellier slopes m_a, NRM, ARM, and δ^{18}O of SU-92-18 are tested against each other and against Sint-200.

The zero-coherence level for the analysis of this core is now circa 0.31 because of the smaller amount of data, as compared to the number of data points in the Sint-stacks. First of all, NRM/ARM corresponds fairly well to Sint-200 (Figure 8.6a), and the routine check whether NRM/ARM is coherent with ARM indicates slight coherence, for example at 0.035 kyr^{-1}. More importantly, NRM/ARM with δ^{18}O gives squared coherences above zero coherence at precessional frequencies, leading one to suspect a slight but significant climatic influence. The middle panel shows that NRM and ARM are similar (Figure 8.6b), as already noted from Figure 8.3b. These remanent magnetizations have common features with the oxygen isotopes near the precession frequency band (circa 0.03–0.05 kyr^{-1}). Ideally, a proper normalization of NRM by ARM should eliminate all environmental influences, but apparently this is not the case. Finally, the paleointensity slope m_a is subjected to the coherence check (Figure 8.6c). The agreement of m_a with the
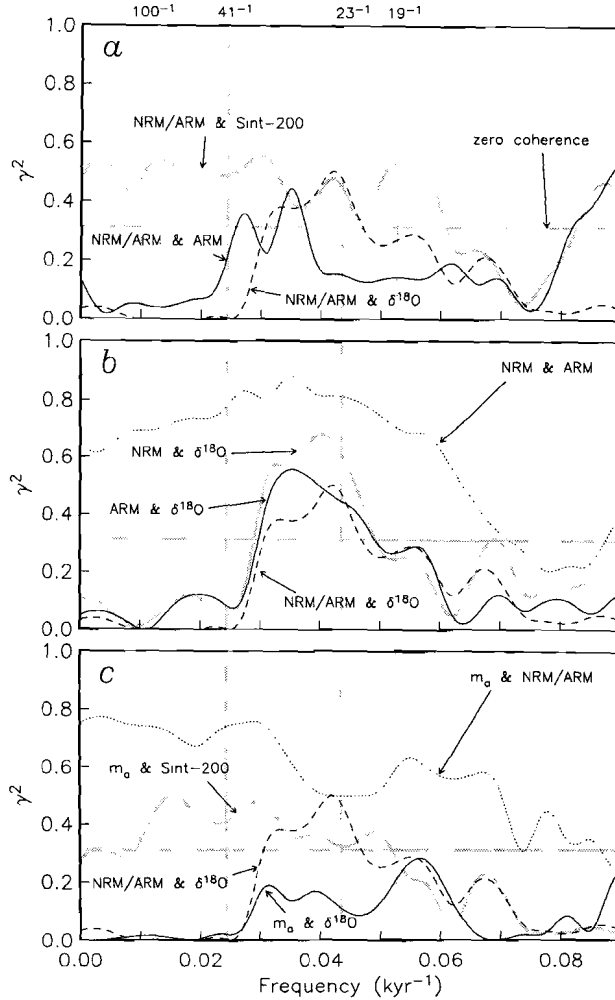
Figure 8.6: *Squared coherence tests for SU-92-18. (a) The paleointensity estimate NRM/ARM is coherent with Sint-200 (which includes the Açores core). The test whether ARM did a fair job in normalizing the NRM (i.e., NRM/ARM & ARM) shows slight coherence; it is less pronounced than the coherence of NRM/ARM and $\delta^{18}O$. (b) The NRM and ARM are highly coherent, which could eventually validate the use of ARM as a normalizer. Both NRM and ARM have coherent features with oxygen isotopes, and also their ratio NRM/ARM is above the zero-coherence level. (c) The pseudo-Thellier slope m_a is coherent with the original paleointensity determination, though a dip is observed at the precession frequencies. The squared coherence of m_a with $\delta^{18}O$ has dropped below the zero-coherence level, suggesting that m_a has lost the climatic contamination that conflicted with the geomagnetic character in NRM/ARM.*

faster NRM/ARM method [*Lehman et al.*, 1996] is evident, although a dip can be recognized in the precession interval. Also, Sint-200 and m_a correlate fairly well over a rather broad frequency interval. However, whereas NRM/ARM & $\delta^{18}O$ cohere, the more elaborate paleointensity determination seems to have lost its resemblance with oxygen isotopes. The pseudo-Thellier approach is designed to suppress climate influences (see Chapters 2–4), in contrast to NRM/ARM which appears to retain a climatic contamination. However, one should take care in interpreting the γ^2 plots. Possibly, the squared coherences of m_a and NRM/ARM with $\delta^{18}O$ are too close to the zero-coherence level to be distinguished as significantly coherent. Also, deviating data in either record can strongly influence the spectral method. Furthermore, the records have been interpolated and are possibly too short and not densely enough sampled for spectral purposes. Finally, in 5% of the cases the squared coherence exceeds zero coherence from chance. Most probably, the 'safe' conclusion to be drawn is that the records NRM, ARM, and their ratio cohere with $\delta^{18}O$. Consequently, a stack of more or less comparable paleointensity records (Sint-200) is likely to contain climate influences.

8.4   Ineffective normalization

As a first order approximation, the natural remanent magnetization (NRM) depends on the paleomagnetic field and a response function of the sediment

$$\text{NRM}(X,t) = M(t) \cdot f(X,t) \tag{8.1}$$

with $M(t)$ as the desired true field behavior of the geomagnetic intensity as a function of age t. The non-linear function f depends on many variable factors, such as grain size, carbonate content, sedimentation rate, bioturbation, diagenesis, all driven by environmental conditions. Its arbitrary parameter X represents climate, which is perhaps best approximated by the data of $\delta^{18}O$ [*Imbrie et al.*, 1984] and to a lesser extent by, for instance, magnetic susceptibility χ. The sediment function f is usually approximated by bulk magnetic parameters or laboratory induced magnetizations, such as anhysteretic remanence (ARM), that is

$$\text{ARM}(X,t) = g(X,t) \approx f(X,t) \tag{8.2}$$

Normalization of NRM by ARM will give a relative paleointensity estimate

$$\frac{\text{NRM}(X,t)}{\text{ARM}(X,t)} = M(t) \cdot \frac{f(X,t)}{g(X,t)} \tag{8.3}$$

Only if $g(X,t)$ is linearly related to $f(X,t)$, the ratio of equation (8.3) is proportional to the true field behavior $M(t)$, and consequently a relative paleointensity independent of X is accomplished. From Figure 8.3 it is obvious that the ratio

NRM/ARM corresponds in a number of cases to the sedimentary response function $\delta^{18}O(X, t)$; the most 'pure' function of X, which is independent of magnetic field strength. Also the squared coherence γ^2 in Figure 8.6 suggests involvement of climate X in the paleointensity curve NRM/ARM.

Oftentimes, other normalizers of NRM, such as χ or IRM, yield very consistent paleointensity estimates within a particular core. It is likely that these responses are again not linearly related to the complex $f(X, t)$ in equation (8.1), but are comparable to $g(X, t)$ of ARM in equation (8.2). Stacking several records like SU-92-18 will give a more or less coherent estimate for $M(t)$. Its reliability in representing solely the geomagnetic paleointensities must be questioned when correlations with purely environmental functions like $\delta^{18}O$ are evident.

8.5 Discussion

8.5.1 Climatic influence in beryllium data

Is it possible that the stacked ^{10}Be deposition rates from marine sediments are contaminated by a climatic signal ? There are several studies on ^{10}Be data that indicate climatic involvement.

First, a ^{10}Be study on the youngest 80 kyr of SU-92-18 [*Robinson et al.*, 1995] shows that circa half of the ^{10}Be/^{9}Be ratio can be explained by variations in the global geomagnetic intensity as inferred from NRM/ARM. The authors argue that the remaining differences could be caused by uncertainties in the assumed relationship or inaccuracies in either record. Instead of resulting from a change in cosmic-ray intensity through variation of the paleomagnetic field strength [*Robinson et al.*, 1995], the ^{10}Be/^{9}Be increase during the last glacial maximum can also be explained by a changed import of Antarctic Bottom Water [*Von Blanckenburg et al.*, 1996].

Second, strong climatic controls are found in high resolution profiles of ^{230}Th$_{ex}$ and ^{10}Be from the southernmost Atlantic Ocean (Weddell Sea), that deliver a stratigraphy similar to the $\delta^{18}O$ variations [*Frank et al.*, 1995]. These records are not included in the present ^{10}Be-stack [*Frank et al.*, 1997] because of their variable contributions of old, rapidly resedimented particles and changes in bottom water currents on interglacial–glacial time scales. This very local phenomenon of the Antarctic continental margin is not representative for the variable advection in the entire Atlantic ocean, still a direct link with climate is evident.

Third, in a study on Fe–Mn crusts [*Von Blanckenburg et al.*, 1996], it is suggested that fluctuations in ^{9}Be-normalized records of ^{10}Be are caused by variations in the Atlantic-Ocean circulation as well. The change in the global thermohaline conveyor pattern could well effect the distribution of dissolved ^{10}Be/^{9}Be in the deep sea. However, the ^{10}Be stack [*Frank et al.*, 1997] incorporates only accumulation rates normalized by ^{230}Th$_{ex}$. This is done to obtain ^{10}Be deposition

rates primarily influenced by boundary scavenging effects and production rate variations.

Finally, increased ^{10}Be/^{230}Th$_{ex}$ values during glacial periods may be attributed to enhanced scavenging intensity due to increased productivity [Kumar et al., 1993]. Such non-geomagnetic variations can also be explained by increased terrigenous input of dust [Frank, 1996; Jansen et al., 1987].

Thus, there is evidence that beryllium-10 records in the Atlantic Ocean are not only affected by the geomagnetic field strength, but also by changes induced by global climate. It is argued [Frank et al., 1997] that although the major part of the long ^{10}Be records cluster in the Southern Atlantic Ocean, the equal distribution north and south of the Polar Front averages out drastically different paleoflux conditions. Consequently, the ^{10}Be stack is thought to represent a global behavior.

It is difficult to unambiguously link circulation in the Atlantic Ocean and/or other glacial–interglacial phenomena to changes in the ^{10}Be stack. Moreover, it is beyond the compass of the present study to solve this debate. Merely the observation that Sint-Be acts in several cases as δ^{18}O, together with (indirect) evidence that ^{10}Be is influenced by climate, makes the assumption that the entire ^{10}Be stack is not influenced by ocean circulation variations or glacial–interglacial successions [Frank et al., 1997] seem optimistic.

8.5.2 Climatic influence in NRM paleointensity data

The correspondences between the conventionally determined Sint-200 and δ^{18}O records may also be attributed to the sedimentary response to climate. Certainly, amplitude variations in the magnetic intensity must have occurred in the past, but the traditional normalization for obtaining relative paleointensity behavior from natural remanences apparently fails to eliminate all climatic influences. The compilation Sint-200 [Guyodo and Valet, 1996] cannot be used in a one-to-one case versus the δ^{18}O curve [Imbrie et al., 1984], therefore, an individual high-resolution record with detailed oxygen isotope and paleomagnetic data was subjected to the squared coherence test. Core SU-92-18 suggests both sedimentary magnetization NRM and rock-magnetic parameter ARM have reacted to environmental features. Their ratio implies that pure geomagnetic paleointensity is not achieved through this normalization procedure (Figure 8.3 and 8.6). Other paleointensity techniques seem to provide better estimates with respect to climatic influence. The pseudo-Thellier approach [Tauxe et al., 1995] for sedimentary paleointensity data (see also Kruiver et al. [1998]) shows subtle differences with the standard normalization methods. However, it causes the squared coherences near precessional frequencies to drop below the zero-coherence level.

Instead of a delayed acquisition of magnetization, the phase shift between the magnetizations and δ^{18}O can be explained by the shift of a few thousand years between carbonate content and δ^{18}O [Ruddiman and McIntyre, 1981]. Magnetite

concentration in the North Atlantic is in phase with carbonate content, therefore a comparable delay between NRM (or ARM) and $\delta^{18}O$ is expected.

8.5.3 Pure geomagnetic signal

The youngest circa 50 kyr indicate an interesting discrepancy between $\delta^{18}O$ and the paleointensity stacks (Figure 8.1). The last glacial maximum is some 15 kyr younger than the minimum in magnetic intensity, which seems be too large a shift, certainly in this very recent period. In addition, this interval is most densely covered with ^{10}Be and normalized NRM data, so we may assume a more accurately determined geomagnetic character. Moreover, both paleointensity stacks coincide very well with the U/Th calibration results of the ^{14}C time scale [*Bard et al.*, 1990; *Laj et al.*, 1996; *Bard*, 1997]. Whereas the paleointensity low at circa 40 ka does not coincide with a glacial maximum, the rest of the paleointensity trend in this youngest part is quite similar to climatic behavior. This could suggest that only anomalous geomagnetic intensity was around 35–40 ka and the monotonously increasing values since are climatic artifacts. Independent support for this is given by the relative paleointensity data from Site 983 which do not indicate an increasing trend for the last 35 kyr [*Channell et al.*, 1997].

With respect to the cross-spectral analyses of the entire stacks, the highest coherence between Sint-200 and Sint-Be (Figure 8.2b) favors the assumption that both are indeed affected by the then prevailing magnetic fields. The agreement confirms the concentration of periodicities in the Brunhes paleointensity data in the ~33 kyr band [*Tauxe and Wu*, 1990; *Tauxe and Shackleton*, 1994]. However, the $\delta^{18}O$ stack does not contain much spectral power between obliquity and precession (41^{-1} and ~23^{-1} respectively), therefore coherences with both paleointensity stacks are bound to be low in this interval. Before hypotheses on orbital influence on the geomagnetic field can be tested with relative paleointensity records from sedimentary data, one must be certain that all sedimentary artifacts are accounted for.

8.6 Conclusion

The Sint-200 stack of several relative paleomagnetic intensity records for the last 200,000 years undoubtedly demonstrates an overall internal coherence. Independent support, from inverting the stacked ^{10}Be record to 100% paleofield intensity fluctuations, has been taken as a validation of the applicability of sediments for paleointensity research. Alternatively, I suggest that the good agreement of the stacked paleointensity records stems—to a certain extent—from similar influences of the Pleistocene climate, rather than from geomagnetic intensity variations alone.

A detailed look at a conventionally determined paleointensity record suggests that after normalization of the natural remanent magnetizations, the magnetic signals resemble the climatically controlled $\delta^{18}O$ records from the same core. 'Impure' paleointensity records, which contain climatic components, are likely to result in coherent stack. Other more time consuming relative paleointensity estimates suggest to do a better job in removing the climatic influence.

Whereas it is not proved that fluctuations in the sedimentary paleointensity records are in fact partially controlled by variations in global climate as opposed to being of geomagnetic origin, there are certainly grounds for suspicion.

Chapter 9

A geomagnetic paleointensity stack from Ontong-Java Plateau sediments for the Matuyama Chron

9.1 Introduction

The time-dependent behavior of the geomagnetic field is an interesting feature within Earth sciences. Not only the historical recordings by mankind, but also registrations in rocks throughout the Phanerozoic show variations of both direction and intensity of the Earth magnetic field. Lava extrusions provide readings of the paleofield in a theoretically well-constrained manner. Since volcanic eruptions take place only sporadically, it is difficult—if not impossible—to construct a continuous record of the geomagnetic behavior through time and space. Therefore, paleomagnetists turn to sedimentary sequences that allow construction of long and continuous records of the paleomagnetic field, also because such records can be inter-correlated, for instance by means of oxygen isotope data. Unfortunately, the acquisition of remanent magnetization in sediments follows processes too complex to be simulated in laboratory experiments. Therefore, only relative estimates of paleointensity can be obtained from sediments by normalization of the natural remanent magnetization (NRM) by the amount of magnetic material that is involved in the NRM. Several normalization procedures are used, all with drawbacks [*Tauxe*, 1993].

The number of sedimentary records spanning the recent normal polarity interval the Brunhes Chron (0–778 ka) is increasing rapidly (see e.g., the global stack of *Guyodo and Valet* [1996]). However, also longer records than 778 thousand

---

[1]Submitted by Y.S. Kok and L. Tauxe to *J. Geophys. Res.*

year passed in review. Five years ago *Valet and Meynadier* [1993] presented the
first long sedimentary record of relative paleointensities spanning the last 4 million
year (VM93). It indicated a striking "saw-toothed pattern": a gradual decrease of
magnetic field strength followed by a polarity reversal and a subsequent vigorous
recovery of the paleointensity. Rather than assuming a geomagnetic origin of this
behavior, *Kok and Tauxe* [1996a] presented a thought experiment that provided
an alternative explanation calling on the acquisition of long-term viscous magneti-
zation. Such a contamination obscures an originally constant primary magneti-
zation. Somewhat later, experimental data [*Kok and Tauxe*, 1996b] showed that
thermal treatment of the cores examined by *Valet and Meynadier* [1993] removed
viscous magnetizations and the asymmetrical pattern around the Gilbert–Gauß
reversal they caused[1]. Contrary to the long-term trend, the finer scale features
in the VM93 record seemed to survive thermal treatment. Thus, these are con-
sidered not to be a viscous relaxation effect, but either geomagnetically or—less
preferably—climatically induced.

The aims of this study are (1) to obtain new relative paleointensity data
throughout the reversed Matuyama Chron (0.778–2.852 Ma), and (2) to construct
a paleointensity stack from Ontong-Java Plateau sediments for this period using
thermal techniques which can remove viscous magnetizations.

9.2   Previous work on Leg 130 sediments

Leg 130 of the Ocean Drilling Program (ODP) sampled sediments and basement
lavas from the north-eastern margin of the Ontong-Java Plateau (OJP). OJP is
one of world's largest submarine plateaus and extends over an area of more than
1000×1500 km^2 in the western equatorial Pacific Ocean. More than a kilometer
of pelagic sediments, spanning late Cretaceous to Quaternary ages, overlay the
volcanic plateau.

Shipboard paleomagnetic studies during the leg showed sudden declines of
the magnetic signal below a certain critical depth: the intensity reduction event
[*Musgrave et al.*, 1993]. *Tarduno* [1994, 1995] suggested on the basis of data from
one of the Leg 130 Sites—which suffered from intensity reduction at a very shallow
depth—that the combination of hysteresis and low-temperature data can be used
to discriminate paleointensity features from magnetic mineral reduction.

A shore-based paleomagnetic study [*Gallet et al.*, 1993] documented three short
normally polarized intervals in the reversed Matuyama Chron. The youngest
of these anomalous zones corresponded to the Cobb Mountain subchron (circa
1.21 Ma), whereas the older two were shown to be caused by overprints of the
present-day normal field. Thermal demagnetization techniques indicated that
these viscous contaminations obscured the low paleointensities of reversed polarity

---

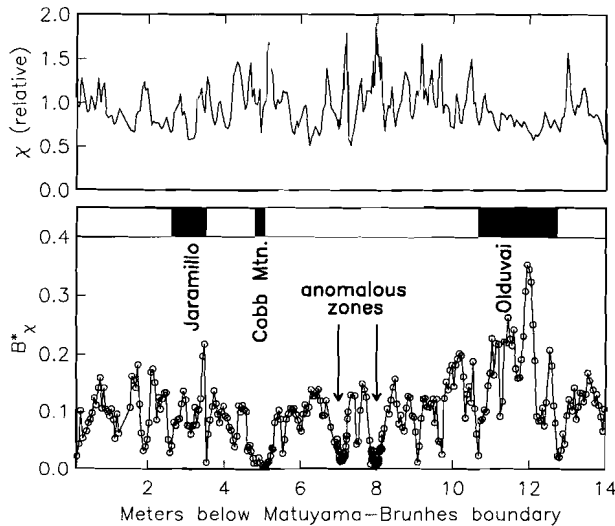[1]This debate is described in more detail in Part II, Chapters 5–7.

Figure 9.1: *Relative paleointensity data from the Matuyama Chron of core 803A. Redrawn from Tauxe [1993] but with susceptibility χ record added for completeness.*

in the two older intervals. By that time, thermal treatment of deep-sea sediments was an unusual technique, certainly with respect to relative paleointensities of the geomagnetic field. In her review, *Tauxe* [1993] shows the relative paleointensity record of core 130-803A (Figure 9.1). It consists of NRM intensities after 300°C normalized by magnetic susceptibility χ, covering the youngest three quarters of the Matuyama Chron (circa 2.1–0.78 Ma).

9.3 Thellier-Thellier experiments

In this study, we have followed the procedure for absolute geomagnetic paleointensity determination of *Thellier and Thellier* [1959] and modified by *Coe et al.* [1978]. The thermal demagnetization of NRM is interwoven by partial thermal remanent magnetization (pTRM) acquisition in a laboratory field. In the ideal case, when plotted against each other, these remanences are linearly related, and the slope translates to an absolute paleointensity estimate. Tests whether the magnetic phases of the sediment remain unchanged are performed by the so-called pTRM check. An earlier pTRM is re-acquired and should, for unaltered samples, give the same outcome as the original reading.

In fact, the above described Thellier-Thellier experiments provide absolute paleointensity information only on thermally blocked remanent magnetizations. Sedimentary magnetizations stem from largely unknown depositional processes. Nevertheless, sediments subjected to the Thellier-Thellier method allows one to monitor the stability of magnetization during the thermal process. Furthermore, in paleomagnetism thermal demagnetization of sedimentary NRM is generally preferable to alternating field techniques with respect to separating secondary from primary magnetizations. So far, several studies incorporated sedimentary Thellier-Thellier techniques to obtain relative paleointensity data [*Hartl and Tauxe*, 1996; *Kok and Tauxe*, 1996b; *Meynadier et al.*, 1998]. All our thermal experiments have been carried out in the magnetically shielded room of Scripps Institution of Oceanography using the methods described by *Hartl and Tauxe* [1996]. We subjected the section of core 803B spanning the lower Olduvai reversal to the Thellier-Thellier approach. Two examples of these experiments are given in Figures 9.2 and 9.3. One of the typical features is a relatively increased NRM unblocking in the intervals 100-150°C and 425–450°C. In the Arai plot [*Nagata et al.*, 1963] (Figures 9.2, 9.3c) we observe a linear behavior in the 250–375°C interval. Generally, the pTRM checks at 200°C and 350°C are lower than the original pTRM at these temperatures. Although the discrepancies are more than 5%, we suggest that the Thellier-Thellier for these experiments are acceptable.

Crucial in experimental data is some estimate of an error. We use the jackknife resampling technique (described in Chapter 3) to obtain non-symmetric uncertainty bounds about the best-fit slope through the NRM–pTRM data. All

Figure 9.2: *Thellier-Thellier results for a sample of the Olduvai normal subchron. (a) Zijderveld diagram indicates decay towards the origin on progressive thermal demagnetization. The cores are unoriented so declinations (closed symbols) do not reflect the normal direction during this polarity interval. (b) NRM decay and pTRM acquisition as function of temperature field. The decay of the NRM is monotonic, the dashed line depicts the decay of the sum of the vector differences, and the unblocking of the latter is shown by bins. Also shown is the pTRM acquisition curve up to 400° C (thick line). (c) When the NRM and pTRM curves are joined, they construct the so-called Arai plot. Triangles indicate the pTRM checks that, in principle, fall on the earlier acquired pTRM; the checks at 200 and 350° C suggest slightly lower values than the original pTRM. The best-fit slope is calculated in the 250–375° C interval. (d) and (e) Results for the jackknife resampling scheme to obtain an estimate in the best-fit slope m_T. The resampling provides 21 jackknife estimates, of which the central 90% is bounded by the dashed lines and used as an asymmetric uncertainty about the best-fit slope.*

Depth 17.17 m

a

N

E, Down

b

c

250 – 375°C
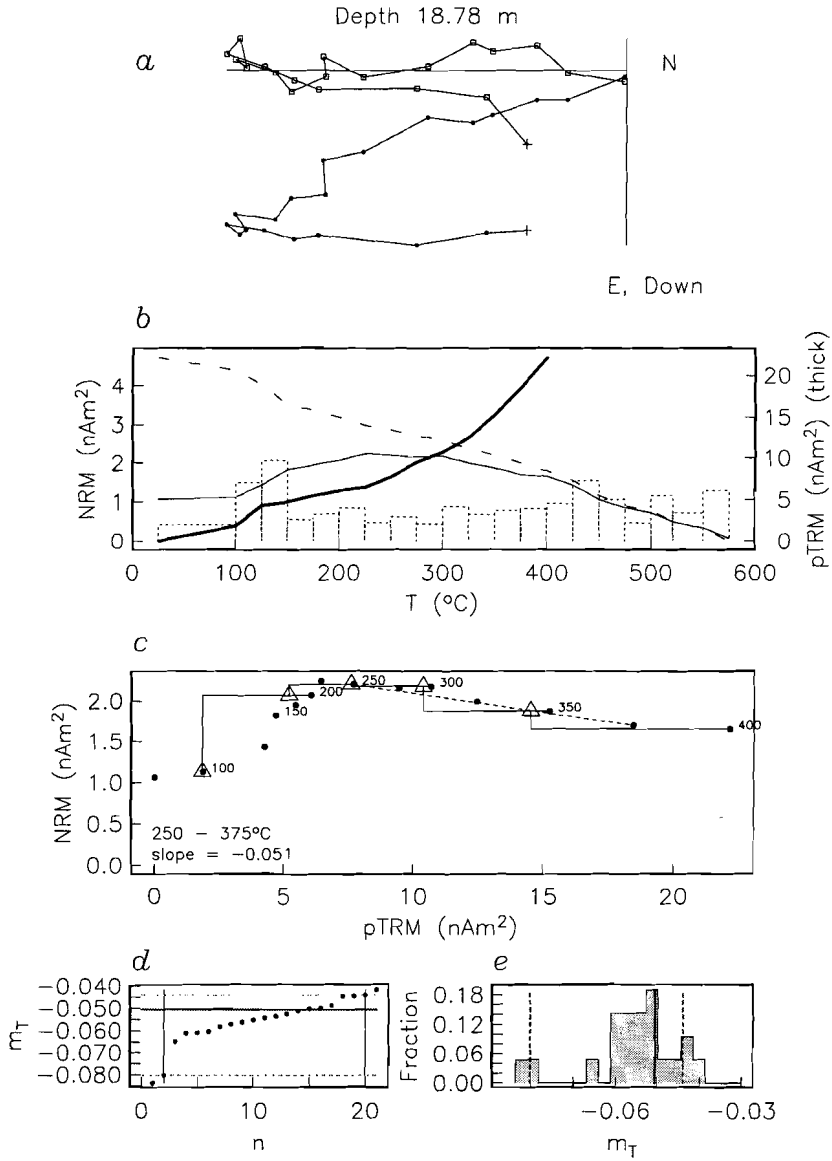slope = −0.161

d

e
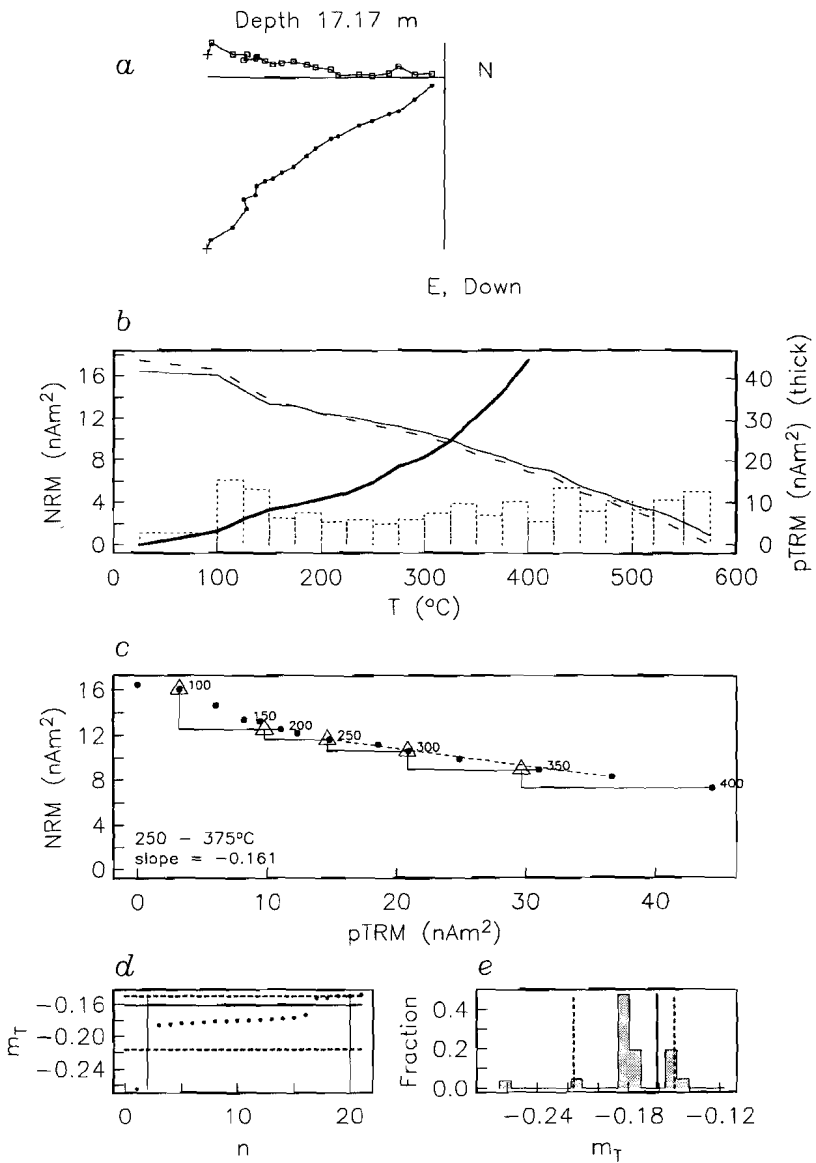
Figure 9.3: *Same as Figure 9.2 for a reversed sample located near the Matuyama–Olduvai transition. The reversed primary magnetization is overprinted by a normal component at circa 250°C.*
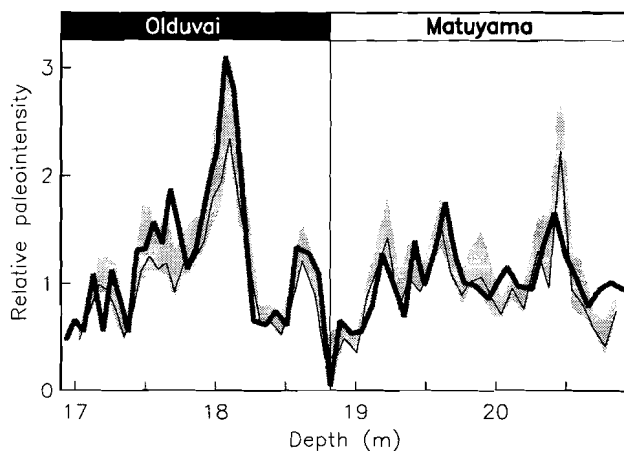
Figure 9.4: *Estimates for geomagnetic paleointensity from a section of Hole 803B. The fast paleointensity method—250° C demagnetization of NRM normalized by 250° C acquisition of pTRM, indicated by the thick line—is compared with the Thellier-Thellier slopes (thin line and gray error estimate). The different paleointensity estimates do not differ significantly and justify the use of the 250° C-method.*

samples acquired an additional 21 estimates of which the two extreme values are discarded. In Figures 9.2, 9.3d and e give indications for the uncertainty in the best-fit line. Since the full Thellier-Thellier procedure is very time-consuming, we prefer to use a faster method that mimics the full method. *Gallet et al.* [1993] suggested that 250 to 300°C is necessary to eliminate a hard viscous overprint. It appears that the Thellier-Thellier slopes—with their error indications—are well approximated by ratio of NRM intensity at 250°C and the pTRM at this step (Figure 9.4). Thus, the rest of the samples of our collection has been subjected to the following faster procedure: 100°C and 250°C demagnetization, and the 250°C pTRM acquisition in the laboratory field of 40.0 μT.

9.4   Results

9.4.1   Hole 803B

From Hole 803B, we have examined two sections , 803B-3H and 4H. In this study, the abrupt changes in the declination records indicate core breaks. The magnetostratigraphy indicates that it comprises the Olduvai, La Réunion and the Gauß normal polarity intervals. An interesting feature is found around the Gauß–Matuyama boundary; the significantly higher paleointensity values after the reversal that generate a saw-toothed pattern, disappear on thermal treatment. This seems to confirm the earlier results of *Kok and Tauxe* [1996b] who suggested that the saw-toothed patterns in the Plio–Pleistocene—as found by *Valet and Meynadier* [1993]—can be explained as an artifact caused by insufficient removal of VRM.

The low paleointensity estimates in the youngest part of the core coincide with relatively high values of pTRM. Here, variations in pTRM correspond in a reciprocal way to paleointensity changes. Therefore, the interval 14–16 m is less suitable for paleointensity estimates. Another observation is that the paleointensity values in the Olduvai are substantially higher than the surrounding Matuyama paleointensity estimates. In this normal polarity interval the paleointensities seem to be are overestimated. Possibly, this is the effect of Brunhes-related viscous magnetization that is not removed in spite of the thermal demagnetization, but variations in pTRM values are suspect as well.

The La Réunion polarity interval appears where pTRM is relatively low, which could suggest a lithological connection. The deepest part of section 3H (22–23.5 m) also indicates low paleointensity values, which do not correspond to the higher Matuyama values of section 4H (23.8–27.4 m).

9.4.2   Hole 803C

From Site 803 we have used one section 803C-1H to overlap the core break in 803B (Figure 9.6). Again, paleointensity values in the oldest part of the Matuyama tend to decrease more than the ones in the Gauß Chron. A striking feature is the zone of anomalous directions between 24 and 24.5 m, where demagnetization to 100°C still suggests normal polarities in the reversed Matuyama Chron. However, after the 250°C step the declinations and inclinations become reversed. They coincide with a low paleointensity interval, reminiscent of the findings of *Gallet et al.* [1993]. La Réunion is also in this core in concert with a low pTRM intensity zone. The anomalous inclinations in an interval around 22 m are also linked with low paleointensities, where declinations do not indicate a jump of some 180°. This zone corresponds to the low paleointensity values in Figure 9.5, but also low pTRM intensities are observed.
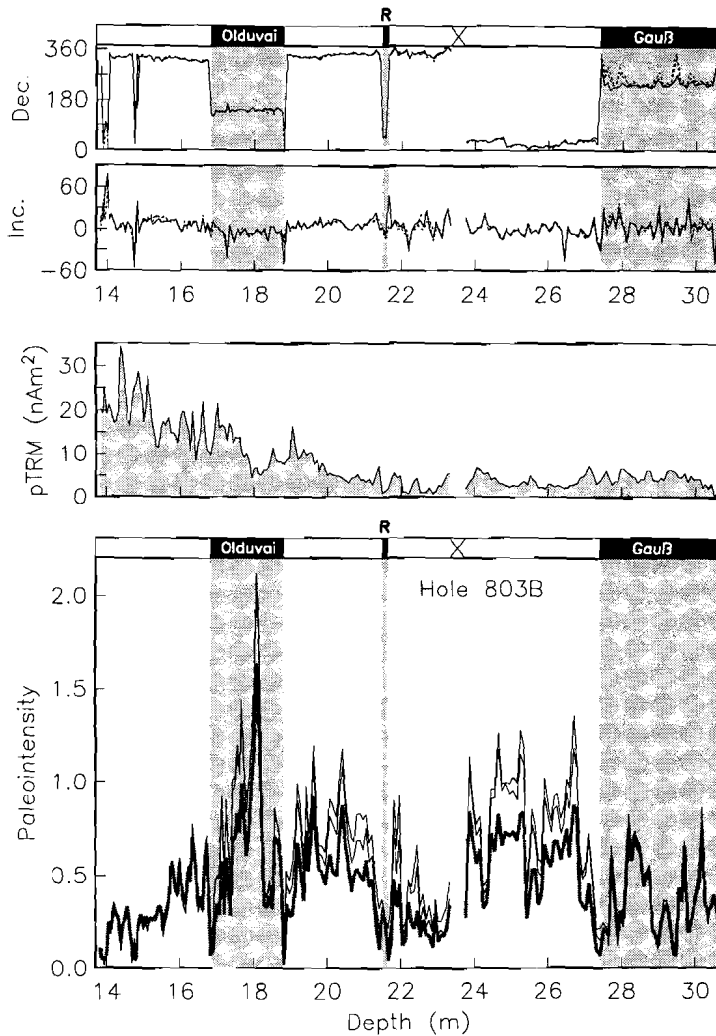
Figure 9.5: Paleomagnetic results for Hole 803B sections 3H and 4H as a function of depth in core. Upper panels show directions during the thermal demagnetization process; dashed lines for 25 and 100° C, and solid line the direction at 250° C. The cores are unoriented so declination can only be used as an arbitrary direction per section. The cross indicates the core break, The normalizing factor pTRM acquired at 250° C is indicated in the middle panel. The lower panel shows the paleointensity changes after treatment at elevated temperatures. Thin lines are NRM intensities after 25 and 100° C, think line is the 250° C step.
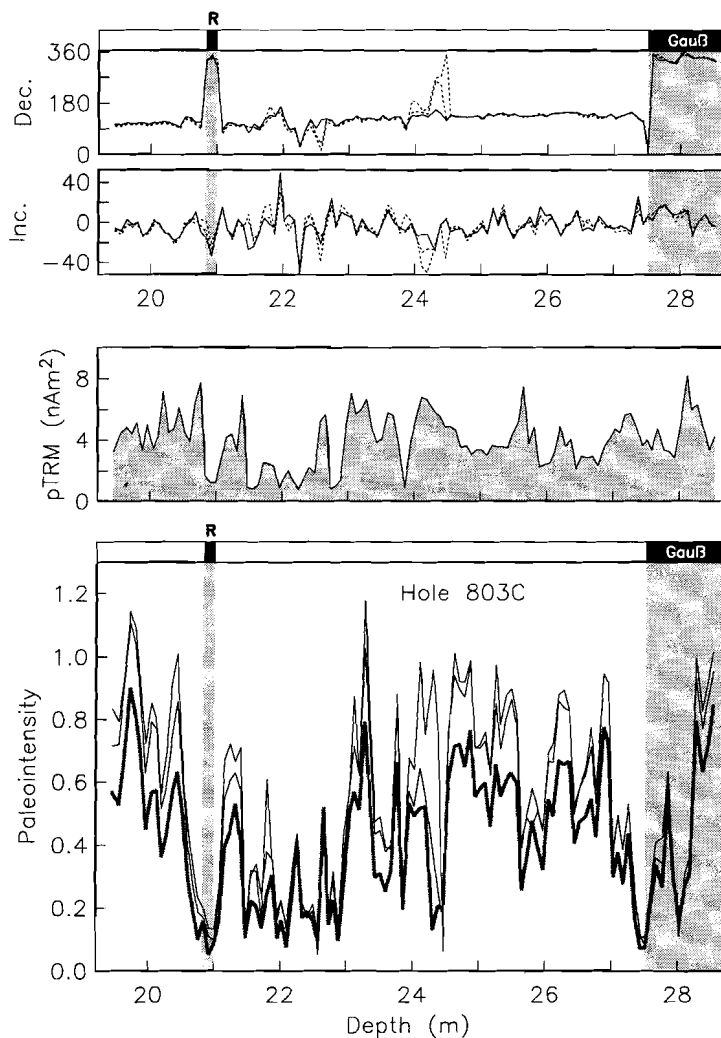
Figure 9.6: *Same as Figure 9.5 but for 803C-1H. Note the anomalous directions in the zone between 24 and 24.5 m. Whereas no or little thermal demagnetization suggest an excursion with normal directions, the 250° C step reveals reversed directions and merely a decreased paleointensity in this interval. More deviating directions are found near 22 m; inclinations indicate highly anomalous paleofields, but the declinations give no clear indications for normal polarity magnetizations. Again, a low in paleointensity can be linked to this behavior.*
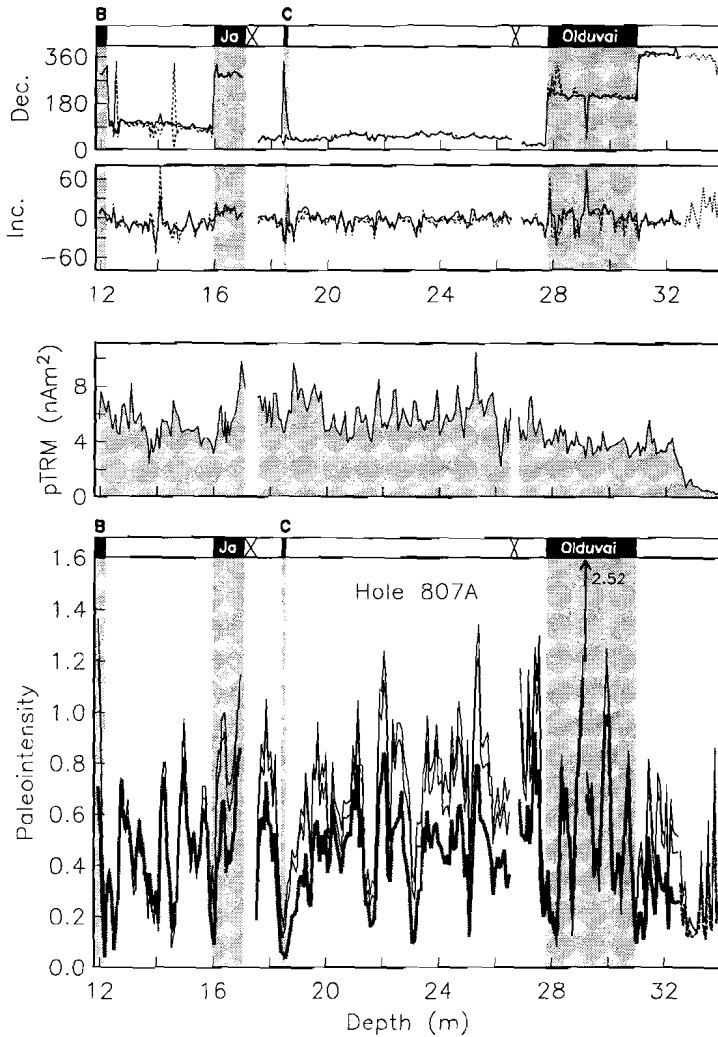
Figure 9.7: *Same as Figure 9.5 and 9.6 but for 807A-1H, 2H, and 3H. B = Brunhes, Ja = Jaramillo, C = Cobb Mountain. The extreme paleointensity value in the Olduvai at 29.18 m corresponds to anomalous directions. In this hole, there are no indications for apparent normal directions between the Olduvai and the Cobb Mountain linked to the lows in paleointensity as found in 803A by Gallet et al. [1993]. Below circa 32.4 m the intensity reduction event caused the magnetic signal to be of inferior quality.*

9.4.3　Hole 807A

The hole 807A record is the longest of this study. It contains three sections 807A-
1H, 2H, and 3H and spans from the oldest part of the Brunhes polarity interval
to approximately La Réunion normal subchron. However, the intensity reduction
event plagues the deepest part of this section (below 32.4 m); data below this
horizon will be omitted from further analyses. Anomalous inclination behavior
around 14 m is not linked to reversing directions in the declinations, but again
to a paleointensity low. One extreme paleointensity value in the Olduvai zone
corresponds to anomalous directions. This data point has a normal pTRM value
but an unusually high NRM value.

Event	Age (Ma)	———Depth (m)———			
		803A	803B	803C	807A
Matuyama–Brunhes	0.778	7.94			12.19
Upper Jaramillo	0.990	10.43			15.98
Lower Jaramillo	1.070	11.32			—
Upper Cobb Mountain	1.201	12.66			18.42
Lower Cobb Mountain	1.211	12.81			18.58
Upper Olduvai	1.785	18.47	16.82		27.80
Lower Olduvai	1.942	20.54	18.82		31.03
Upper La Réunion	2.129		21.49	20.84	
Lower La Réunion	2.149		21.66	21.00	
Gauß–Matuyama	2.582		27.40	27.51	
average SAR (cm/kyr)		1.06	1.33	1.48	1.59

Table 9.1: *Summary of locations and ages of reversals from the Leg 130 collection.
Ages are according to Lourens et al. [1996], Tauxe et al. [1996], and Cande and
Kent [1995]. SAR = sediment accumulation rate estimated from the ages.*

9.5　Reality check on the records

Tauxe [1993] tested the 803A record for coherence of the susceptibility χ with a
thermally derived paleointensity estimate. Portions of the spectra were slightly
coherent, particularly between circa $\frac{1}{41}$ and $\frac{1}{26}$ kyr^{-1}. She suggested that unre-
moved lithological variations corresponding to obliquity of the Earth's orbit still
have an influence on the paleointensity determinations.

We test the all the Leg 130 records this study (Figure 9.8). It is clear that
variations in sediment accumulation rate have occurred, and because we do not
date all the separate records, individual age models are not available. Therefore,
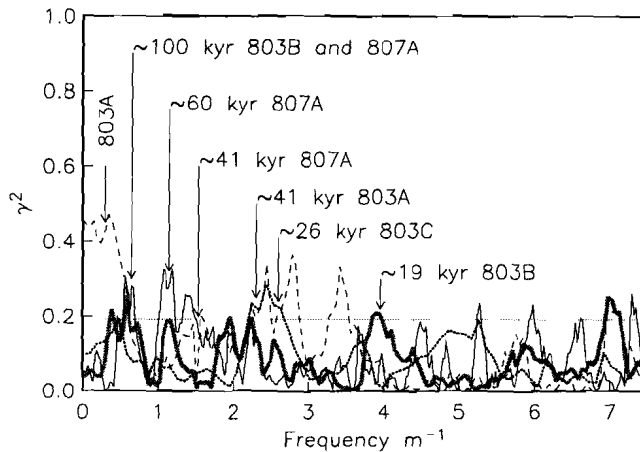
Figure 9.8: *Squared coherence analysis of the paleointensity curves 803A (dashed), 803B (gray), 803C (dotted), and 807A (line) versus their susceptibility profiles as function of frequency per meter. The labels indicate the matching periods in kyr. Squared coherences* γ^2 *above the zero-coherence level (horizontal gray line) are significant at a 95% level. Coherences near the 100 kyr period for the eccentricity of the Earth's orbit are found. This suggests that rock-magnetic parameter* χ *and the paleointensity estimates are not completely independent.*

we deal with frequencies per meter. As an indication of frequencies per kyr, the vertical arrows with their labels indicate periods in kyr (deduced from average sediment accumulation rate from Table 9.1). Hole 803A shows the stronger coherences than originally shown by *Tauxe* [1993] where only 500-kyr windows are used. The phase diagram of 803A (not shown) for the significant coherences at the shortest frequencies indicate a 180° shift between χ and paleointensity which suggest that normalization by χ was not ideal. However, the left end of the frequency spectrum is not as well sampled by the spectral analyses and can therefore not be attributed too much weight (see also discussion by *Constable et al.* [1998]). Significant coherences (within 95% certainty) are found near the Milankovic period for eccentricity of 100 kyr for 803B and 807A. Also other frequencies connected with Earth's climate can be recognized. However, these coherences are only slightly above the zero-coherence level.

9.6   Stacking the records

The next step is the compilation shown in Figure 9.9. It includes an extended section of 804C (this study and [*Hartl and Tauxe*, 1996]) around the Matuyama–Brunhes reversal. This record is too short to be unambiguously linked to the patterns in 803A and 807A. The overall image is that many coherent features can be recognized. We use the program AnalySeries [*Paillard et al.*, 1996] to tie the individual records together. Obvious coherent signatures in the separate paleointensity records are connected, and linear interpolation is performed between these correlation points. We translate all records to a common-depth scale (Figure 9.10). For the youngest part of the stack, the 803A record forms the base for the depth scale from the beginning of the Olduvai until the oldest part of the Brunhes. The oldest part of the stack is based on the depths of 803B and connected to the depth scale of the youngest part (at 12.74 m common-depth). Most of the paleointensity and polarity variations found in the individual records can be transferred to a coherent stack. The main discrepancies are found in the Olduvai zone, but the overall agreement is very good. Interesting features in the stack are

- absence of general saw-toothed behavior,

- the double dip at the Matuyama-Brunhes boundary (30 cm),

- the rather broad paleointensity minimum around the Cobb Mountain subchron (at 5 m),

- the two paleointensity lows at respectively 7 and 8 m,

- the low paleointensity zone between 16 and 17 m, preceding the La Réunion zone.

Next, the data of Figure 9.10 are averaged and dated by taking the reversal boundary ages indicated in Table 9.1. Most of them are from *Lourens et al.* [1996], except for the ages of the youngest reversal which is dated at 778 kyr ago [*Tauxe et al.*, 1996], and the Cobb Mountain subchron dated 1.201–1.211 Ma [*Cande and Kent*, 1995]. Figure 9.11 shows the stack which we refer to as the OJP-stack for the Matuyama Chron.
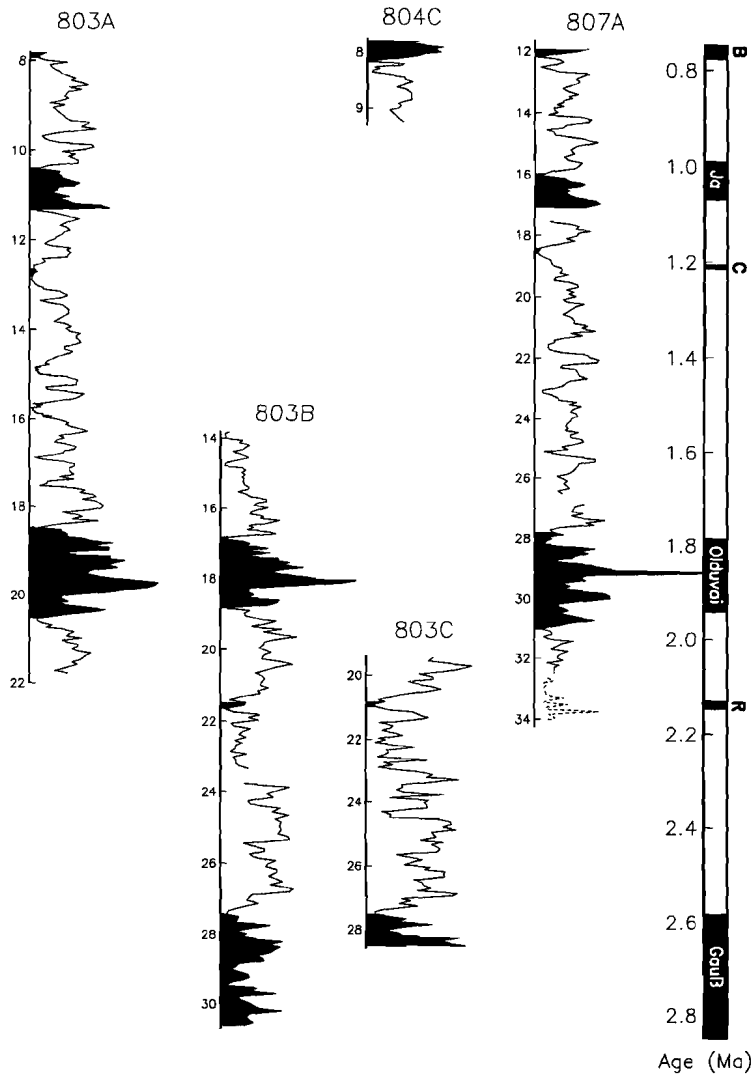
Figure 9.9: *Overview of all paleointensity records. Abbreviations as in previous plots and filled parts of the records indicate normal polarities which correspond to features in the geomagnetic polarity time scale (on the right).*
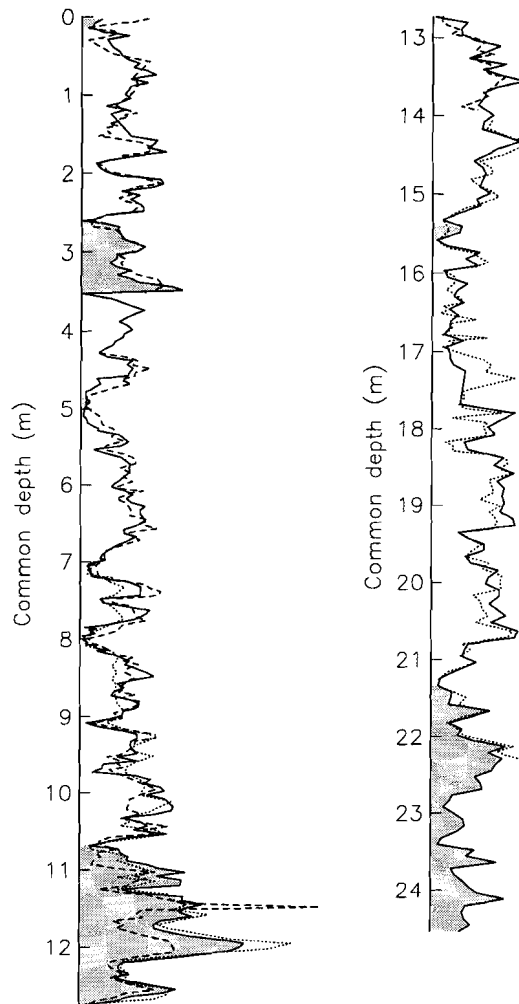
Figure 9.10: Common-depth record of the paleointensity curves after coherent paleointensity variations are tied together. The youngest part (on the left) is based on the 803A depth scale and overlapping records are plotted on the same scale. The oldest part (on the right) uses 803B depths as guide. Practically everywhere, each interval is covered by at least two records.
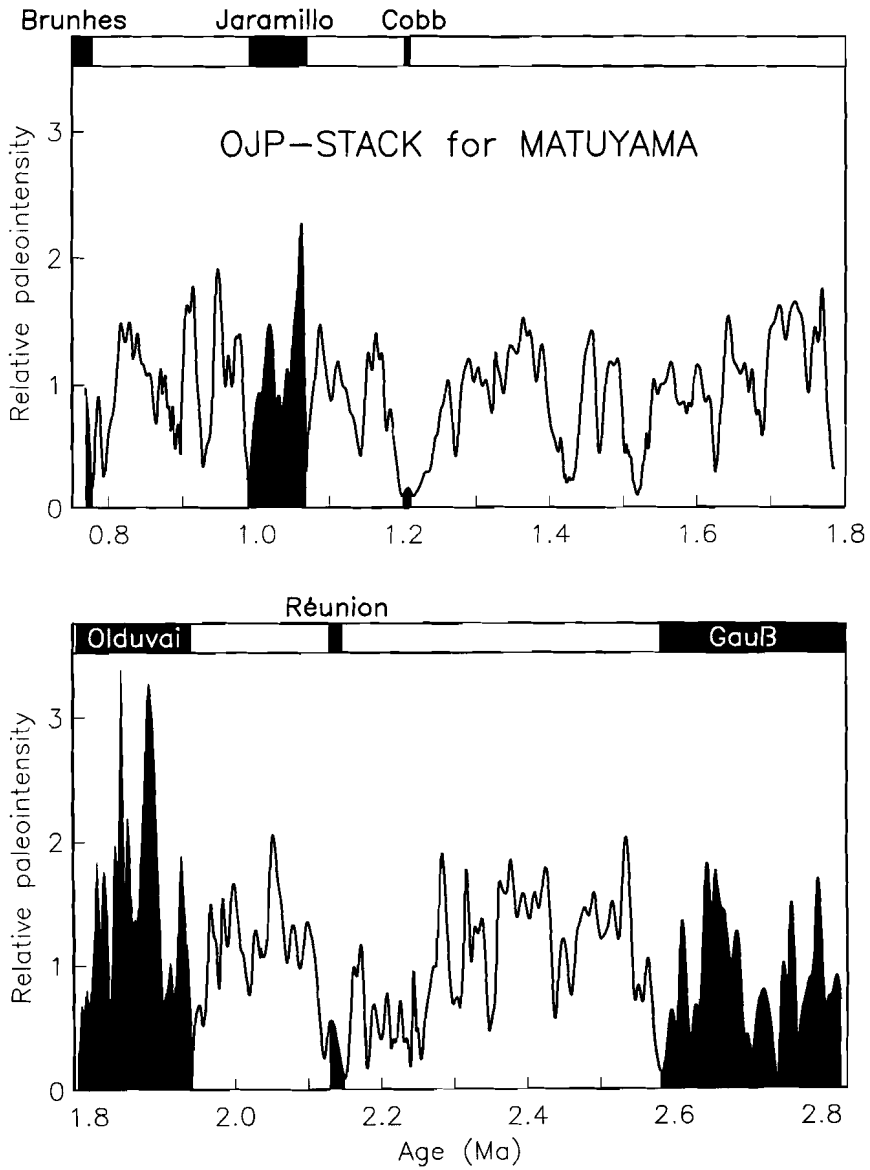
Figure 9.11: *Ontong-Java Plateau stack pinned at the reversals to the polarity time scale from Table 9.1.*

9.7   Comparison with other paleointensity data

The paleointensities of the Matuyama Chron were previously poorly documented. Records that do cover this reversed polarity zone are the 4-million year Pacific record [*Valet and Meynadier*, 1993] (VM93) and the 5-million year record of core MD90-0940 from the Indian Ocean [*Meynadier et al.*, 1994] (M94). We tuned these records at the reversal boundaries to the ages from Table 9.1. Figure 9.12 shows the three curves spanning the Matuyama Chron. Both 'French' records display evidence of the typical saw-toothed pattern. On the contrary, the records used to obtain the OJP stack do not indicate an off-set in paleointensity values around reversals after thermal demagnetization.

Once again, we use squared coherence analyses to quantify the correspondence between the independent records. We analyze *all* data including decreases in paleointensity related to reversals. If we suppose that paleointensity and reversals are linked, then this is a valid approach. The ages *within* the polarity intervals is not synchronous for the three records, but at this stage we have no reliable time control.

Power spectral densities (PSD) of the three data sets are shown in Figure 9.13a. Features of interest are (1) the relatively low PSD values for OJP and M94 at circa 0.013 kyr^{-1} (75 kyr), and (2) the corresponding signatures of OJP and VM93 in the interval with periods between 29 and 27 kyr.

Figure 9.13b indicates the squared coherence γ^2 of the frequency spectra. Significantly coherent peaks are found at several intervals. A striking feature is found at the lowest frequencies: VM93 & M94 are well above the zero-coherence level which is the expression of the long-term saw-toothed pattern in these records. According to these analyses, the only frequency at which all three records cohere is near $1/150$ kyr^{-1}. Such frequencies cannot be linked to a saw-tooth (which was absent in OJP). Also the period of about 75 kyr, where both M94 & OJP show relatively low PSDs, can be labeled as a significantly coherent period. VM93 is not coherent with the other two records at this period. The phase spectrum of the squared coherences γ^2 is plotted in Figure 9.13c. Only the "saw-tooth" and the 150-kyr components indication variations that are in phase (phase $= 0°$). Higher frequency components are all offset, which suggests time-lags in the records. However, it is more appropriate to explain the offsets by the dating problems within the intervals of stable polarity.

There is no indication that the eccentricity of the Earth's orbit with a period of 100 kyr is present in the records. However, significant coherences in M94 & OJP are found roundabout the obliquity period of 41 kyr. We did find slightly coherent values at frequencies just below $1/41$ kyr^{-1} for some of the individual paleointensity records (Figure 9.8), which suggests a minor lithological factor. Alternatively, it is suggested that periods between circa 35 and 42 kyr are a genuine expression of the paleomagnetic field, in concert with findings for the
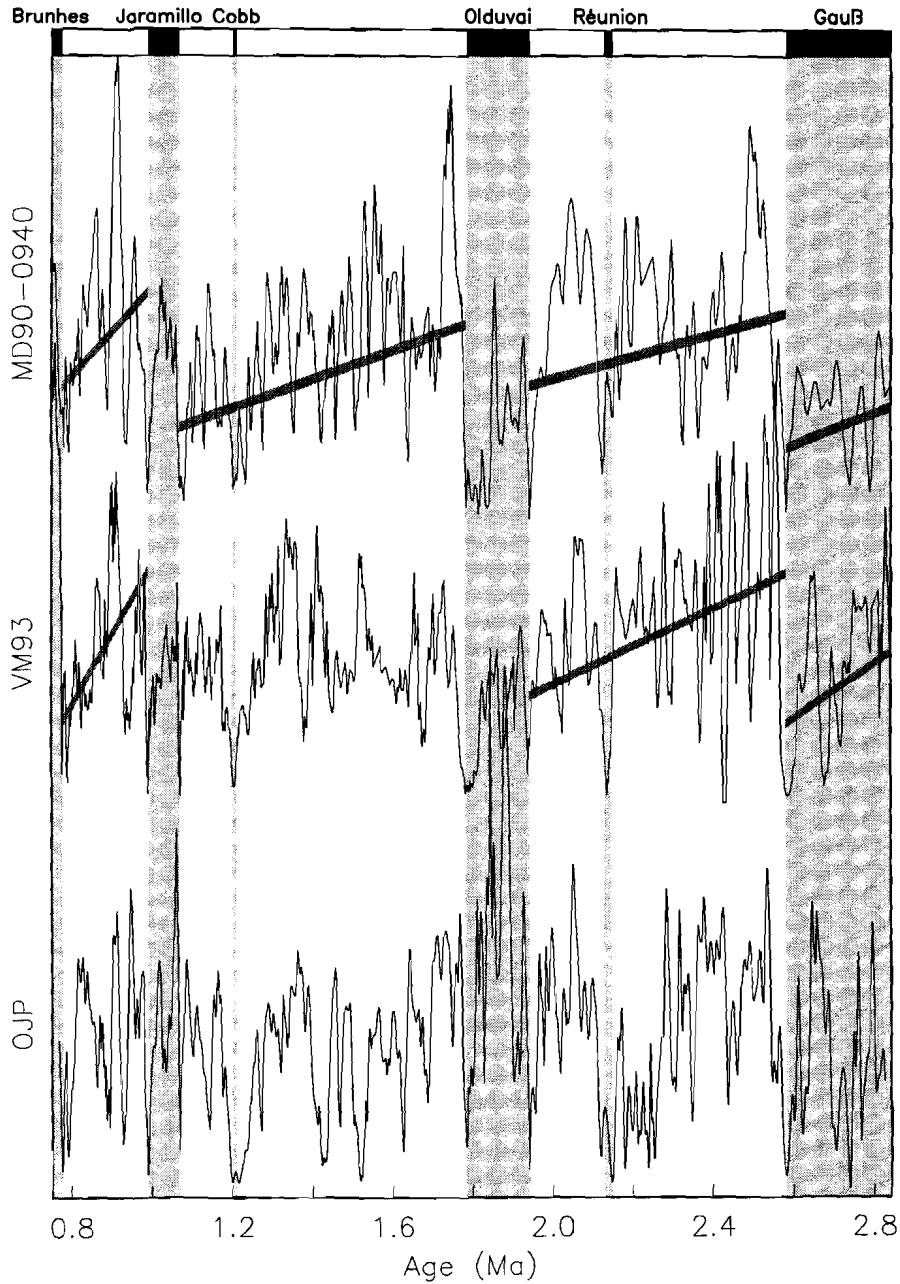
Figure 9.12: *Comparison of paleointensity data of this study (OJP) with two other sedimentary records, from the Indian (upper panel) and Pacific (middle) Ocean. The saw-toothed behavior in MD90-0940 and VM93 is absent in OJP.*
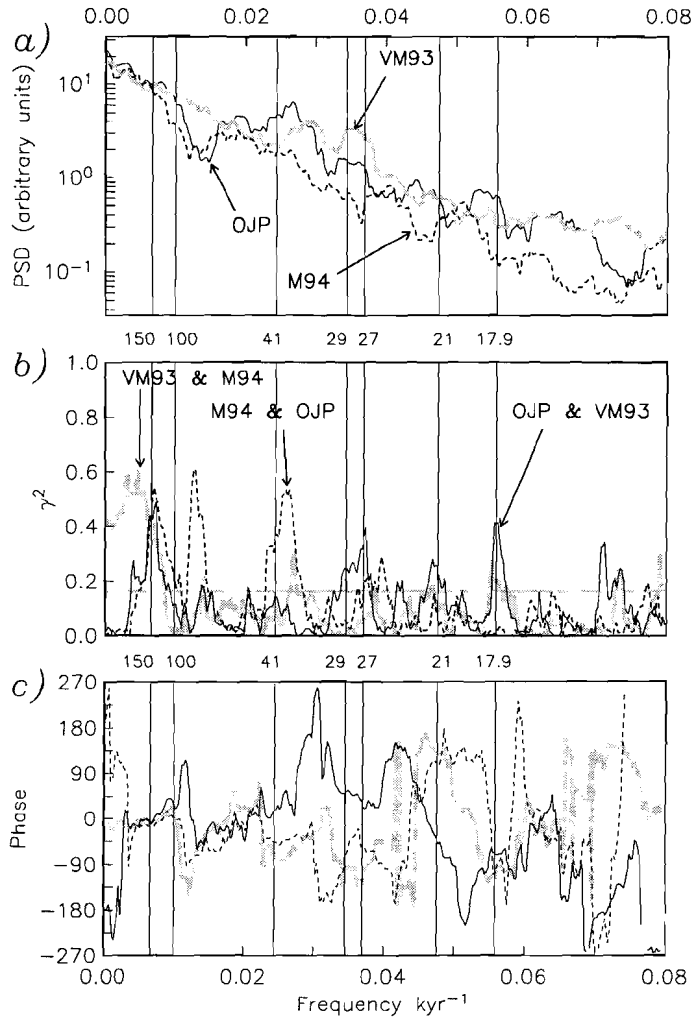
Figure 9.13: (a) PSD shows the behavior of the three 2-million year records. An interesting deviation is found around circa 75 kyr^{-1}, where OJP and M94 have relatively little power. (b) Squared coherences γ^2 indicate a significant correspondence at periods of circa 150 kyr for all possible combinations. Much longer periods (shorter frequencies) could correspond to the saw-toothed pattern that is absent in OJP. Significant peaks near the obliquity period of 41 kyr and at precessional cycles of circa 21 and 18 kyr suggest either climatic influence, or true geomagnetic behavior. (c) Phase diagram of the squared coherence of (b) (same labels) shows that the three records are in phase for the shortest frequencies. Other coherent features of (b) could indicate time lags.

Brunhes OJP stack [*Tauxe and Shackleton*, 1994]. It also corresponds to obliquity-like frequencies in Brunhes paleointensity records, of which the records of the normalizers do not show a 41-kyr component [*Channell et al.*, 1998]. On the other hand, the other two combinations of paleointensity curves tested here do not indicate such features, which tones down the assumption of a geomagnetic origin for these periods.

More coherent periods are found between circa 26.5 and 30 kyr, and at 21 and 18 kyr for OJP & VM93. These periods correspond to the astronomical precession of 26 kyr and the Milanković precessional periods, so one might suggest a link with orbital variations. Possibly, the reason for coherences at and near the climatic precessional frequencies is that there exists a contamination in the magnetic data that is unremoved (see Chapter 8). In general, the γ^2 for the records on practically all frequencies is below zero-coherence, which is a disappointing finding. If all records are readings of the paleomagnetic intensity variations, one expects coherent features over longer frequency intervals. However, we reinforce that the time control is merely based on the ten reversal ages. Between these tie-points, variations in sediment accumulation rates are likely to have occurred. Such variations would disturb the periodic behavior, to the detriment of the coherence estimates and their phase diagrams.

9.8   Conclusions

Thermal experiments were used to obtain relative paleointensities of the geomagnetic field. Earlier work on one of the cores showed that thermal demagnetization techniques were able to identify some anomalous zones in the reversed Matuyama Chron as low-intensity instead of normal-polarity intervals [*Gallet et al.*, 1993]. Thellier-Thellier experiments were carried out to determine the behavior during thermal treatment. These paleointensity determinations allow us to give error estimates in our best-fit slope values. Based on the Thellier-Thellier results, it turned out that we are allowed to demagnetize the sediments to 250°C and normalize them by the pTRM acquired at the same temperature.

The magnetostratigraphy of the four records showed that ages range from Gauß (circa 2.8 Ma) to the oldest part of the Brunhes normal Chron (circa 0.75 Ma). The normal Olduvai subchron is characterized by anomalously high paleointensity values. Possibly, despite the thermal demagnetization techniques, the Olduvai has acquired some unremoved viscous magnetization from the Brunhes Chron that adds to the paleointensity. Surrounding parts from the Matuyama are affected in the opposite direction and show lower relative paleointensity estimates. The Jaramillo subchron does not show anomalous high paleointensity values, however.

The paleointensity records are tied together and dated through pinning the reversals to calibrated ages. The resulting Ontong-Java Plateau stack (OJP) is compared with two other long sedimentary records that span the Matuyama

Chron. Unlike these data sets, OJP does not favor asymmetrically distributed paleointensity values around reversals.

Squared coherence analyses of the frequency spectra indicate a common period of circa 150 kyr in the three paleointensity curves. Other coherences are found at circa 75 and 40 kyr, but are not evident in all records, probably also as a consequence of the not ideal time control. Coherent frequencies near or at precessional values might be ascribed to non-geomagnetic features such as climate, but at present there is a lack of hard evidence.

Bibliography

Bard, E., 1997. Radionuclide production by cosmic rays during the last ice age. *Science*, 277, 532–533.

Bard, E., B. Hamelin, R.G. Fairbanks & A. Zindler, 1990. Calibration of the ^{14}C timescale over the past 30,000 years using mass spectrometric U/Th ages from the Barbados corals. *Nature*, 345, 405–410.

Brassart, J., E. Tric, J.-P. Valet & E. Herrero-Bervera, 1997. Absolute paleointensity between 60 and 400 ka from the Kohala Mountain (Hawaii). *Earth Planet. Sci. Lett.*, 148, 141–156.

Cande, S.C. & D.V. Kent, 1995. Revised calibration of the Geomagnetic Polarity Time Scale for the Late Cretaceous and Cenozoic. *J. Geophys. Res.*, 100, 6093–6095.

Channell, J.E.T., D.A. Hodell & B. Lehman, 1997. Relative geomagnetic paleointensity and δ^{18}O at ODP Site 983 (Gardar Drift, North Atlantic) since 250 ka. *Earth Planet. Sci. Lett.*, 153, 103–118.

Channell, J.E.T., D.A. Hodell, J. McManus & B. Lehman, 1998. Orbital modulation of the Earth's magnetic field intensity. *Nature*, 394, 464–468.

Chave, A.D. & C.R. Denham, 1979. Climatic changes, magnetic intensity variations and fluctuations of the eccentricity of the Earth's orbit during the past 2,000,000 years and a mechanism which may be responsible for the relationship - a discussion. *Earth Planet. Sci. Lett.*, 44, 150–152.

Coe, R. S., 1967. The determination of paleo-intensities of the Earth's magnetic field with emphasis on mechanisms which could cause non-ideal behavior in Thellier's method. *J. Geomag. Geoelectr.*, 19, 157–178.

Coe, R. S., S. Grommé & E. A. Mankinen, 1978. Geomagnetic paleointensities from radiocarbon-dated lava flows on Hawaii and the question of the Pacific nondipole low. *J. Geophys. Res.*, 83, 1740–1756.

Constable, C. & L. Tauxe, 1996. Towards absolute calibration of sedimentary paleointensity records. *Earth Planet. Sci. Lett.*, 143, 269–274.

Constable, C.G., L. Tauxe & R.L. Parker, 1998. Analysis of 11 Myr of Geomagnetic Intensity variation. *J. Geophys. Res.*, 103, 17735–17748.

Denham, C. R., 1981. Viscous demagnetization and the longevity of paleomagnetic polarity messages. *Geophys. Res. Lett.*, 8, 137–140.

Dunlop, D. J., 1973. Theory of magnetic viscosity of lunar and terrestrial rocks. *Rev. Geophys. Space Phys.*, 11, 855–901.

Dunlop, D. J., 1983. Viscous magnetization of 0.04–100 μm magnetites. *Geophys. J. R. Astr. Soc.*, 74, 667–687.

Dunlop, D. J. & Ö. Özdemir, 1997. *Rock magnetism: Fundamentals and frontiers.* Cambridge University Press.

Efron, B., 1982. *The Jackknife, the Bootstrap and Other Resampling Plans.* SIAM (Regional Conf. Ser. in App. Math.).

Frank, M., 1996. Reconstruction of late Quaternary environmental conditions applying the natural radionuclides ^{230}Th, ^{10}Be, ^{231}Pa and ^{238}U: A study of deep-sea sediments from the eastern Atlantic sector of the Antarctic Circumpolar Current system. *Rep. Polar Res.*, 186, 136 pp.

Frank, M., A. Eisenhauer, W. J. Bonn, P. Walter, H. Grobe, P. W. Kubik, B. Dittrich-Hannen & A. Mangini, 1995. Sediment redistribution versus paleoproductivity change: Weddell Sea margin sediment stratigraphy and biogenic particle flux of the last 250,000 years deduced from ^{230}Th$_{ex}$, ^{10}Be and biogenic barium profiles. *Earth Planet. Sci. Lett.*, 136, 559–573.

Frank, M., B. Schwarz, S. Baumann, P. W. Kubik, M. Suter & A. Mangini, 1997. A 200 kyr record of cosmogenic radionuclide production rate and geomagnetic field intensity from ^{10}Be in globally stacked deep-sea sediments. *Earth Planet. Sci. Lett.*, 149, 121–129.

Gallet, Y., J. Gee, L. Tauxe & J.A. Tarduno, 1993. Paleomagnetic analyses of short normal polarity magnetic anomalies in the Matuyama Chron. *Proc. Ocean Drilling Program, Scientific Results*, 130, 547–559.

Gee, J., H. Staudigel, L. Tauxe, T. Pick & Y. Gallet, 1993. Magnetization of the La Palma Seamount Series: Implications for Seamount Paleopoles. *J. Geoph. Res.*, 98, 11743–11768.

Guyodo, Y. & J.-P. Valet, 1996. Relative variations in geomagnetic intensity from sedimentary records: the past 200,000 years. *Earth Planet. Sci. Lett.*, 143, 23–36.

Halgedahl, S.L. & R.D. Jarrard, 1987. Paleomagnetism of the Kuparuk River formation from oriented drill core: evidence for rotation of the Alaska Plate. In I. Tailleur & P. Wymer (Eds.), *Alaskan North Slope Geology*, pp. 581–617. Bakersfield, CA: Society of Economic Paleontologists and Mineralogists, Pacific Section.

Hartl, P. & L. Tauxe, 1996. A precursor to the Matuyama/Brunhes transition-field instability as recorded in pelagic sediments. *Earth Planet. Sci. Lett.*, 138, 121–135.

Hartl, P., L. Tauxe & T. Herbert, 1995. Earliest Oligocene increase in South Atlantic productivity as interpreted from "rock magnetics" at Deep Sea Drilling Project Site 522. *Paleocanography*, 10, 311–325.

Herguera, J.C., 1994. Nutrient, mixing and export indices: a 250 kyr paleoproductivity record from the western equatorial Pacific. In R. Zahn (Ed.), *NATO ASI Series, I, 17, Carbon cycling in the glacial ocean: Constraints on the ocean's role in global change*, pp. 481–519. Berlin: Springer-Verlag.

Imbrie, J., J.D. Hays, D.G. Martinson, A. McIntyre, A.C. Mix, J.J. Morley, N.G. Pisias, W.L. Prell & N.J. Shackleton, 1984. The orbital theory of Pleistocene climate: support from a revised chronology of the marine $\delta^{18}O$ record. In A.L. Berger, J. Imbrie, J. Hays, G. Kukla & B. Saltzman (Eds.), *Milankovitch and Climate*, Vol. 1, pp. 269–305. Dordrecht: D. Reidel Publishing Company.

Jackson, M., W. Gruber, J. Marvin & S. K. Banerjee, 1988. Partial anhysteretic remanence and its anisotropy: applications and grainsize-dependence. *Geophys. Res. Lett.*, 15, 440–443.

Jansen, J.H.F., C. Alderliesten, A.J. van Bennekom, K. van der Borg & A.F.M. de Jong, 1987. Terrigenous supply of [10]Be and dating with ^{14}C and [10]Be in sediments of the Angola Basin (SE Atlantic). *Nucl. Instr. and Meth.*, B29, 311–316.

Johnson, E.A., T. Murphy & O.W. Torreson, 1948. Pre-history of the Earth's magnetic field. *Terr. Magn. atmos. Elect.*, 53, 349–372.

Kent, D. V., 1973. Post-depositional remanent magnetisation in deep-sea sediment. *Nature*, 246, 32–34.

Kent, D. V., 1982. Apparent correlation of paleomagnetic intensity and climatic records in deep-sea sediments. *Nature*, 299, 538–539.

Kent, D. V. & N. D. Opdyke, 1977. Paleomagnetic field intensity variation recorded in a Brunhes epoch deep-sea sediment core. *Nature*, 266, 156–159.

King, J. W., S. K. Banerjee & J. Marvin, 1983. A new rock magnetic approach to selecting sediments for geomagnetic paleointensity studies: application to paleointensity for the last 4000 years. *J. Geophys. Res.*, 88, 5911–5921.

Kok, Y. S., 1998. Climatic influence in NRM and ^{10}Be derived geomagnetic paleointensity data. *Earth Planet. Sci. Lett.*, submitted. Chapter 8, this thesis.

Kok, Y. S. & L. Tauxe, 1996a. Saw-toothed pattern of relative paleointensity records and cumulative viscous remanence. *Earth Planet. Sci. Lett.*, 137, 95–99. Chapter 5, this thesis.

Kok, Y. S. & L. Tauxe, 1996b. Saw-toothed pattern of sedimentary paleointensity records explained by cumulative viscous remanence. *Earth Planet. Sci. Lett.*, 144, E9–E14. Chapter 6, this thesis.

Kok, Y. S. & L. Tauxe, 1998a. Long-τ VRM and relative paleointensity estimates in sediments. *Earth Planet. Sci. Lett.*, submitted. Chapter 4, this thesis.

Kok, Y.S. & L. Tauxe, 1998b. Comment on "Saw-toothed variations of relative paleointensity and cumulative viscous remanence: Testing the records and the model" by L. Meynadier, J.-P. Valet, Y. Guyodo and C. Richter. *J. Geophys. Res.*, submitted. Chapter 7, this thesis.

Kok, Y.S. & L. Tauxe, 1998c. A geomagnetic paleointensity stack from Ontong-Java Plateau sediments for the Matuyama Chron. *J. Geophys. Res.*, submitted. Chapter 9, this thesis.

Kruiver, P. P., Y.S. Kok, M.J. Dekkers, C.G. Langereis & C. Laj, 1998. A pseudo-Thellier relative paleointensity record, rock magnetic and geochemical parameters in relation to climate during the last 276 kyr in the Azores region. *Geoph. J. Int.*, in press.

Kumar, N., R.F. Anderson, R.A. Mortlock, P.N. Froehlich, P.W. Kubik, B. Dittrich-Hannen & M. Suter, 1993. Increased biological productivity and export production in the glacial Southern Ocean. *Nature*, 362, 45–48.

Laj, C., A. Mazaud & J.C. Duplessy, 1996. Geomagnetic intensity and ^{14}C abundance in the atmosphere and ocean during the past 50 kyr. *Geoph. Res. Lett.*, 23, 2045–2048.

Lal, D., 1988. Theoretically expected variations in the terrestrial cosmic-ray production rates of isotopes. *Soc. Ital. Fis. Bologna*, 95, 216–233.

Lehman, B., C. Laj, C. Kissel, A. Mazaud, M. Paterne & L. Labeyrie, 1996. Relative changes of the geomagnetic field intensity during the last 280 kyears from piston cores in the Açores area. *Phys. Earth Planet. Inter.*, 93, 269–284.

Levi, S. K. & S. Banerjee, 1976. On the possibility of obtaining relative paleointensities from lake sediments. *Earth Planet. Sci. Lett.*, 29, 219–226.

Lourens, L.J., A. Antonarakou, F.J. Hilgen, A.A.M. van Hoof, C. Vergaud-Grazzini & W.J. Zachariasse, 1996. Evaluation of the Plio-Pleistocene astronomical timescale. *Paleoceanography*, 11, 391–413.

Lowrie, W., 1973. Viscous remanent magnetization in oceanic basalts. *Nature*, 243, 27–29.

Mangini, A., A. Eisenhauer & P. Walter, 1990. Response of Mn in the ocean to the climatic cycles in the Quaternary. *Paleoceanography*, 5, 811–821.

Mazaud, A., 1996. 'Sawtooth' variation in magnetic intensity profiles and delayed acquisition of magnetization in deep sea cores. *Earth Planet. Sci. Lett.*, 139, 379–386.

McFadden, P.L. & R.T. Merrill, 1998. Sawtooth paleointensity and reversals of the geomagnetic field. *Phys. Earth Planet. Int.*, 103, 247–252.

Meynadier, L., J.-P. Valet, F. Bassinot, N. J. Shackleton & Y. Guyodo, 1994. Asymmetrical saw-tooth pattern of the geomagnetic field intensity from equatorial sediments in the Pacific and Indian Oceans. *Earth Planet. Sci. Lett.*, 126, 109–127.

Meynadier, L., J.-P. Valet, Y. Guyodo & C. Richter, 1998. Saw-toothed variations of relative paleointensity and cumulative viscous remanence: Testing the records and the model. *J. Geophys. Res.*, 103, 7095–7105.

Mullender, T. A. T., A. J. van Velzen & M. J. Dekkers, 1993. Continuous drift correction and separate identification of ferrimagnetic and paramagnetic contributions in thermomagnetic runs. *Geophys. J. Int.*, 114, 663–672.

Musgrave, R.J., M.L. Delaney, R. Stax & J.A. Tarduno, 1993. Magnetic diagenesis, organic input, interstitial water chemistry, and paleomagnetic record of the carbonate sequence on the Ontong Java Plateau. *Proc. Ocean Drilling Program, Scientific Results*, 130, 527–546.

Nagata, T., Y. Arai & K. Momose, 1963. Secular variation of the geomagnetic total force during the last 5000 years. *J. Geophys. Res.*, 68, 5277–5282.

Néel, L., 1949. Théorie du trainage magnétique des ferromagnétiques en grains fins avec applications aux terres cuites. *Ann. Geophys.*, 5, 99–136.

Néel, L., 1955. Some theoretical aspects of rock magnetism. *Adv. Phys.*, 4, 191–243.

Paillard, D., L.D. Labeyrie & P. Yiou, 1996. Macintosh program performs time-series analyses. *Eos*, 77, 379.

Pick, T. & L. Tauxe, 1993. Holocene paleointensities: Thellier experiments on submarine basaltic glass from the East Pacific Rise. *J. Geophys. Res.*, 98, 17949–17964.

Prévot, M. & M. Perrin, 1992. Intensity of the Earth's magnetic field since Precambrian from Thellier-type paleointensity data and inferences on the thermal history of the core. *Geophys. J. Int.*, 108, 613–620.

Pullaiah, G., E. Irving, K. L. Buchan & D. J. Dunlop, 1975. Magnetization changes caused by burial and uplift. *Earth Planet. Sci. Lett.*, 28, 133–143.

Raisbeck, G. M., F. Yiou & S. Z. Zhou, 1994. Paleointensity puzzle. *Nature*, 371, 207–208.

Richter, G., 1937. Über die magnetische Nackwirkung am Carbonyleisen. *Ann. Physik*, 29, 605–635.

Robinson, C., G. M. Raisbeck, F. Yiou, B. Lehman & C. Laj, 1995. The relationship between [10]Be and geomagnetic field strength records in central North Atlantic sediments during the last 80 ka. *Earth Planet. Sci. Lett.*, 136, 551–557.

Ruddiman, W. F. & A McIntyre, 1981. Oceanic mechanisms for amplification of the 23,000-year ice-volume cycle. *Science*, 212, 617–627.

Schwartz, M., S. P. Lund & T. C. Johnson, 1996. Environmental factors as complicating influences in the recovery of the quantitative geomagnetic-field paleointensity estimates from sediments. *Geophys. Res. Lett.*, 23, 2693–2996.

Shackleton, N. J., A. Berger & W. R. Peltier, 1990. An alternative astronomical calibration of the lower Pleistocene time scale based on ODP Site 677. *Trans. R. Soc. Edinburgh Earth Sci.*, 81, 251–261.

Shackleton, N. J., S. Crowhurst, T. Hagelberg, N. G. Pisias & D. A. Schneider, 1995. A new Late Neogene time scale: application to Leg 138 Sites. *Proc. Ocean Drill. Prog. Sci. Res.*, 138, 73–101.

Tarduno, J. A., 1994. Temporal change of magnetic dissolution in the pelagic realm: Gauging paleoproductivity? *Earth Planet. Sci. Lett.*, 123, 39–48.

Tarduno, J. A., 1995. Superparamagnetism and reduction diagenesis in pelagic sediments: Enhancement or depletion? *Geophys. Res. Lett.*, 22, 1337–1340.

Tauxe, L., 1993. Sedimentary records of relative paleointensity of the geomagnetic field in sediments: theory and practice. *Rev. Geophys.*, 31, 319–354.

Tauxe, L., T. Herbert, N. J. Shackleton & Y. S. Kok, 1996. Astronomical calibration of the Matuyama-Brunhes boundary: Consequences for magnetic remanence acquisition in marine carbonates and the Asian loess sequences. *Earth Planet. Sci. Lett.*, 140, 133–146.

Tauxe, L., T. Pick & Y. S. Kok, 1995. Relative paleointensity in sediments; a pseudo-Thellier approach. *Geophys. Res. Lett.*, 22, 2885–2888. Chapter 2, this thesis.

Tauxe, L. & N. J. Shackleton, 1994. Relative paleointensity records from the Ontong-Java Plateau. *Geophys. J. Int.*, 117, 769–782.

Tauxe, L. & G. Wu, 1990. Normalized remanence in sediments of the Western Equatorial Pacific: Relative paleointensity of the geomagnetic field? *J. Geophys. Res.*, 95, 12337–12350.

Thellier, E. & O. Thellier, 1959. Sur l'intensité du champ magnétique terrestre dans le passé historique et géologique. *Ann. Geophys.*, 15, 285–378.

Tric, E., J.-P. Valet, P. Tucholka, M. Paterne, L. LaBeyrie, F. Guichard, L. Tauxe & M. Fontugne, 1992. Paleointensity of the geomagnetic field during the last 80,000 years. *J. Geophys. Res.*, 97, 9337–9351.

Tucker, P., 1980. Stirred remanent magnetization: a laboratory analogue of post-depositional realignment. *J. Geophys.*, 48, 153–157.

Tucker, P., 1981. Paleointensities from sediments: normalization by laboratory redepositions. *Earth Planet. Sci. Lett.*, 56, 398–404.

Valet, J.-P. & L. Meynadier, 1993. Geomagnetic field intensity and reversals during the past four million years. *Nature*, 366, 234–238.

Valet, J.-P., L. Meynadier, F. C. Bassinot & F. Garnier, 1994. Relative paleointensity across the last geomagnetic reversal from sediments of the Atlantic, Indian and Pacific oceans. *Geophys. Res. Lett*, 21, 485–488.

Verosub, K. L., E. Herrero-Bervera & A. P. Roberts, 1996. Relative geomagnetic paleointensity across the Jaramillo subchron and the Matuyama/Brunhes boundary. *Geophys. Res. Lett.*, 23, 467–470.

Von Blanckenburg, F., R. K. O'Nions, N. S. Belshaw, A. Gibb & J. R. Hein, 1996. Global distribution of beryllium isotopes in deep ocean water as derived from Fe-Mn crusts. *Earth Planet. Sci. Lett.*, 141, 213–226.

Wollin, G., W.B.F. Ryan & D.B. Ericson, 1978. Climatic changes, magnetic intensity variations and fluctuations of the eccentricity of the Earth's orbit during the past 2,000,000 years and a mechanism which may be responsible for the relationship. *Earth Planet. Sci. Lett.*, 41, 395–397.

Worm, H.-U., 1997. A link between geomagnetic reversals and events and glaciations. *Earth Planet. Sci. Lett.*, 147, 55–67.

Samenvatting (Summary in Dutch)

Een van de interessante eigenschappen van onze levende planeet betreft haar zwakke doch merkbare magnetische veld. Verscheidene bacteriën en dieren gebruiken het aardmagneetveld ter navigatie, bijvoorbeeld tijdens hun migraties. De mensheid ontdekte de mogelijkheden van de magnetische kracht voor kompassen die naar het magnetische noorden wijzen. De richtingen van het geomagnetisch veld zijn echter niet stabiel, waardoor correcties tussen de magnetische en geografische polen cruciaal zijn voor positionering. Historische registraties laten niet alleen zien dat de richting van het aardmagneetveld verandert, ook de intensiteit vertoont variaties in de tijd. Kennis van deze tijdafhankelijke eigenschappen van het magneetveld resulteert in een beter begrip van de processen die zich in het binnenste van onze planeet afspelen en de 'geodynamo' aandrijven. De aard en evolutie van de geodynamo zijn intrigerende onbekenden binnen de aardwetenschappen.

Directe observaties van het geomagnetisch veld beslaan slechts een zeer klein gedeelte van de geologische geschiedenis. Gelukkig bestaan er gesteenten met bepaalde ijzeroxides en ijzersulfides die tijdens hun vorming informatie over het heersende veld opslaan (remanente magnetisatie). Ofschoon het magnetisch signaal uiterst zwak is, kunnen 'paleomagnetici' met behulp van moderne apparatuur geomagnetische data achterhalen van lang vervlogen tijden (zelfs van het Archaïcum, 2.5–4 miljard jaar geleden). Dankzij dit fenomeen hebben we ontdekt dat het aardmagneetveld vaak van polariteit heeft gewisseld. Circa 780 duizend jaar geleden vond de laatste duidelijke omkering plaats. .

Voor alle paleomagnetische studies is het van groot belang de primaire magnetisaties te isoleren uit de totale natuurlijke remanente magnetisatie (NRM) van gesteenten. Paleomagnetici gebruiken in wezen twee procedures om de NRM te scheiden in de gewilde primaire en toegevoegde secundaire magnetisaties: in een magnetisch vacuüm worden gesteentemonsters blootgesteld aan verhoogde temperaturen (thermische demagnetisatie) of aan elektromagnetische wisselstroomvelden (AF demagnetisatie).

Vulkanische gesteenten zijn bij uitstek geschikt voor absolute bepalingen van de paleointensiteit van het aardmagneetveld. Zij kunnen jammergenoeg slechts momentopnamen van het paleomagneetveld geven, hetgeen een continue registratie belemmert. Dit in tegenstelling tot sedimentaire opeenvolgingen, welke bovendien wereldwijd kunnen worden gemonsterd en gecorreleerd. Het voornaamste nadeel van sedimentaire paleomagnetische studies is het gebrek aan kennis van het acquisitieproces van detritische remanente magnetisatie (DRM, een primaire vorm van NRM). De intensiteit van de DRM is in eerste benadering evenredig met het magneetveld tijdens afzetting, maar ook variërende processen zoals sedimentinvoer, bioturbatie, consolidatie en compactie zijn van invloed. Het is daarom

uiterst belangrijk dat de sedimentaire magnetisaties juist gecorrigeerd worden. Benaderingen van de 'magnetiseerbaarheid' van het sediment zijn magnetische susceptibiliteit χ of in het laboratorium geïnduceerde remanenties. Zij worden gebruikt om de DRM te normaliseren. Alvorens zulke correcties uitgevoerd kunnen worden, dient men er zich van te vergewissen dat de overgebleven magnetisatie louter primair is. Een voorbeeld van ongewilde secundaire magnetisatie betreft viskeuze remanente magnetisatie (VRM). Elk gesteente dat lang genoeg aan een extern veld wordt blootgesteld, zal een secundaire magnetisatie opdoen in de vorm van VRM. Daar DRM-acquisitie een nogal inefficiënt proces is, kan de VRM de totale NRM veel doen groeien naar de maximale of evenwichtsmagnetisatie. De tijdconstanten die de mate van deze groei bepalen, zijn de relaxatietijden τ die variëren van milliseconden tot astronomische waarden. Zij zijn afhankelijk van korrelgrootte, temperatuur en mineralogische samenstelling. Zelfs in het uitzonderlijke geval dat de τ-distributie binnen een sedimentkern constant zou zijn, dan kan de VRM-contributie aan de NRM van de jongste sedimenten drastisch verschillen van die van de oudste. Deze tijdafhankelijke effecten worden ingrijpender als het paleomagnetisch veld tussentijds van polariteit is veranderd. Variërende verdelingen van τ in sedimentaire opeenvolgingen resulteren in een nog complexere registratie van VRM. Een standaard demagnetisatie van NRM is in dat geval niet afdoende en kan leiden tot foutieve interpretaties.

Opbouw van het proefschrift

Dit proefschrift bestaat uit drie delen: Deel I behandelt drie methodologische studies, deel II gaat over het zaagtandpatroon dat sommige paleointensiteitsregistraties van de laatste 4 miljoen jaar kenmerkt, en deel III betreft enkele geomagnetische paleointensiteitscompilaties.

Deel I: Relatieve paleointensiteiten in sedimenten: Methoden

In **Hoofdstuk 2** wordt de pseudo-Thelliermethode ter normalisering van sedimentaire paleointensiteitsregistraties gepresenteerd. Deze vertoont overeenkomsten met de Thellier-Thelliertechniek [*Thellier and Thellier*, 1959] welke 'unblocking' van NRM vergelijkt met 'blocking' van gedeeltelijke thermo-remanente magnetisatie (p-TRM). In plaats van de thermische experimenten gebruiken we wisselvelddemagnetisatie van de NRM en vergelijken deze met verwerving van anhysteretische remanente magnetisatie (ARM) ten behoeve van een degelijkere afschatting van de paleointensiteit. We suggereren dat dit het voordeel heeft variërende hoeveelheden VRM te kunnen verwijderen van de NRM.

Hoofdstuk 3 bespreekt een statistische methode voor Thellier-Thellier of pseudo-Thellier-experimenten. Zoals gebruikelijk worden de paleointensiteiten bepaald door middel van lineaire regressie van het best passend verband tussen de

NRM en de in het laboratorium geïnduceerde remanenties. Met behulp van een zogenaamde jackknife-hermonsteringsmethode verwijderen we successievelijk dataparen van de groep om aan de hand van de kleinste-kwadratenmethode de helling opnieuw te berekenen. Deze extra paleointensiteitsbepalingen worden gebruikt als een onzekerheidsindicatie in de oorspronkelijke determinatie. In tegenstelling tot de standaardafwijking van de oorspronkelijke paleointensiteit produceert de jackknife-hermonstering dikwijls asymmetrische betrouwbaarheidsgrenzen.

In **Hoofdstuk 4** gebruiken we de pseudo-Thelliermethode (zoals beschreven in Hoofdstuk 2) om VRM-contributies aan de NRM te bepalen. Het verband tussen NRM-demagnetisatie en ARM-verwerving is typisch niet-linear. De concave gedeelten van de curve die NRM als functie van ARM beschrijft, worden toegeschreven aan VRM-componenten die eerder worden gedemagnetiseerd dan de DRM. Daar de coërciviteiten van VRM en DRM gedeeltelijk samenvallen, wordt in het begin van het proces ook een gedeelte van de gezochte DRM verwijderd. Terwijl deze kromme gedeelten worden weggelaten uit paleointensiteitsbepalingen, concentreren we ons hier echter op hun implicaties als lange-relaxatietijd VRM indicatoren. In hoofdstuk 2 wordt de lange-τ VRM-bijdrage geschat met het verschil tussen de conventionele NRM/ARM en de best passende lijn. Hier suggereren we een andere methode die niet vereist dat beide paleointensiteitwaarden zijn bepaald. Resultaten van onze lange-τ VRM wijzen op correlaties met paleoklimaatcurven en ouderdomafhankelijke groei van VRM. Bovendien zien we een scherpe verandering in korrelgrootte en lijkt de lange-τ VRM verkregen gedurende het Pleistoceen samen te hangen met korte-τ effecten opgemerkt in de laboratoriumomgeving.

Deel II: Zaagtandpatroon in paleointensiteitsregistraties

De waarneming van het zogenaamde zaagtandpatroon [*Valet and Meynadier*, 1993] in paleointensiteitsregistraties heeft veel stof doen opwaaien in de paleomagnetische gemeenschap. De Franse onderzoekers merkten een typisch driehoekig patroon op in hun paleointensiteitsbepalingen voor de laatste 4 miljoen jaar. Tijdens een interval van stabiele polariteit lijkt de sterkte van het aardmagneetveld af te nemen tot er een ompoling plaatsvindt, gevolgd door hoge intensiteiten in het nieuwe interval met tegengestelde polariteit. Een dergelijk paleointensiteitspatroon zou onverwacht gedrag van de geodynamo met zich meebrengen. Verschillende studies hebben dit zogenaamde zaagtandpatroon bevestigd, terwijl sommige anderen geen bewijs voor dergelijk gedrag vonden. **Hoofdstuk 5** suggereert dat het zaagtandfenomeen wordt veroorzaakt door cumulatieve viskeuze remanentie (CVR). Het richt zich met name op viskeuze magnetisaties verkregen over miljoenen jaren. Een CVR model dat distributies van lange relaxatietijden τ gebruikt, bijvoorbeeld 50±25 Myr, is in staat een van origine constante paleointensiteitwaarde te veranderen naar een zaagtandpatroon.

Hoofdstuk 6 onderzoekt in meer detail één van de omkeringen uit de curve van *Valet and Meynadier* [1993]. We gebruiken hier thermische demagnetisatie-technieken op een herbemonsterd gedeelte en merken op dat het asymmetrische patroon verdwijnt. We concluderen dat het zaagtandpatroon wordt veroorzaakt door een kunstmatige component die de primaire magnetisaties verdoezelt. De Thellier-Thellier-experimenten helpen bovendien onze parameters van het model uit Hoofdstuk 5 vast te stellen. Het model reproduceert het oorspronkelijke asym-metrische contrast rond de omkering verrassend goed, hetgeen suggereert dat de vervuiling die de zaagtand genereert van lange-τ viskeuze origine is.

Onze Franse collega's hebben alternatieve verklaringen van het zaagtandpa-troon categorisch getracht te weerleggen. In **Hoofdstuk 7** beargumenteren we dat hun recente weerlegging [*Meynadier et al.*, 1998] gebaseerd is op een foutieve interpretatie van ons werk. Zij hebben één voorbeeld van een distributie van re-laxatietijden uit zijn verband gerukt en toetsen het tegen thermisch 'blocken' van daadwerkelijke sedimenten. Logischerwijs verschillen de eigenschappen sterk, omdat ons voorbeeld slechts een ondergroep beslaat van het wel zeer omvangrijk scala van relaxatietijden aanwezig in het gesteente. We benadrukken dat het spec-ifieke voorbeeld 50 ± 25 Myr in staat is een zaagtand te genereren, maar dat het bestaan van veel langere relaxatietijden (i.e., $\gg 100$ Myr) expliciet wordt genoemd in Hoofdstukken 5 en 6.

Deel III: Stacks

In **Hoofdstuk 8** wordt beargumenteerd dat gepubliceerde paleointensiteitencom-pilaties die de laatste 200 kyr omvatten ook zijn beïnvloed door niet geomagne-tische gebeurtenissen. Twee recente, op onafhankelijke wijze afgeleide, stacks van paleointensiteiten vertonen goede overeenkomsten. De eerste—Sint-200 [*Guyodo and Valet*, 1996]—bestaat uit een verzameling van NRM-intensiteitsregistraties gecorrigeerd door een van de gebruikelijke normalisatietechnieken. De tweede 200-kyr stack gebruikt verscheidene genormaliseerde ^{10}Be-registraties als een indicatie van de mate van kosmogene productie, welke wordt vertaald naar relatieve geo-magnetische intensiteitsvariaties [*Frank et al.*, 1997]. Hun globale gelijkenis wordt optimistisch uitgelegd als een validatie van de gebruikte technieken en materi-alen ter verkrijging van paleointensiteitsvariaties. Als alternatief wordt gesteld dat beide curven—tot op zekere hoogte—nog steeds worden gestuurd door het klimaat tijdens het Pleistoceen. In het algemeen worden klimaatsinvloeden eenvoudig her-kend in sedimentaire reeksen. Bijvoorbeeld zuurstofisotopendata (δ^{18}O) van sedi-menten kunnen een nauwkeurige weerspiegeling geven van de glaciale–interglaciale chronologie (daarom worden δ^{18}O-curven vaak gebruikt ter datering en synchro-nisatie van sedimentaire kernen). Beide stacks van paleointensiteit, maar in het bijzonder de ^{10}Be-data, vertonen coherente kenmerken met de δ^{18}O-curve, hetgeen suggereert dat ze naast geomagnetisch gedrag ook het klimaatsinvloeden verto-

nen. Om deze bewering kracht bij te zetten worden spectraal-analysetechnieken gebruikt, zowel voor de stacks als voor een individuele registratie opgenomen in Sint-200. Deze laatste vertoont dat NRM, ARM, maar ook hun quotiënt coherent zijn met zuurstofisotopen, hetgeen wordt uitgelegd als een ontoereikendheid in de normalisatietechniek. Meer recent ontwikkelde paleointensiteitbepalingen zouden deze invloed onderdrukken.

Tenslotte wordt in **Hoofdstuk 9** een paleointensiteitscompilatie voor het Matuyama Chron gepresenteerd. Sedimentaire magnetisaties van vier kernen van het Ontong-Javaplateau (OJP) worden geanalyseerd met thermische technieken. Thellier-Thellierexperimenten [*Thellier and Thellier*, 1959] worden gebruikt ter bepaling van de magnetische eigenschappen en laten zien dat thermische demagnetisatie tot 250°C volstaat voor paleointensiteitbenaderingen. De gecorreleerde curven vormen een coherente OJP-stack, welke wordt gedateerd op de ompolingen van het paleomagnetisch veld. Er zijn geen aanwijzingen voor het bestaan van een zaagtandpatroon in deze stack. Een samenhangend verschijnsel met twee andere curven die het Matuyama Chron beslaan, is een periodiciteit van 150 kyr. Hierbij dient opgemerkt te worden dat, behalve op de tien ijkpunten, de tijdcontrole te wensen overlaat. Dit zou—ten dele—kunnen verklaren waarom de drie paleointensiteitsregistraties van de Matuyama verder geen samenhangde frequenties vertonen.

Acknowledgments

Everybody who got this far in "Reading the muddy compass" is thanked very much for their interest in this study or at least just their curiosity. I wouldn't have been able to complete this thesis without the help of many people. First of all the 'ever-patient advisor' Lisa Tauxe who wrote the proposal and got GOA to fund this project. She has initiated me in the art of paleointensity research. I thank her for her support, the valuable discussions, her friendship, and the hospitality in The Netherlands and California. As a matter of fact, working with Lisa was almost like paleomagnetism. Her *excursion* to the Netherlands was aborted, leaving me *locked in the mud.* After she left Utrecht a *decrease in paleointensity* (DIP) was observed. Sometimes there was evidence of a *decline* or even *anti-podal* behavior. Furthermore, *delayed acquisition* played a role during the last two years. The global trend of our working relationship could be typified as a segment of a *saw-toothed paleointensity record*, but we have strong reason to believe that this is not a genuine feature, merely an *overprint* of reality. It must have been quite a task for Lisa to deal with my obstinacy.

Professor J.D.A. Zijderveld is thanked very much for agreeing to be my promotor. With his promise we could have the defense in Utrecht, instead of somewhere else.

Next, the Fort people are thanked for having the pseudo *anomaly* among them: I didn't spend much time measuring (I probably spent more hours playing saxophone in the catacombs), nor was my computer 'normal', still it was a pleasant time. The discussions I had with Cor Langereis were valuable, as were his comments and suggestions on the many of the manuscripts. Furthermore, I am grateful to the entire Fort team: Willy van Beek, Cor de Boer, Mark Dekkers, Jaume Dinarés, Charon Duermeijer, Ton van Hoof, Teresa Juárez, Wout Krijgsman, Pauline Kruiver, Henk Meijer, Tom Mullender, Ingeborg van Oorschot, Hilde Passier, Thomas Pick, Michael Urbat, Adry van Velzen, Piet-Jan Verplak, Nicole van Vugt, Hans Wensink, and Tanja Zegers, if not for scientific reasons, then on matters concerning life in general. Thomas Pick is not only thanked for his involvement in paleointensities, but also for introducing me to Chet Baker.

Data has been kindly provided by Jean-Pierre Valet, Carlo Laj, Catherine Kissel, Alain Mazaud, and I particularly thank Martin Frank for providing preprints of manuscript and data and his positive attitude towards science. Constructive reviews of Rob Coe, Martin Frank, Jean-Pierre Valet and several anonymous referees are much appreciated. I am indebted to the paleomagnetists of consequence Dennis Kent, Carlo Laj, and Rob van der Voo for carefully reading and judging this thesis.

Without help from Lisa Tauxe, Bryan Conlon, Pauline Kruiver, and John Miller (ODP), sampling would have been a drag. The curators of ODP in College Station and Laurent Labeyrie in Gif-sur-Yvette are acknowledged for letting me

sample their sedimentary cores. Steve DiDonna sampled several boxes as well, moreover he prepared *all* my glass cylinders by burning holes in them. He and Jeff Gee (great ovens!) are thanked for their essential assistance while I was turning the paleomagnetic laboratory at Scripps upside down. The other zombies Jason Hicks and Teresa Juárez cheered up my sentences to the shielded room. Also Harm van Avendonk, Kim Cobb, Elena Pérez, and Mark van Zuylen are thanked for being around in La Jolla.

I appreciate to have been housed at Harm van Avendonk's, Renate Hartog's and—last but not least—Jason Phipps Morgan's during my visits to California. My extended stays at the latter's house were honored by the presence of Teresa Juárez, Marije van Koolwijk, Cor "le Chef" Langereis, Steve Tait, Martine Huleux, Sylvia de Vries, Jurgen Kok, and even JPM himself.

Next, Lisa Tauxe (Scripps), Rob Coe (Santa Cruz), Jonathan Glen (IPGP), and Carlo Laj c.s. (Gif-sur-Yvette) are thanked for showing me around in their laboratories. Harmen Bijwaard's help as 'naïve' reader has improved many of the manuscripts, and Susanne Buiter helped me during struggles with LaTeX. My never-failing izabella has been set up by Jörg Schmalzl, Thomas Pick, and Theo van Zessen. Without the very nice plotxy program by Bob Parker and Loren Shure I would have been helpless; it must have been called over hundred thousand times (all figures in this thesis are made with 'p'). Also cross (Bob Parker), Gif-sur-Yvette's AnalySeries (Paillard *et al.*), and parts of Lisa's and Thomas' code were very helpful. John Bolte is thanked for taking me on a train journey, in order to indirectly meet Nathalie.

Finally, I would like to thank the support of my family, and—most certainly—Nathalie (ba oui, je t'aime!).

Bunnik, 27 September 1998.

Curriculum Vitae

December 10, 1970	Born in Den Burg (Texel), The Netherlands
1983–1989	VWO (secondary school) in Den Burg, The Netherlands
1989–1994	Study of Geophysics at Universiteit Utrecht, The Netherlands
1994–1998	PhD student (oio) at the Paleomagnetic Laboratory "Fort Hoofddijk", Universiteit Utrecht, The Netherlands
1996–1998	Working visits to Scripps Institution of Oceanography, University of California San Diego, USA (total 7 months)

Stellingen behorende bij het proefschrift

Reading the muddy compass

Yvo S. Kok

1. Saw-toothed patterns in paleointensity records can be explained by cumulative viscous remanence.

   Chapter 5

2. Stepwise thermal demagnetization of magnetic remanence is a proper way to get rid of a saw-toothed pattern around a geomagnetic polarity reversal.

   Chapters 6 and 9

3. A distribution of relaxation times spanning the interval 0–100 Myr is merely a subset of all relaxation times present in rocks. However, it is sufficient for modeling saw-toothed patterns when the tooth of time works for circa 4 million year.

   Chapters 5, 6 and 7

4. When independently derived paleointensity curves show strong similarities, it does not necessarily mean that they indicate 100% geomagnetic behavior.

   Chapters 5 and 8

5. Correlation coefficients are only meaningful when significance levels are provided and when the data sets are Gauß-Laplace distributed.

Chapter 8

6. It is noteworthy that paleointensities from sediments can be obtained by conveyor-belt production, much simpler and faster than acceptable for better-understood volcanic rocks.

Chapter 1

7. The *real* millenium problems are (1) the growing number of computer-related physical and mental injuries, and (2) MS Win-*dough*'s addiction to disk space, processor speed and memory.

8. PALEOINTENSITY = A POET'S TINY LINE.

9. Working longer than 4 years on a Dutch PhD study is like driving faster than 50 km per hour in built-up areas.

10. An 800-kyr periodicity is observed in the geomagnetic polarity pattern for last 5 million year (see Figure 1). It is insinuated that circa 190 kyr ago, at short reversed polarity period heralded the present 800-kyr sequence; in approximately 600 kyr we are to expect a reversal of the Earth's magnetic field...
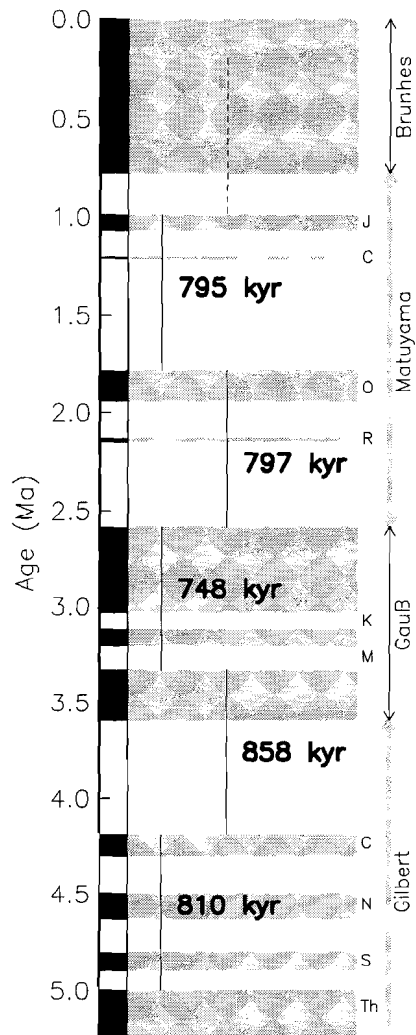
Figure 1: Alternative look at the Geomagnetic Polarity Time Scale with ~800 kyr periods starting with a reversed zone. The Early Matuyama with the normal La Réunion (R) and Olduvai (O) resembles the Late Matuyama with Cobb Mountain (C) and Jaramillo (J) polarity intervals. It is also interesting that the Olduvai is twice as long as the Jaramillo and both are 8 times longer than their respective "precursors" La Réunion and Cobb Mountain.